SYNAPTIC LEARNING RULES FOR LOCAL SYNAPTIC INTERACTIONS: Theory and Application to Direction Selectivity

Thesis by Chunhui Mo

In Partial Fulfillment of the Requirements
for the Degree of
Doctor of Philosophy

California Institute of Technology
Pasadena, California
2003
Defended May 20, 2003

Acknowledgements

I would like to thank my advisor, Dr. Christof Koch, whose constant support has made this research work possible. He provided me with the critical guidance to advance my research in the right direction and stay focused on important questions. He sets high standards for research quality and scientific ethics. I can always count on his encouragement when I venture into creative areas and his patience when I make slow progress.

I am very grateful to my thesis committee, Drs. Scott Fraser, Gilles Laurent, Steven Quartz, and Erin Schuman, who have provided me with invaluable feedback over the years. Special thanks go to Gilles for stimulating scientific discussions and Erin for valuable insights in the experimental side of learning and calcium dynamics.

I thank all Koch lab members for tolerating my big background jobs on their desktop machines. All my friends, fellow BMB and CNS students, and Techers have made my stay at Caltech an enjoyable experience. Thank you.

This “reverse-phi” modeling project originated in a joint discussion with Tomaso Poggio and Margaret Livingstone. I would like to thank both for their help and criticism. I would also like to thank Drs. Kevin Archie, Bartlett Mel and Terry Sejnowski for providing cell models, help and criticism.

Finally, I would like to thank my parents for motivating me to go through the graduate school and my friend Ying Gong for constant encouragement. Thanks for the critical reading of my thesis!

This research was supported by grants from the NSF-sponsored Engineering Research Center at Caltech, the National Institutes of Health, and the National Institute of Mental Health.

Abstracts

This thesis is organized in two parts, both concerned with local synaptic interactions within the dendritic tree. The first part is focused on how specific synaptic arrangements that can be used to compute direct ion selectivity can be learned in an unsupervised manner. The second part consists of a double synaptic veto model that can account for the observed reverse-phi selectivity of direction-selective cells. We propose an activity-based, local learning model that may account for the direction selectivity in neurons in the visual cortex based on the local veto operation among excitation and inhibition. We implement the learning rule with local calcium concentration changes and a BCM type learning curve (Bienenstock, Cooper and Munro, 1982). Our biophysical simulations suggest that a model cell implementing our learning algorithm develops direction selectivity organically after unsupervised training. The learning rule is also applicable to cells with multiple direction-selective subunits on dendrites and is stable under a number of starting conditions.

Reverse-phi motion is the illusory reversal of perceived direction of movement when the stimulus contrast is reversed in successive frames. Livingstone (2000) showed that direction-selective cells in striate cortex of the alert macaque monkey showed reversed excitatory and inhibitory regions when two different contrast bars were flashed sequentially during a two-bar interaction analysis. We carry out detailed biophysical simulations of a direction-selective cell model

implementing a synaptic shunting scheme. Our results suggest that a simple synaptic-veto mechanism with strong direction selectivity for normal motion cannot account for the observed reverse phi-motion effect. A direct interaction between the ON and OFF pathway, missing in the original shunting-inhibition model, is essential to account for the reversal of response. We propose a double synaptic-veto mechanism in which ON excitatory synapses are gated by both delayed ON inhibition at their null side and by delayed OFF inhibition at their preferred side. The converse applies to OFF excitatory synapses. Mapping this scheme onto the dendrites of a direction-selective neuron permits the model to respond best to normal motion in its preferred direction and to reverse-phi motion in its null direction.

Table of Contents

Chapter One

Introduction

This thesis consists of two major parts. The first part, a detailed description of a synaptic learning rule for local synaptic interactions between excitation and shunting inhibition on a direction-selective cell's dendrite is given in Chapters Two and Three. The second part, a double synaptic veto mechanism that can account for the observed "reverse-phi" selectivity of cortical direction-selective cells, is introduced in Chapter Four which has been published as Mo and Koch (2003). This chapter serves as a guided tour to give readers a quick overview of each chapter and the motivation behind.

The ability to detect motion direction is arguably one of the most important functions of all vision systems. Direction-selective cells in the retina of the rabbit (Barlow and Levick, 1964; reviewed by Vaney *et al*., 2001), the pretectal nucleus of the optical tract (NOT) of the wallaby (Ibbotson and Price, 2001), the lobular plate of the fly (Egelhaaf and Borst, 1992), and the visual cortex of the cat and monkey (Goodwin *et al*., 1975; Emerson and Gerstein, 1977; Ganz and Felder, 1984; Emerson *et al*., 1993;Jagadeesh *et al*., 1993; Livingstone, 1998) have been extensively studied (reviewed by Clifford and Ibbotson, 2003). Over the years, both feed-forward (Koch and Poggio, 1985; Livingston, 1998; Anderson *et al*., 1999) and feedback (Suarez *et al*., 1995; Douglas *et al.*, 1995; Maex and

Orban, 1996; Ernst *et al*., 2001; Rao and Sejnowski, 2001) schemes have been proposed. Recent experimental evidence suggests the asymmetrical delayed inhibition is likely to be one of the mechanisms that underlie cortical direction selectivity (Livingstone, 1998). Such a mechanism may be based on shunting inhibition, *i.e.,* an increase in a chlorine based GABA_A conductance that reverses close to the cell's resting position, as proposed by Koch and Poggio (1985).

One important open question is: how can the required synaptic specific interaction among excitations and inhibitions be obtained in an unsupervised manner? The wiring requirement for such a scheme is the following: excitation in visual space can reside on either side of the inhibitory zone, but not on both sides, in which case the model receives symmetric input in space-time and is thus not direction-selective. Cats reared in a stroboscopically illuminated environment develop normal orientation-selective neurons in cortex but direction-selective neurons are virtually abolished. This effect remains after long periods of normal visual exposure (Cynader and Chernenko, 1976; Humphrey and Saul, 1998; Saul and Feidler, 2002; rabbit visual cortex: Grigonis *et al.,* 1988). The results suggest the establishment of direction-selective properties of cortical cells is likely to go through a visual-experience driven, activity-based learning phase. The learning process for direction selectivity may be independent of the establishment of orientation selectivity. In this study, we propose an activity-based, local learning model that may account for direction selectivity in V1 cells

or other types of computations based on local veto operation among excitation and inhibition. We assume that the inhibitory connection is fixed and the learning process only occurs at excitatory synapses in chapter two and through most of chapter three, because very little experimental evidence exists for inhibitory learning. A global, activity-based inhibitory learning scheme that works with our local excitatory learning rule is also addressed in the last section of chapter three. Given the fact no calcium flow through an inhibitory channel when it is open, it is unclear if our calcium based local learning mechanism can be applied to the learning of inhibitory synapse. We here adopt a global inhibitory learning mechanism as described by Soto-Trevino *et al*. (2003). In cat area 17, 40% of cells are found to have their inhibition tuning preference different from their spike outputs in an intracellular study investigating synaptic mechanisms of orientation and direction selectivity (Monier *et al*, 2003). The excitation tuning preference of these cells is the same as either the spiking output or the inhibition. The lack of homogeneities in input combinations might reflect the result of an activity based, excitation-inhibition differential learning process during development.

Various modified versions of the original Hebbian learning rule that can account for the development of direction selectivity have been proposed (Bienenstock *et al*., 1982; Feidler *et al*., 1997; Blais *et al*., 2000; Rao and Sejnowski, 2001). Our learning rule is based on the peak calcium concentration change at spines following a synaptic input. We use a BCM type learning curve (Bienenstock *et al*., 1982) without implementing a non-linear sliding threshold that is yet to be

experimentally verified. Direction-selective cells in the monkey V1 can respond to movement within 0.1 degree, which is much smaller than their receptive field size (Livingstone, 1998), suggesting cortical direction-selective cells have direction-selective subunit structures on their dendrites (Emerson, 1997). We use compartmental simulations and a model cell with very simple geometry to test our learning rule, different from all previous studies that treat the post synaptic cell as a point-neuron or simply an integration unit (Koch and Segev, 2000; Koch *et al*., 2003). This allows us to investigate the development of direction-selective subunit structures at the dendritic level.

The effect of post-synaptic calcium concentration on LTP and LTD has been shown by (Yang and Zucker, 1999) in their photolysis experiments. Fast rising calcium concentration changes in dendritic spines mediated by action potential and long sustained rising mediated by synaptic inputs have been observed in calcium imaging experiment (Sabatini and Svoboda, 2002). A comparison of the calcium dynamics that is discovered in their study and that is implemented in our model is given in the discussion section of Chapter two. We assume calcium-dependent synaptic weight changes can be achieved biochemically through the calcium-dependent phosphorylation of a-amino-3-hydroxy-5-methyl-4-isoxazolepropionic acid (AMPA) subtype of glutamate receptors (AMPARs) as described by Castellani *et al*. (2001).

Phi motion refers to our perception of motion when discrete bars are presented in

a continuous spatial and temporal sequence. Reverse-phi motion was first demonstrated by Anstis (Anstis, 1970; Anstis and Rogers, 1975). Subjects perceive the reverse direction of motion when the contrast of a moving object reverses in the second frame of a two-frame shift experiment. Reverse-phi like effects have also been reported during electrophysiological experiments from direction-selective complex cells in the cat striate cortex (Emerson *et al*., 1987), the H1 cell in the fly's lobula plate (Egelhaff and Borst, 1992), and the optical tract of the wallaby (Ibbotson and Clifford, 2001). Recent recordings from direction-selective cells in the alert monkey show that cells in both cortical areas V1 and MT reverse facilitation and suppression regions in the 2-bar interactions map when two different contrast bars are presented (Livingstone *et al.,* 2000; Conway and Livingstone, 2001). This implies that these cells respond to reverse-phi motion in the reversed direction. In Chapter Four, we show how the circuitry for the normal direction selectivity can be adapted to account for the reverse-phi selectivity. Our results suggest that a simple synaptic-veto mechanism with strong direction selectivity for normal motion cannot account for the observed reverse phi-motion effect due to the fact that a direct interaction between the ON and OFF pathways is missing in the original shunting inhibition model. We show a double synaptic-veto mechanism, derived from the traditional asymmetrical delayed shunting inhibition model, can account for both normal and reverse-phi motion direction selectivity. In such a scheme, ON excitatory synapses are gated by both delayed ON inhibition at their null side and by delayed OFF inhibition at their preferred side. The converse applies to OFF excitatory synapses. Mapping

this scheme onto the dendrites of a direction-selective neuron permits the model to respond best to normal motion in its preferred direction and to reverse-phi motion in its null direction.

Both the learning model and the reverse-phi model use shunting inhibition to achieve dendritic specific veto of excitatory inputs. The shunting inhibition's local "gating" effect is discussed in Chapter Five, as well as the optimal inhibition and excitation input locations in our model. Recent experiments in the retina provide evidence in favor of at least some nonlinear interactions between excitatory and shunting inhibitory inputs that take place within the dendrites of direction-selective ganglion cells (Taylor *et al.*, 2000; for a dissenting view, see Borg-Graham 2001). Large conductance changes that reverse around the cell's resting potential have been observed in V1 during visual stimuli (Anderson *et al.*, 2000; Borg-Graham *et al*., 1998). Our results suggest shunting inhibition may be important for forming direction-selective synaptic connections as well as the final direction selectivity.

Finally, in Chapter Six we discuss whether our learning rule described in chapters two and three can account for the "double-veto" synaptic placement we proposed in chapter four. Reverse-phi motion stimuli do not appear to be a common feature of natural spatiotemporal scenes. It therefore remains unclear why cortical cells should invert their direction selectivity for reverse-phi motion. We believe that the synaptic circuitry responsible for detecting reverse-phi motion

has to be established as a by-product of developing normal direction selectivity, rather than a stand-alone training process. We show such connections may be established due to the background firing of inhibitory input cells, which causes bias in the learning outcome.

Chapter Two

A Synaptic Learning Rule for Local Synaptic Interactions between Excitation and Shunting Inhibition

2.1 Introduction

The ability to distinguish object movement directions is important to all motion processing systems. In the cat and monkey, V1 is the first stage in the visual pathway where direction-selective (DS) cells are encountered. Cats reared in a stroboscopically illuminated environment develop normal orientation-selective neurons in cortex but direction-selective neurons are virtually abolished. This effect remains after long periods of normal visual exposure (Cynader and Chernenko, 1976; Humphrey and Saul, 1998; Saul and Feidler, 2002). Therefore, direction selectivity is likely to require structured synaptic input during early developmental stages. These neurons are thus excellent targets for the study of activity-dependent synaptic weight changes. Hebb proposed his famous learning rule based on the correlation between pre- and post-synaptic activities (Hebb, 1949). Long-term potentiation (LTP) and the long-term depression (LTD) are likely to be among the synaptic manifestations of such a learning rule (Bliss and Lomo, 1973; Dudek and Bear, 1992; Reviewed by Malenka and Nicoll, 1999). However, a computational study showed that the simple Hebbian learning rule performs poorly in direction-selective synapse placement (Feidler *et al.*, 1997). This is not surprising since the basic requirement for direction selectivity is a non-

linear interaction between two different inputs in space-time. In a natural environment, as many stimuli are expected to move in the preferred than in the null direction. While there exists a correlation between pre- and post-synaptic firing in the preferred direction, this is not the case for motion in the opposite, null, direction.

There are various modified versions of the original Hebbian learning rule that can account for the development of direction selectivity. The principal component analyzer model proposed by Oja in 1982 adds a non-linear decay term to achieve stability (Oja, 1982), although itself is not a direction selective learning rule. A post-synaptic "gating" rule links synaptic weight changes with post-synaptic activities (Feidler *et al*., 1997). The BCM learning rule, originally proposed to account for orientation selectivity and binocular interactions, has been extended to the generation of direction-selective units (Bienenstock *et al*., 1982; Feidler *et al*., 1997; Blais *et al*., 2000).

Intracellular calcium concentration is one of the biophysical variables critical to LTP induction, suggesting it may be an important messenger bridging the gap between firing frequency changes and synaptic modifications (Lynch *et al.*, 1983; Yang *et al*., 1999; Zucker, 1999; Kalikulov *et al*., 2002). NMDA receptors are likely to be the entry points of calcium at spines since an antagonist of NMDA receptors inhibits the induction of LTP (Collingridge *et al*., 1983). The age-dependent time course change of the NMDA current has been proposed to

account for the age-dependent decline of visual cortical plasticity (Carmignoto and Vicini, 1992). Glutamate receptors may involve in regulating spine structure plasticity (Fischer *et al*., 2000). Calcium influx through NMDA channels can cause a large, localized and transient increase in the postsynaptic calcium level (MacDermott *et al*., 1986; Gamble and Koch, 1987; Zador *et al*., 1990; Helmchen *et al*., 1999; Sabatini *et al*., 2001; Sabatini *et al*. 2002). The existence of voltage-gated gated calcium channels in hippocampal cells and their contribution to synaptic plasticity have been reported (Dingledine, 1982; Cummings *et al*.). A simulation study by Castellani *et al*. (2001) suggests a BCM type learning curve can be achieved by calcium-dependent protein kinases and phosphatases activity changes that in turn modify the phosphorylation state of AMPA receptors and thus their conductance. Enzymes involved in this process reside in the postsynaptic density (reviewed by Kennedy, 2000) and may involve with the long-term calcium-dependent regulation in neuronal gene expression (reviewed by Bito *et al*., 1997).

A great deal is known about direction-selective cells through experimental, modeling and theoretical investigations. The motion energy model (Adelson and Bergen, 1985), as well as the equivalent Reichardt model (Reichardt, 1961; Santen and Sperling, 1985), interprets observed physiological and psychophysics data well. At the biophysical level, network models that rely on excitatory feedback (Douglas *et al*., 1995; Maex and Orban, 1996; Rao and Sejnowski, 2001) and feed-forward models (Koch and Poggio, 1985; Livingston,

1998; Anderson *et al*., 1999) have been proposed to account for direction-selective synaptic arrangements in the cortex. The asymmetry in the summation of excitatory inputs at dendrites alone is not sufficient to account for the directional response based on modeling study by Anderson *et al*. (1999). Asymmetrical delayed inhibition is likely to be one of the mechanisms that underlie direction selectivity. Such a mechanism based on shunting or silent inhibition was proposed for the cortex by Koch and Poggio (1985). A bar moving in the preferred direction reaches the excitatory input before the inhibitory one, which only acts after an additional delay (Fig. 2-1a). The excitatory input reaches the soma and causes the cell to spike because of the temporal offset between the two inputs. In the opposite, null direction, the excitatory input is "vetoed" by the inhibition if the bar's speed is approximately matched to the delay. The wiring requirement for such a scheme is simple: excitation in visual space can reside on either side of the inhibitory zone, but not on both sides, in which case the model receives symmetric input in space-time and is thus not direction-selective. Large conductance changes that reverse around the cell's resting potential have been observed in V1 during visual stimuli (Anderson *et al.*, 2000; Borg-Graham *et al*., 1998). Given the local effect of shunting inhibition, it is interesting to investigate its possible role in synaptic learning.

Both retinal and cortical direction-selective cells have subunit structures within their receptive fields (Barlow and Levick, 1965; Emerson *et al.*, 1987; Livingstone *et al*., 2001). A comparison of two fictitious cortical DS cells with and without

subunit structures is shown in Fig. 2-1b. Both cells receive inputs from the same group of LGN cells but the one with subunit structures utilizes its resources more efficiently and has superior position-invariant direction tuning. Synaptic logic models involving complex, branch-specific synapse placements had long been proposed (Poggio, 1982; Koch and Poggio, 1987). Recent work by Mel and colleages suggests that the large dendritic tree of cortical pyramidal neurons may function as a two-layer neural network (Poirazi *et al*., 2003). The standard form of Hebbian learning rule and all of its variations describing changes only in the overall connection strength between the pre- and post-synaptic neurons cannot account for structure plasticity (Mel, 2002) and local learning, for they do not distinguish among post-synaptic connection locations. We here demonstrate, using a highly idealized compartmental simulation of a single post-synaptic neuron, how a learning rule for local synaptic interactions between excitation and shunting inhibition could, in principle, account for direction selectivity and subunits learning at the dendrite level.

2.2 Methods

All compartmental simulations were carried out using the program NEURON (Hines and Carnevale, 1997). The idealized cell morphology of a direction-selective neuron included eight dendrites (width 0.5 µm, length 100 µm) that were directly connected to the soma (width 16 µm, length 16 µm). Each dendrite was unbranched and had 20 compartments, for a total of 180 compartments. The dendrites were passive except for an N-type calcium conductance, while the cell body contained sodium and potassium conductance that gives rise to fast Hodgkin-Huxley-like action potentials. Given our model cell's low L value/large space constant (L=0.45 at the tip of the dendrite), large sodium conductance is not needed at dendrites to sustain back-propagating spikes as opposed to a simulation study by Tsay and Yuste (2002) using a big layer five pyramidal neuron model. There was no spike adaptation mechanism in our model. The biophysical parameters included: R_i=250 Ω•cm, C_m=0.5 µF/cm^2, E_{leak}=-60 mV, R_m=10 kΩ•cm^2, g_{Na}=0.030 S/cm^2, g_K=0.028 S/cm^2, E_{NMDA}=0 mV, g_{NMDA}=0-2 nS, $\tau_{NMDA\ on}$=0.1 ms, $\tau_{NMDA\ off}$=80 ms, E_{AMPA}=0 mV, g_{AMPA}=0-2 nS, $\tau_{AMPA\ on}$=0.1 ms, $\tau_{AMPA\ off}$=2 ms, E_{GABA}=-60 mV, g_{GABA}=5.0 nS, $\tau_{GABA\ on}$=1 ms, $\tau_{GABA\ off}$=80 ms. Synaptic input was modeled using the point process in NEURON (adopted from Archie and Mel, 2000). The input resistances of the model cell were 570 MΩ, l008 MΩ (L=0.22, transfer resistance 519 MΩ), and 1448 MΩ (L=0.45, transfer resistance 503 MΩ), at the soma, the middle of the dendrite and the tip of the dendrite respectively. The large input resistance allowed a single excitatory

synaptic input around 2ns to elicit spikes at the soma. Real cells may have much lower input resistance at soma, but they may also require several simultaneous excitatory inputs to elicit spikes. The large input resistance was due to our cell's limited size (dendrite: 100 µm in length, 0.5 µm in diameter. Soma: 16 µm in diameter). Increasing the dendrite length to 200 µm and diameter to 1.5 µm and connecting a large compartment that was 500 µm in length and 5 µm in diameter decreased the model cell's input resistance to around 70 MΩ. Our learning model converged as expected using this alternative geometry setting when we increased the excitatory and inhibitory input connection strength by ten folds to make them large enough to elicit spikes.

The N-type voltage-gated calcium conductance was taken from (Benison *et al*., 2001) and mapped to dendrites with a density of 1 mS/cm2. We assume that excitatory synapses are located to dendritic spines and that the rapid rise in intracellular calcium concentration at the postsynaptic site inside the spine following synaptic activation have two main sources (Fig. 2-2a): calcium current through the NMDA synapse, I_{Ca_NMDA},, and calcium current, I_{CaN}, that is located in the dendrite and a certain amount of which diffuses up into the spine. I_{Ca_NMDA} was calculated as one third of the total current through the NMDA synapse but with a reversal potential E_{Ca}=130mv. Of the I_{CaN} entering the dendritic compartment associated with the spine, 5% was assumed to contribute to the calcium concentration at the spine (Koch, 1999). These scaling factors were chosen to bring the amounts of calcium entering through NMDA channels and

through N-type voltage gated calcium channels within the same order of magnitude. The final calcium concentration at the spine was given by a simple decay equation

$$\frac{d[Ca^{2+}]}{dt} = I_{Ca\_NMDA} + I_{CaN} - \frac{[Ca^{2+}]}{t_{Ca^{2+}}}$$

The stimulus was a 1-D bar moving across the receptive fields of 6 LGN cells (Fig. 2-1b) at 10 deg/sec (for details, see section 4.2). Each of the middle four LGN cells provided delayed input to one dendritic branch of the model cell while the LGN cell immediately to the right and the LGN cell immediately to the left provided delayed excitation. The delay was 10 ms. There were a total of 8 excitatory synapses and 4 inhibitory synapses in the model (Fig. 2-1d). Each geniculate input was assumed to directly excite its appropriate dendrite at a single synaptic cluster (here modeled as one deterministic excitatory synapse), and—via a local interneuron—to inhibit a dendrite. This was modeled by a single deterministic inhibitory synapse that was delayed by 10 ms with respect to excitation. Excitatory synapses were mapped to the dendrite compartment 60µm away from the soma; inhibitory synapses located 50µm away from the cell body. In the main model, inhibition was assumed to be of the shunting type, with a reversal potential E_{GABA}=-60mV (the cell's resting potential is -60 mV). The temporal dynamics of the excitatory (NMDA) and inhibitory (GABA) synaptically induced conductance changes were as described by (Destexhe and Sejnowski, 1994).

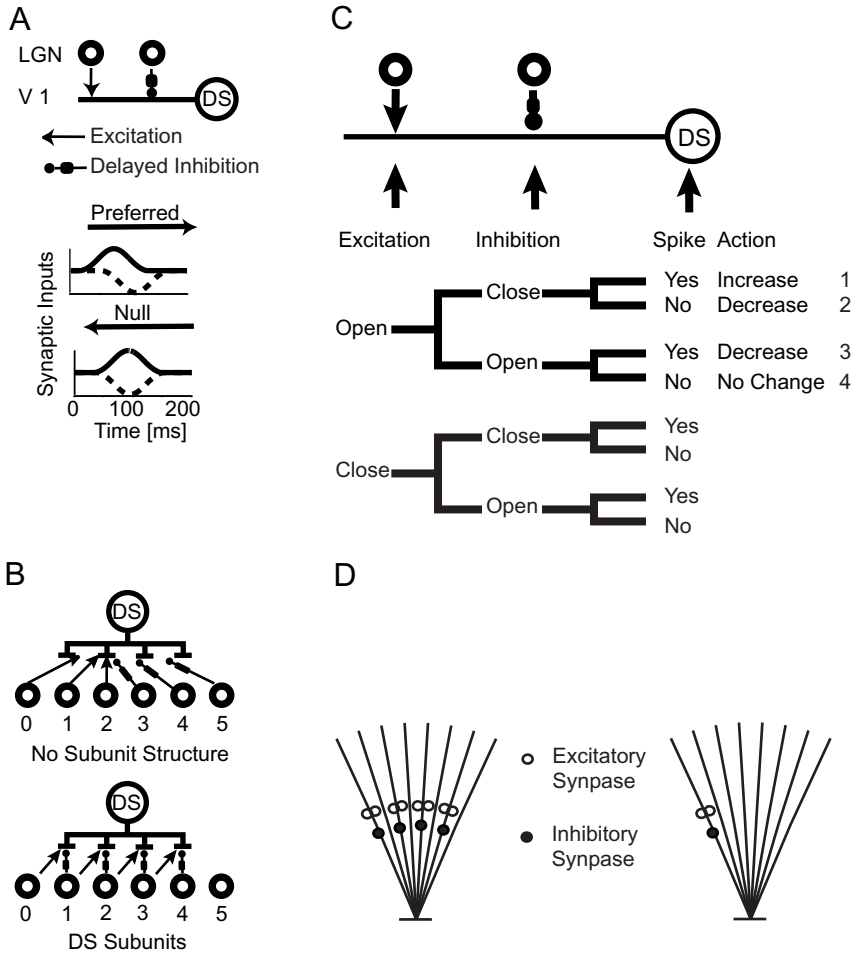

Fig. 2-1. Illustration of a direction selective (DS) mechanism and basic kinds of information available to an excitatory synapse to determine its learning strategy (A) A DS neuron in V1 receives two LGN inputs, one excitatory and one delayed inhibitory (via a cortical interneuron). Solid curves show excitatory synaptic conductance changes during the preferred and null direction motion stimuli. Dashed curves show inhibitory synaptic conductance changes plotted in negative. The difference in temporal alignment of these two inputs during motion stimuli forms the base of the V1 cell's direction selectivity. (B) Connection diagram for two DS cells with (bottom) and without (top) DS subunits on their dendrites. Both receive inputs from the same LGN cell array. The DS cell on the top has no subunit structures. A bar needs to move across the middle line between LGN input cell 2 and 3's receptive fields to elicit directional response. The DS cell at the bottom has one DS subunit on each of its four dendrites and thus has much better position invariant direction selectivity within its receptive field. (C) Three types of information available to an excitatory synapse on a remote dendrite of a DS cell to determine whether or not its own activity is contributing to the direction selectivity of the host cell. (D) The model neuron and relative excitatory and inhibitory synapses placement. Left: multiple DS subunits. Right: single unit model.

2.3 A local learning scheme for direction selectivity

We considered what kinds of information were available to an excitatory, geniculate synapse that just landed on a dendrite of a cortical neuron to correctly judge whether its activity contributed or degraded the direction selectivity (DS) of the host cell, assuming the inhibitory input was already connected and fixed. There are three major pieces of information accessible to local mechanisms: the state of the excitatory input, the state of the local inhibitory input and whether or not the host cell generates a somatic action potential within a small time window and this spike propagates back into the dendrite to the postsynaptic site of excitation. Assuming binary states (e.g., excitatory input is either on or off), this gives rise to eight possible scenarios (for instance, both excitation and inhibition are active and the host cell spikes). We assume the excitatory synapse can only be modified when it is active; this reduces the combinations to four scenarios (Fig. 2-1c). In scenario one, there is no inhibition and the cell spikes after the excitatory synapse opens. The assumption is that the excitatory synapse directly contributes to the cell's direction selectivity and thus its connection strength should increase. In scenario two, there is no inhibition and no spike when the excitatory synapse opens. The fact that the DS cell isn't spiking suggest that the stimulus moves in the null direction; yet the excitatory input is not gated by the inhibition and counteracts the cell's direction selectivity. Its connection strength should decrease. In scenario three, both the excitation and the inhibition are open, yet the cell fires an action potential. The assumption is that this scenario

corresponds to the null direction motion and that the excitatory synapse lands on a spot with incorrect matching of inhibition. Its connection strength should therefore decrease. In scenario four, the excitation is successfully blocked by inhibition, suggesting a null direction movement, in which case the blocking by inhibition is legitimate. On the other hand, this could also correspond to a preferred direction movement. The cell generates an action potential in the presence of inhibition, yet this spike, propagating back from the soma into the dendrite, is blocked by inhibition from reaching the site of excitation. Given this ambiguity, the best possible action is to do nothing and keep the excitatory weight constant.

An excitatory synapse can adjust its weight if it can distinguish these four scenarios. We next mapped out local calcium concentration changes during these scenarios and used this biophysical variable to "inform" the excitatory synapse about which action it should take during the learning process.

2.4 Calcium dynamics at spine and the local learning rule

Fig. 2-2a illustrates a dendritic branch with two spines with independent excitatory inputs. Inhibition was mapped to a dendritic compartment located between the excitatory inputs and the soma, fulfilling the "on-the-path" requirement (Koch *et al*., 1982). We mapped the two excitatory synapses into one, electrical equivalent, dendritic compartment (Koch, 1999). Calcium can enter the spine in two ways: either through NMDA channels at the spine or

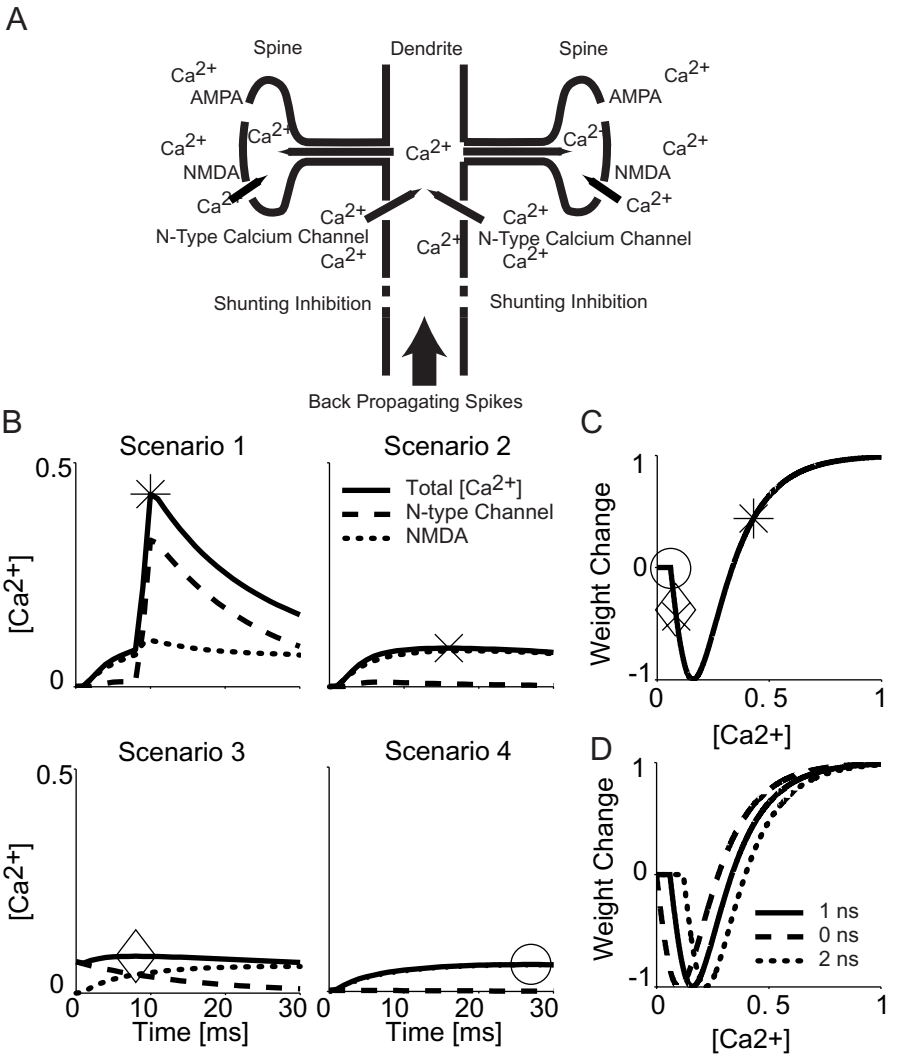

Fig. 2-2. Calcium dynamics at a spine and a BCM type learning curve based on local calcium concentration change (A) A schematic drawing of calcium entrance points at spines and the local dendritic branch. Calcium can enter spines directly through NMDA channels or indirectly through N-type voltage-gated calcium channels that could be activated by back-propagating somatic action potentials. Shunting inhibition is located between the spine and soma and can block back-propagating somatic spikes and clamp the membrane voltage to reduce the amount of calcium entrance. (B) Local calcium concentration changes following synaptic activation for four different learning scenarios. Solid curves show the total calcium concentration. Dashed (resp. dotted) curves show the calcium concentration changes due to calcium entering through N-type voltage gated calcium channels (resp. local NMDA channels). Peak calcium exposures within 30 ms are marked. (C) A BCM type learning curve (gNMDA=1ns). Peak calcium concentration reached in each of the four scenarios described above and the corresponding synaptic weight changes are marked on the curve. Calcium concentrations are in an arbitrary unit. The synaptic weight change is relative to the maximum allowed learning step size in each trial. (D) A linear sliding threshold is chosen for the learning curve. Three learning curves shown are calculated at gNMDA=0ns (dashed), gNMDA=1ns (solid), gNMDA=2ns(dotted).

through the N-type voltage gated calcium channels inserted into the dendritic membrane. We reason that calcium can enter the spine from the dendrite but cannot exit to the dendrite from the spine; given the large volume difference between the spine head and the dendrite, and given various calcium pumps along the thin neck of the spine. Therefore, the two spines are chemically independent, although they are electrically equivalent (Zador and Koch, 1990).

The excitatory and inhibitory inputs and the back-propagating spike from the soma affect the total calcium concentration at the spine in their own way. The excitatory input directly correlates with the calcium current entering through NMDA channels, which is spine/synapse specific. Its time course is mainly determined by the conductance change of the local NMDA synapse. Back-propagating action potentials signal the global activation state of the DS cell. N-type voltage-gated calcium channels are mainly activated when there is a back-propagating spike. Given the NMDA synapse's reversal potential (set to zero), the synaptic input current alone cannot elevate the membrane potential high enough to cause significant activation of the N-type voltage gated calcium channel. The on-the-path shunting inhibition affects the time course of both calcium currents. It clamps the membrane voltage when open, thereby reducing the amount of calcium current entering through NMDA channels. Furthermore, it completely blocks back-propagating spikes, which in turn blocks calcium entrance through N-type voltage gated calcium channels. The clamping and blocking effects are branch specific due to the local action of shunting inhibition.

The total calcium concentration at the synapse results from the addition of the two currents assuming instant diffusion of the intracellular free calcium from dendrites into spine. We modeled all internal calcium buffers and calcium pumps using a single decay constant.

We implemented the above calcium scheme and computed the resultant changes in free, intracellular calcium concentration ($[Ca^{2+}]$) at the spine for the four scenarios considered earlier (Fig. 2-2b). In scenario one, there is no local inhibition and the cell spikes after the excitatory synapse opens. Calcium enters through both channels. Changes of $[Ca^{2+}]$ are high. In scenario two, there is neither local inhibition nor a back-propagating spike immediately after the excitatory synapse opens. Calcium mainly enters through NMDA channels. Changes of $[Ca^{2+}]$ fell into an intermediate range. In scenario three, the excitatory input is blocked by the inhibition but the cell spikes. The amount of calcium entering through NMDA channels is reduced by inhibition. Meanwhile residual calcium enters through voltage N-type gated calcium channels due to the back-propagating action potential immediately before the synapse opens, adding to the total calcium concentration. Changes of $[Ca^{2+}]$ again fall into an intermediate range. In scenario four, excitation is blocked by inhibition in the absence of any action potential. Only a limited amount of calcium enters through the NMDA synapse due to the clamping effect of shunting inhibition. Changes of $[Ca^{2+}]$ are low.

As we mentioned earlier, the proper action for scenario one is to increase the weight of the excitatory synapse. Changes of $[Ca^{2+}]$ in this case are high. The proper action for scenario two and three is to decrease the synaptic weight. Changes of $[Ca^{2+}]$ in these cases are medium. The proper action for scenario four is to keep the synaptic weight unchanged. Changes of $[Ca^{2+}]$ are low. In order to link the synaptic weight change with maximum calcium exposure, we map the peak calcium exposures to a BCM type learning curve (Fig. 2-2c). The amplitude of each excitatory synapse from the geniculate input to the target cell is changed in accordance with the maximum calcium concentration just below the synapse reached within 30 ms of synaptic activation. Following the BCM learning curve (Fig. 2-2c), this is associated with the following change in synaptic weight:

$$weightchange = a\sqrt{e^{c(-[Ca^{2+}]-d)} - e^{c(-[Ca^{2+}]-d)} / 2p} + b$$

With a=-2.63, b=1, and c=14. d is a constant that varies continuously between -0.10 and -0.22 as g_{NMDA} varies from 0 to 2 ns. The learning curve is chosen to give a negative output at a medium calcium concentration and a positive one at high calcium concentration (Fig. 2-2c). The parameters a and b are chosen to restrict the function's output to between -1 and 1. The parameter c is a scaling factor that determines the width of the curve and parameter d is a sliding threshold that linearly shifts the curve according to different values of g_{NMDA} (Fig. 2-2d). g_{AMPA} is always set to equal g_{NMDA}.

Instead of implementing a non-linear threshold that will narrow or broaden the learning curve with respect to the average [Ca^{2+}] change during training, we use a linear sliding-threshold to shift the learning curve without changing its shape as shown in Fig. 2-2d. We link the sliding threshold directly to the excitatory synaptic connection strength. This prevents runaway excitation and helps stabilize the synapse (Bienenstock *et al*., 1982; Abbott and Nelson, 2000). The larger the connection strength, the more [Ca^{2+}] accumulates over time, independent of learning scenarios.

2.5 Direction-selective single-unit learning

We first tested our learning rules in a model cell without subunit structures. The connection scheme is shown in Fig. 2-3a. The model initially receives balanced excitatory inputs from both left and right LGN neurons. Two excitatory inputs are mapped into the same compartment on the dendrite. The initial connection strength is 1ns each. Delayed inhibition is fixed at 5 ns and is mapped to a compartment between the excitatory inputs and the soma. During each trial, a bright bar moving to either the left or to the right is randomly presented and the maximum change of [Ca^{2+}] at each excitatory synapse within 30 ms of its opening during the trial is recorded. After each trial, the synaptic weight change is calculated based on the learning curve shown in Fig. 2-2d.

A synapse can only be rewarded if the host cell spikes and this action potential successfully invades the dendrite. Our learning model cannot converge to

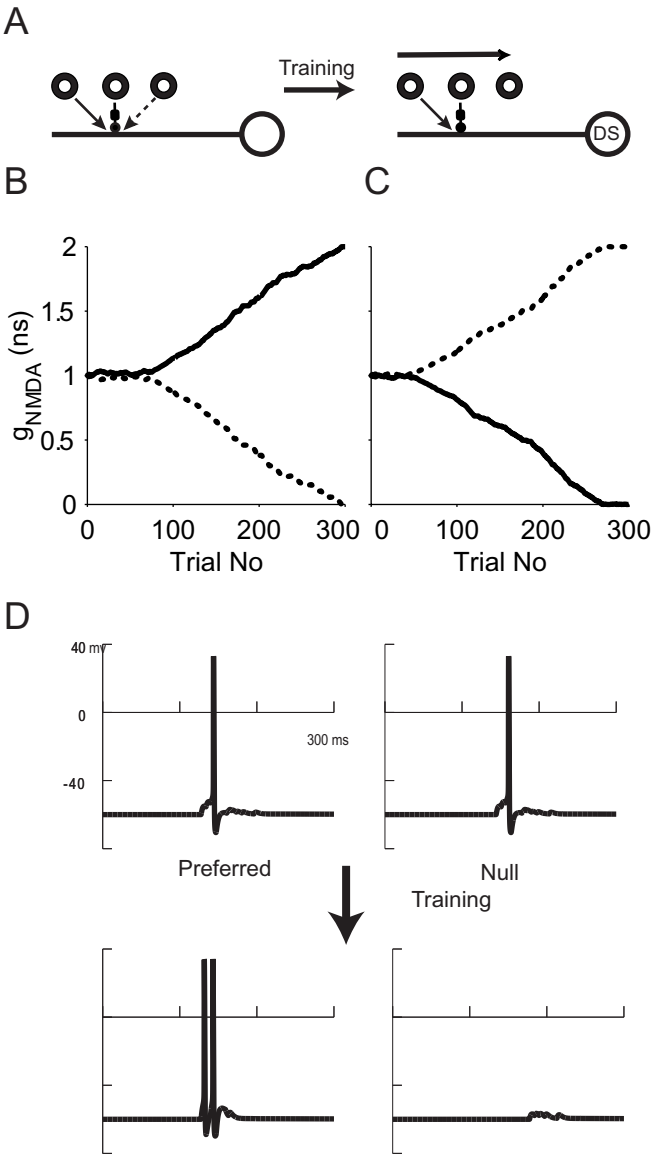

Fig. 2-3. Model cell with a single subunit implementing these rule acquired direction selectivity following unsupervised training (A) The model cell initially receives balanced inputs from the left and right and is not direction selective. After training with random bar movements, the input connection from one side is strengthened while the input connection from the other side is weakened and the model cell becomes direction selective. (B) Synaptic weight changes for motion for the left (solid curve) or right (dashed curve) input during one simulation run. Learning step size is 0.01ns. (C) A different simulation run. The model cell learns to respond to leftward motion only after training. (D) The model cell's response to a bright bar moving at 10^{o}/s across its receptive field before and after training.

direction selectivity if none of the excitatory inputs is strong enough to drive the cell to spike. Therefore, we need to impose a "competition" rule to control the model's excitability. We implemented this by holding the total excitatory connection strength over each local dendrite constant during simulations. This rule is of the "subtraction" type (Abbott and Nelson, 2000); that is, after each trial, half of the value of the synaptic weight above or below the total connection strength is subtracted from or added to both excitatory synapses. If the two excitatory synaptic weights are g_{e1} and g_{e2}, the rule specifies $g_{e1\ new} = g_{e1\ old} - (g_{e1\ old} + g_{e2\ old} - 2\ ns)/2$ (for details see Chapter 3). This competition rule prevents both inputs from slipping to zero. We assume there is no initial bias and the model cell receives balanced input from the left and the right. The outcome is dependent on the training sequence. The synaptic weight changes for both inputs during a simulation run that lasted 300 trials are shown in Fig. 2-3b. Before training, the model cell responds equally for motion in either direction (Fig. 2-3d). During the initial training period, if a rightward moving bar is present, the left excitatory synapse opens first and causes the host cell to spike (scenario one for the left synapse). Then the inhibitory synapse opens and blocks the excitatory input from the right excitatory synapse (scenario three for this synapse). After the trial, the left connection is strengthened and the right one weakened. If a leftward moving bar is shown to the model, the right synapse opens first and causes the model cell to spike (scenario one). Then the inhibitory synapse opens and blocks excitation from the left excitatory input (scenario three). After the trial, the right connection is strengthened and the left weakened. If the training regime

consisted of alternating left and right stimuli, we would expect the synaptic strengths of both sides to oscillate within a range close to the learning step size, but never converge. However, a random training sequence contains consecutive left or right trials and thus causes the oscillation to be larger than one learning step. The longer the training sequence, the larger the oscillation we can expect the model to encounter. Once the oscillation reaches a large enough value such that the connection strength of one excitatory input, say the right input, drops below a value that is enough to elicit a somatic spike, the oscillation stops. Now during its preferred direction motion, a bar moving from the right to left, its weight is decreased according to the scenario two instead of being increased according to scenario one. The right input thus enters a downward spiral and gradually decreases its weight to zero while its counter part, the left input gradually increases its weight to the maximum allowed value. In the simulation shown in Fig. 2-3b, this transition occurs around 80 trials. After training, only the excitatory input to the left side of inhibition remains. The cell acquired direction selectivity for rightward motion, with DI = 1 (Fig. 2-3d). Fig. 2-3c shows another simulation run during which the right excitatory input cell won the competition and the prefer direction of motion is reversed. We ran 100 simulations with a 0.032 ns learning step size, during all of which the model cell converged to a DS cell within 200 trials (in 52 out of these 100 the preferred direction was rightward). An index of direction selectivity (DI) is computed as (preferred direction response – null direction response) / (preferred direction response + null direction response). DI values close to zero indicate a lack of direction selectivity, while the maximal

extent of selectivity yields DI = 1. In all above cases, the model cell reached DI=1 after training.

2.6 Direction-selective multiple subunits learning

How can our learning rule assure that direction selectivity in different dendritic subunits of the host neuron is the same? To answer this question, we tested our DS learning rule in a model cell with four direction-selective subunits on its dendrites. The model connection scheme is shown in Fig 2-4a. Each of the middle four LGN cells (1-4) provides delayed inhibitory input to one dendrite (1-4 from the left) of the model cell. LGN cells 0-3 each provides a left excitatory input to dendrite 1-4 respectively. We refer to this group as the left input connection group. LGN cells 2-5 each provide a right excitatory input to dendrite 1-4 respectively. We refer to this group as the right input connection group and to the connections within a group as “friends” and the connections between groups as “competitors”. The model cell initially has four potential DS subunits on four of its eight dendrites. The learning goal is to have all members within one group out-compete their competitors after training. If the four subunits were completely independent and all received the exact same sequence of visual stimuli, we would expect them to converge to the same direction selectivity. Unfortunately, neither of these two conditions is true. Although at each trial the same moving bar is presented to each subunit, the exact timing of the bar reaching the receptive field of each geniculate cell is different. Both NMDA and GABA synapses have long off ramps. Their late currents can cause differences in the

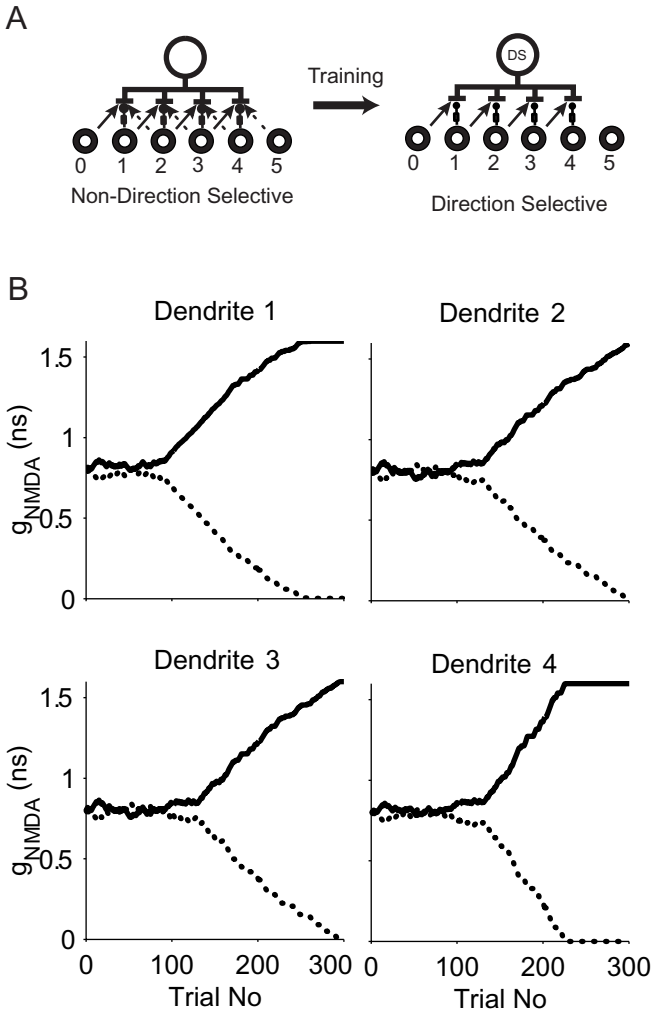

Fig. 2-4. The model with four DS subunits after unsupervised training with a balanced initial setting. (A) All four dendrites initially received balanced excitatory inputs. After training with random bar movements, the input connection from one side is strengthened while the input connection from the other side is weakened. Due to coupling among dendrites and the local nature of shunting inhibition, all subunits are selective for the same direction of motion. (B) Synaptic weight changes for the left (solid curves) and right excitatory inputs (dashed curves) at each dendrite during one simulation run. Learning step size is 0.003ns. The cell learns to respond to the rightward motion only after training.

status of subunits. The shunting inhibition mostly affects local connections but it also has a more global effect. The same curve as in the single-unit learning case is used in our simulations without being tailored to each subunit. These differences can cause different branches to learn to respond to opposite directions of motion. The model cell is thus not direction-selective. The problem can be solved if there are internal links between group members and competition between the groups. The links between group members indeed exist in our model through somatic spikes. For example, the LGN cell 1's input connection to the dendrite 2 and the LGN cell 2's input connection to the dendrite 3 belong to the same left input group. In a rightward movement trial, a late spike caused by LGN cell 1's input will also be counted as a spike caused by LGN cell 2 given the overlap of their input time courses. In case LGN cell 2's connection strength drops below the transition threshold, this would "rescue" it from scenario two to scenario one. The same spike, however, will not help the LGN cell 2's connection to dendrite 1, which belongs to the right input group. The inhibitory input to dendrite 1 always opens before LGN cell 2 on dendrite 1 during a rightward movement trial, and thus blocks any back-propagating spike from reaching LGN cell 2's connection point. So this "link forward" effect only benefits group friends but not competitors. A similar "link backward" effect also exists. An early spike caused by LGN cell 2 will also be registered as LGN cell 1's own spike if it happens within 30 ms of LGN cell 1's firing. The "rescue" effort only occurs during the preferred direction movement while there are no linkages among group members during the null direction movement. If a group member is stuck

far away from the divergent point, long consecutive same direction trials are required to increase its connection strength above the spiking threshold. To speed up convergence, we imposed an additional “majority” rule. We linearly scaled the learning step size of each trial with respect to the total number of action potentials generated at the soma during that trial. In such a setting, a group member is increased more in its preferred direction and decreased less in its null direction, once its group responds with more spikes than the other one. This creates a direct competition between groups and thus facilitates convergence.

Initially, the model cell receives balanced inputs at each of its dendrites as shown in Fig. 2-4b and is not direction-selective. After 300 trials training, the entire left input group wins over the right input group and the model cell develops four DS subunits on its dendrites sensitive to rightward motion. Each direction-selective subunit reaches its divergent point at different trials and goes through different weight change paths. Note initially, LGN cell 2 provides excitatory input to both dendrite 1 and 3. After training, only the connection to dendrite 3 remains. Therefore the learning process is indeed branch specific. We carried out 100 simulations with a 0.032 ns learning step size, which was increased linearly with the number of action potentials generated according to our majority rule. The model cell converged to achieve uniform DS subunit structures within 200 trials in all cases. DI equals 1 in all cases. The model converged to a right direction-selective unit during 47 simulation runs and to a left direction-selective unit during

the remaining runs.

In the above stimulations, all dendrites receive balanced input from each side. We further tested our learning model in a “random start” configuration. The total input connection strength to a dendrite is still fixed but the relative contribution from the left input cell and from the right input cell is randomly assigned. Such a simulation run is shown in Fig. 2-5a. After 200 training trials, the right input group won at dendrite one while the left input group was leading at dendrite three and four. The competitions between the two groups were about even at dendrite two. Because of the “majority” rule we imposed and the “link forward” and “link backward” effect, the left input group finally increased its “friends’” connection strength at dendrite one and two and destabilized its “competitors”. After 1000 training trials, the model cell developed four rightward motion selective subunits. To test the stability of our learning model in the random start condition, we ran 10 simulations, each at 4 different learning step sizes: 0.1 ns, 0.032 ns, 0.01 ns and 0.003 ns. Training periods are 100 trials, 500 trials, 1000 trials and 2000 trials respectively. DI converged to 1 for all conditions. Another possible scenario during development is that initially all the excitatory geniculate inputs to the V1 cell are very weak and not enough to drive the cell to spike. Gradually, as the input connections are strengthened, the cell starts to spike and competition among input synapses begin. We tested our learning model in such a “developmental” configuration. Initially all connection weight are zero. The weights are increased gradually because of the “competition” rule we imposed.

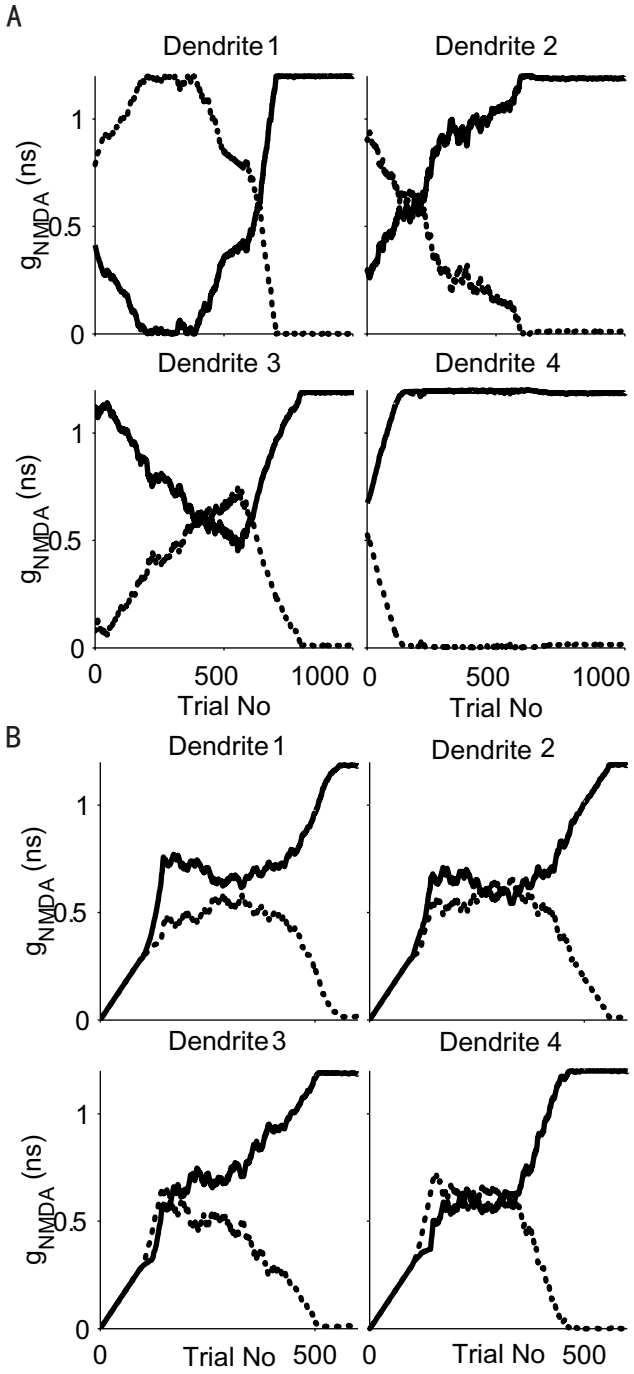

Fig. 2-5. The model with four DS subunits after unsupervised training under the "random start" setting and "development" setting. (A) All four dendrites initially received random excitatory inputs. The total excitatory connection strength at each branch is set to be 1.2ns. Synaptic weight changes for the left and the right excitatory inputs. Learning step size is 0.003ns. The model cell learns to respond to rightward motion only after training. (B) The excitatory input connection strengths to the model are initially zero. Synaptic weight changes for the left and right excitatory inputs. Learning step size is 0.003ns. The model cell learns to respond to rightward motion only after training.

The total excitatory connection strength to a dendrite is below the desired value, so at each trial, both inputs are increased by the maximum allowed learning step size (Fig. 2-5b). During the initial 100 trials, there are no spikes and all the input connections increase at each trial. Once the input connection strength reaches about 0.3 ns, the model cell starts to spike and the connection strength of different input groups starts to diverge. After 600 training trials, the model cell develops four rightward motion selective subunits. To test the stability of our learning model in the development condition, we carried out 10 simulations each at 4 different learning step sizes. The model cell converged to DI=1 under all conditions.

2.7 Discussion

Our learning scheme makes several testable predictions. Firstly, intra-cellular calcium concentration changes should correlate with LTP (high calcium concentration increase) and LDP (moderate calcium concentration increase) at the synaptic level. Postsynaptic calcium elevation experiments using photolysis of caged EGTA in CA1 hippocampal slices suggest such a relationship (Yang and Zucker, 1999). Shunting inhibition can be mimicked using the dynamic clamp (Chance and Reyes, 2002). This, together with two-photon calcium imaging, can be used to determine if shunting inhibition indeed can direct local synaptic modifications via local calcium concentration change. Secondly, our "competition" rule suggests neurons with direction-selective subunit structures on its dendrites have the ability to control independently the total excitatory input

connection strengths to each of their major dendrites. Evidence for such a mechanism, albeit operating at the whole cell level, has been provided by Turrigiano and Nelson (1998). Local protein synthesis (reviewed by Schuman, 1997) may play an important part in this process. In addition, we predict that cats reared in an environment with little motion in one particular direction---achieved by having the animals wear LCD goggles---will show a deficit in direction-selective cells tuned for that direction relative to the opposite direction of motion. In our learning model, random motion plays a key role in breaking the balance between the left and right input cells. Symmetry could also be broken by a bias in the initial connection strength between the left and right input.

Our learning scheme makes a few key assumptions. Delayed inhibition is of the shunting type, pre-connected to fulfilling the on-path condition, and fixed. The training stimuli move at a speed that matches the delay factor of the inhibition. Shunting inhibition is crucial to our multiple subunits learning model in achieving the branch specific veto of excitation and the branch specific blocking of back propagating spikes. We compared the single-unit and the multiple subunits model with four, six and eight subunits in the standard case with hyperpolarizing inhibition with E_{GABA}=-60mV - 90mV (model cell's resting potential is -60mV). The single-unit learning is not dependent on the shunting inhibition while the more subunits the learning model has, the more it relies on shunting inhibition (for details see Chapter Five).

In our simulations, the inhibitory connection strength is fixed. However, the strength of inhibition close to the cell body may be related to calcium levels there, as recently considered (Soto-Trevino *et al*., 2001). We implemented such a global inhibitory learning scheme together with our local excitatory learning mechanism and achieved differential excitation-inhibition learning (for details see Chapter Six).

Fast rising calcium concentration changes in dendritic spine mediated by action potential and long sustained rising mediated by synaptic inputs have been observed in calcium imaging experiments (Sabatini and Svoboda, 2002). The measured calcium decay constant is 12 ms at spines and 15 ms at small dendrites. We used a single decay constant of 15 ms for both calcium sources and assumed instantaneous dendrite-to-spine diffusion. We have no evidence to suggest that a more sophisticated treatment of calcium dynamics will change our conclusion appreciably. Experimental evidence suggests voltage-gated calcium channels exist in spines, while little calcium diffuses between the spine and the dendritic shaft in either directions (Sabatini and Svoboda, 2002; for a dissent view see Majewska *et al*., 2000a; Majewska *et al*., 2000b; Holthoff *et al*., 2002). Such a scheme is computationally equivalent to our model setting given we used instantaneous dendrite to spine uni-direction calcium diffusion and single compartment for the spine and the dendritic shaft. We choose the N-type voltage gated calcium channel to have a voltage sensitive calcium dynamics different from calcium flowing through NMDA channels. The high threshold L type voltage

gated calcium channels should also serve our purpose.

We exploit calcium gain-control mechanisms which dynamically shift the learning curve according to the average, local activity level. The key to the stability of the original BCM learning rule (Bienenstock *et al.*, 1982) is a non-linear threshold that decreases and increases faster than the average response. Such a sliding threshold control requires that the tuning curve be narrowed for small responses and broadened for large responses. For the sake of simplicity, we implemented a linear sliding of the learning curve without changing its shape. The linear sliding can be implemented in many ways, such as by an increased calcium pump within the spine with respect to time-averaged calcium exposure or adaptation of calcium-dependent enzyme activities. Both the duration and the amplitude of post-synaptic calcium concentration have been shown to affect LTP and LTD (Yang and Zucker, 1999). Brief and large postsynaptic calcium concentration changes lead to LTP while sustained and moderate changes cause LTD. However, brief and moderate calcium concentration change can lead to either LTP or LTD. A calcium gain-control mechanism/sliding learning threshold can explain such phenomena. Sustained calcium concentration elevation may shift the learning curve as well as the LTD/LTP transition threshold toward high calcium concentration and thus increase the probability of LTD formation.

Spike-time-dependent plasticity (STDP) is a temporal asymmetry Hebbian learning rule. The synaptic weight change depends on the relative timing of the

pre-synaptic input and the back-propagating spike. STDP was shown in a modeling study to automatically balance synaptic strengths and reduce the spiking latency of the post-synaptic neuron (Song *et al*., 2000). A network of neocortical neurons implementing STDP developed direction selectivity after training (Rao and Sejnowski, 2000; Rao and Sejnowski, 2001). Our learning rules are different from the "prediction and sequence learning" mechanism (Montague and Sejnowski, 1994; Montague *et al*., 1995; Markram, 1997). In our learning scenario one, the excitatory connection is increased if there are back-propagating spikes within a certain period following synaptic activation; while in learning scenario three, the excitatory connection is decreased if there is a spike a few milliseconds before its opening and the back-propagating spike is clamped by inhibition at opening. These fit into the general framework of the STDP with the exception that our learning rules not only take the temporal sequence between the input and the output into account but also the states of local inhibition. The difference is critical for the learning of branch-specific DS subunits.

We assume the direction selectivity of V1 cells is derived from feed-forward connections only. The learning is also restricted to feed-forward connection. There are extensive feedback interactions among V1 cells and these feedback currents are likely to be important for sharpening directional tuning (Douglas *et al.*, 1995; Maex and Orban, 1996). It will be important to see if the same learning principle can be used to establish mutual excitation between cells selective to the same direction of motion and mutual inhibition among cells tuned to opposing

directions of motion. Such network learning may be used to generate two direction-selective cell groups with roughly equal members during the development process.

Chapter Three

A Detailed View of Critical Parameters and Constraints That Affect the Learning Model

3.1. Introduction

We described a local synaptic learning model for local synaptic interactions between excitation and shunting inhibitions in the chapter two. Here we take a detailed look at several important model parameters and additional constrains that affect the stability of the learning model and its convergence speed. The first such parameter is the learning step size, which directly affects the number of training trials required to reach direction selectivity. The smaller the learning step size, the longer the required training period. The subtractive type of "competition" rule affects the stability of both the single-unit learning model and the multi-subunits learning model. It helps to control the post-synaptic cell's excitability. "Linkages" between subunits are needed to have all subunits converge to the same direction selectivity. The "link-back" and "link-forward" effect connect subunits through back propagating spikes. The "majority" rule facilitates the quick convergence of subunits. Here we compare the simulations with and without such a learning rule to show its effect on the learning model.

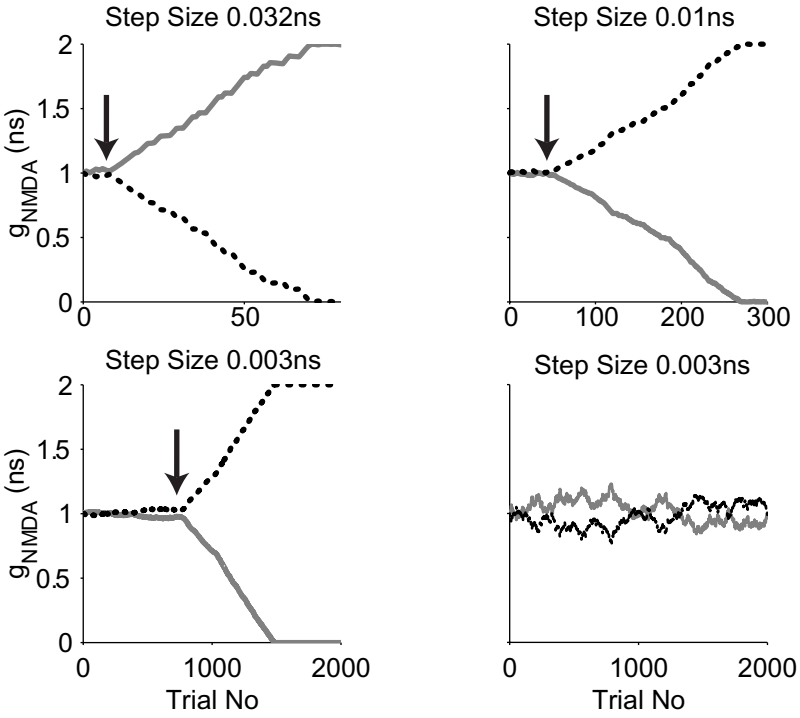

Fig. 3-1. The learning step size determines the number of trials required for the model to reach the divergent point. At 0.032ns, Less than 10 trials are required to reach the divergent point (solid arrow). Around 50 trials are required if the step size is decreased to 0.01ns. Two simulation runs are shown here with a step size of 0.003ns. One reaches the divergent point at around 800 trials. The other fails to reach the divergent point even after 2000 trials training. Solid (Dotted) curve: Synaptic weight changes for the left (right) input cell during one simulation run.

The inhibitory input connection strengths are fixed in all previously described simulations. In section 3.6, we propose a simply global inhibitory synapse learning scheme that links the average spikes at soma with the inhibitory synaptic connection strength. The goal of inhibitory learning is to achieve a targeted average spike number given random direction motion stimuli. We tested the inhibitory learning rule in simulations together with our excitatory synapse learning rule. Our results show such a scheme can achieve excitation-inhibition differential learning.

3.2 The model convergent speed and learning step size

We tested the relationship between the learning step size and the model convergent speed (Fig. 3-1). In our learning model, the synaptic weight change at each step is calculated from the learning curve and then scaled with learning step size set for the simulation. The larger the learning step size, the larger synaptic weight change after each trial. At 0.032ns (maximum allowed conductance is 2ns), the learning model reaches divergent point with 10 trials. About 60 trials are required to reach the divergent point when the learning step is decreased to 0.01ns. Two simulations at learning step size 0.003ns are shown in Figs. 3-1 C and D. The model cell reaches the divergent point around 800 trials in one simulation, but fails to converge within 2000 trials in the other one. In our learning model, the oscillation of synaptic weights is caused by the incoming stimuli sequence. The smaller the learning size, the more consecutive one-direction stimuli needed to cause a large enough oscillation that can push both

inputs to the divergent point. If our learning curve were a step function, such that a synapse were increased or decreased by exactly one learning step size, we would expect the number of consecutive same direction trials needed to be

$N = (g_{\text{initial synaptic weight}} - g_{\text{divergent point}})/\text{step size}$

2^N random trials are thus required to reach the divergent point. The actual situation in our model is more complicated because we use a continuous BCM type learning curve. The synaptic weight changes at each trial are not exactly one learning step, but we would expect the number of training trials needed to reach the divergent point still scales non-linearly with respect to the learning step size. For simulations shown in Fig. 3-1, 10, 60, 800 trials are needed to reach the divergent point for learning step size 0.032ns, 0.01ns, 0.003ns, not far from the 8-fold (2^3) increase in trial length for the every 3 fold decrease in the step size. The learning model converges much faster (only N trials are required), if the stimuli are same direction motions. The bursting spiking waves discovered in developing mammalian retina (Meister *et al*, 1991; Wong *et al*, 1993) may be equivalent to such same direction stimuli.

3.3 The "competition" rule

The Hebbian learning rule is a positive feedback learning rule. Correlated input connections are increased and uncorrelated input connections are decreased during the training process. Such a learning rule causes fluctuations in the excitability of the post synaptic cell. Various constraints have been proposed to prevent the cell from growing overactive or slipping into non-firing territory. We

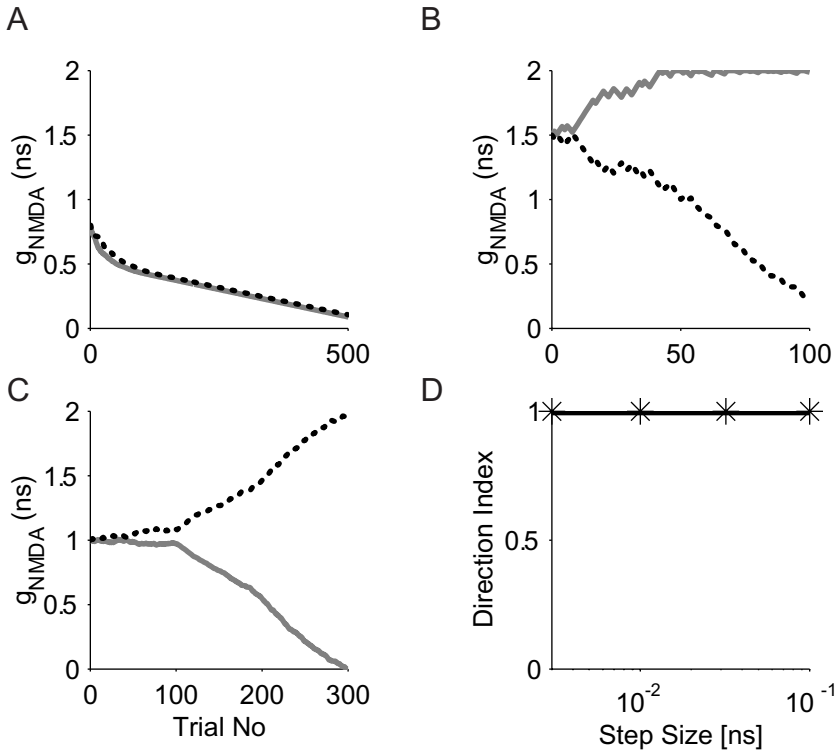

Fig. 3-2. The single-unit learning model's response without the competition rule. A. Synaptic weight changes for the left input cell (solid curve) and the right input cell (dotted curve) during one simulation run that both initial connection strengths were below the spiking threshold. Both connections slip to zero after training. B. Synaptic weight changes during a simulation run that both initial connection strengths are well above the spiking threshold. The model cell is direction-selective after training. C. Synaptic weight changes during a simulation run that both initial connection strengths are just above the spiking threshold. Model cell is direction-selective after training. D. Average DI values of the model cell of 10 simulations each at 4 different learning step size. The initial condition is the same as in C.

use a subtractive type constraint in our learning model. In each trial, the total excitatory input connection strength to each dendrite is held constant. Half the amount that is over/under the targeted value after learning is then subtracted from/added to all synapses on that dendrite. This has the benefit of creating a direct competition between synapses on a dendrite while keeping the total excitability of the model cell constant during simulations.

We first investigated the "competition" rule's effect on the single-unit learning model. Synaptic weight changes for several simulation runs without imposing such a "competition" rule are shown in Fig. 3-2. In our learning model, a synapse can only be rewarded if there is a back propagating spike. Simulations show both connections gradually decrease toward zero during training if neither connection's initial strength is large enough to cause a spike (Fig. 3-2A). If both initial connections are well above the spiking threshold, the learning model is stable and became direction-selective after training as shown in Fig. 3-2B. Although we did not impose the "competition" rule in this case, we still limited the highest synaptic conductance a synapse can reach to 2ns and the lowest to zero. Another simulation run with both initial connection strengths just above the spiking threshold is shown in Fig. 3-2C. To test the stability of our learning model in the same condition as Fig. 3-2C, that is, with initial values strong enough to elicit spikes, we ran 10 simulations each at 4 different learning step sizes: 0.1ns, 0.032 ns, 0.01 ns and 0.003 ns. The training length for each step size was 100 trials, 500 trials, 1000 trials, and 2000 trials respectively. After the training was

completed, a leftward movement trial and a rightward movement trial were presented to the model cell and the resulting spike numbers were recorded. The cell converged to DI=1 in all trials as shown in Fig. 3-2D.

We then tested our multi-subunits learning model without imposing the "competition" rule. The challenge facing the multi-subunits model is to coordinate the learning between subunits. We used the "random start" initial condition to put different subunits into different domain of direction selectivity initially and then tested the model's ability to converge without the "competition" rule. In most cases, the model cell failed to become direction-selective after training as shown in Fig. 3-3A. Note again, in the multi-subunits model, the competition rule was imposed onto each dendrite. We ran 10 simulations each at 4 different learning step sizes: 0.1 ns, 0.032 ns, 0.01 ns and 0.003 ns. Model cell's average DI was close to 0 after trainings. Synaptic weight changes for the left input cells and the right input cells at each dendrite during one simulation run are shown in Fig. 3-3B. Initially, dendrite one is not direction-selective. Dendrite two and three are rightward motion selective while dendrite four is leftward motion selective. After training, connections to dendrite one and four all drop below the spiking threshold while connections to dendrite two and three all reaches maximum. The model cell is thus not direction-selective.

Our results suggest both the single-unit and the multi-subunits learning model require the "competition" rule for stability. The single-unit model can converge

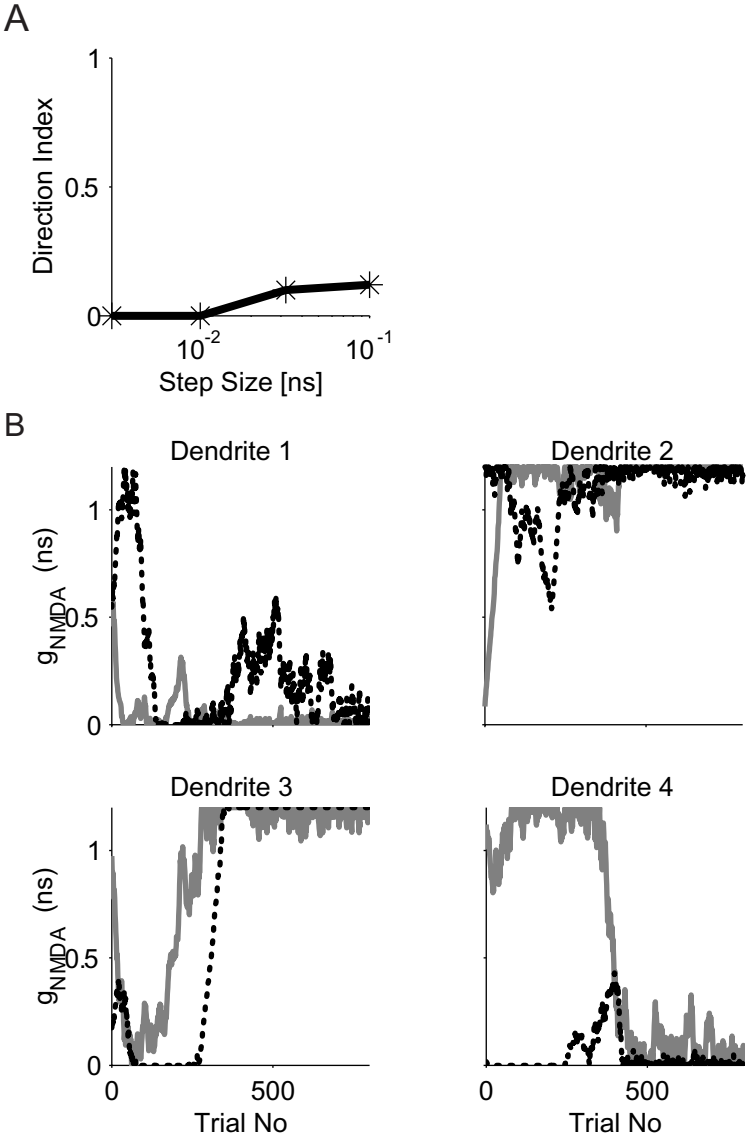

Fig. 3-3. The multi-subunits learning model's response without the competition rule. A. Average DI values of the model cell of 10 simulations each at 4 different learning step size. The initial input connection strengths are random. The learning model converges to low DI values after training without the competition rule. B. Synaptic weight changes for the left input cells (solid curves) and the right input cells (dotted curves) at each dendrite during one simulation run. Learning step size is 0.01ns. The model cell is not direction-selective after learning.

without the “competition” rule if either initial connection strength is above the spiking threshold but not if both initial connections are weak. This is expected given that we do not implement a sliding threshold that scales non-linearly with respect to the average response of the cell as in the original BCM model. Our linear sliding threshold and the “competition” constraints are easy for real neurons to implement than a non-linear sliding threshold.

3.4 Linkages between subunits

The model cell initially has four potential DS subunits on its dendrites. The learning goal is to have all members of one group win over their competitors after training. If the four subunits are completely independent, all receive the exact same sequence of visual stimuli and have the same initial condition, we would expect them to converge to the same direction selectivity. Unfortunately, neither of these conditions is true. Although at each trial the same moving bar is presented to each subunit, the exact timing of the bar reaching the receptive field of each excitatory input is different. Both the NMDA synapses and the GABA synapses we use in simulations have long off ramps. Their late currents cause difference in the status of subunits. The shunting inhibition mostly affects local connections but it also had some global effects. We do not tailor our learning curve to each subunit but rather use the same curve as in the single-unit learning case. In addition, we would expect different subunits to receive different stimuli in a natural setting. Therefore the difference in subunits can cause different branches to learn to be selective to different directions and the model cell itself is

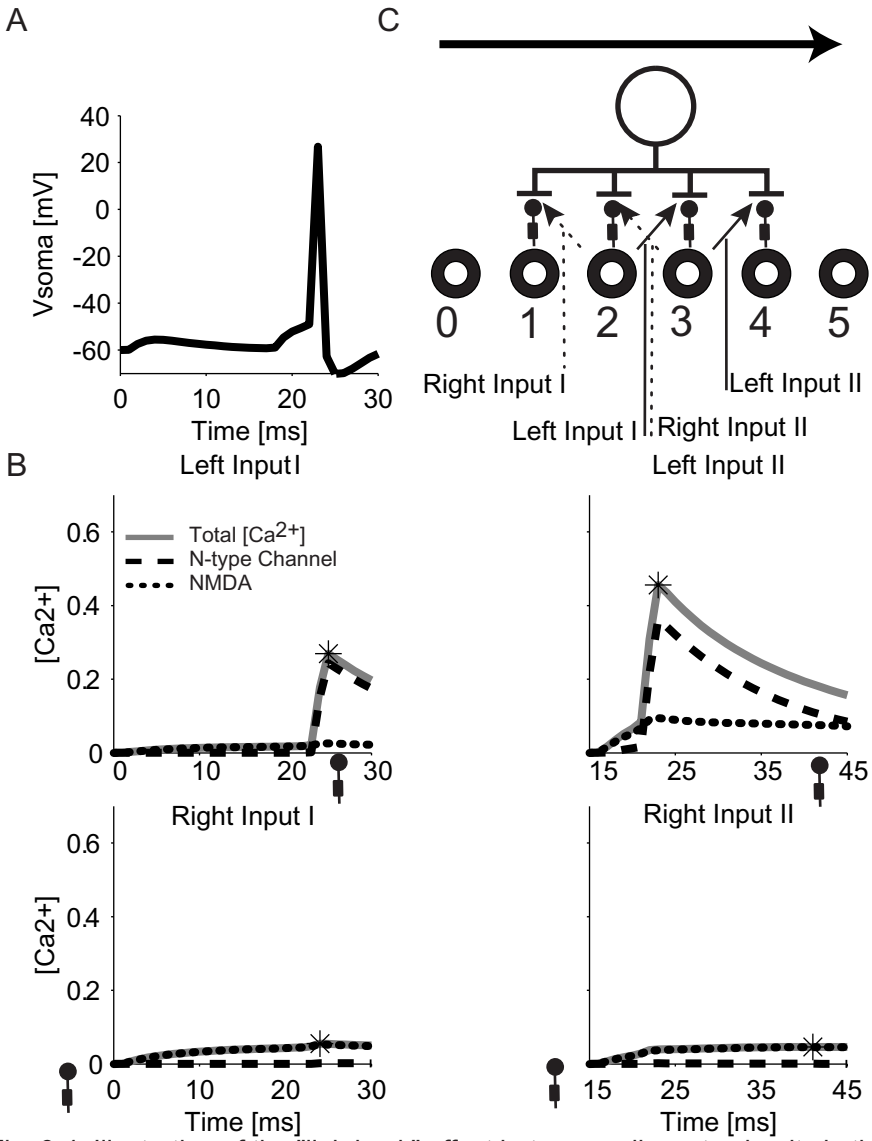

Fig. 3-4. Illustration of the "link-back" effect between adjacent subunits in the same input group A. Somatic voltage change. B. Local calcium concentration changes within 30 ms of the excitatory synapse firing during a rightward motion trial for all four input connections. Solid line: Total calcium concentration. Dashed line: Calcium concentration buildups due to calcium entering through N-type voltage gated calcium channels. Dotted line: Calcium concentration buildups due to calcium entering through NMDA synapses. LGN cell 2's excitatory input occurs at time 0. LGN cell 3's excitatory input occurs 15ms later. The timing of branch specific inhibitions is marked with closed circle. Calcium concentrations are in arbitrary unit. The peak calcium concentration is marked in each case. Left input I is not strong enough to cause a spike initially while left input II is. The spike due to left input II causes left input I to increase its connection strength without affecting all the connections in the right input group. C. A schematic drawing of the input connection to the model. Left input I refers to the LGN cell 2's connection to dendrite 3. Right input I refers to the LGN cell 2's connection to dendrite 1. Left input II refers to the LGN cell 3's connection to dendrite 4. Right input II refers to the LGN cell 3's connection to dendrite 2.

not direction-selective. The problem would be solved if there are internal links between group members and there is competition between the groups. The link between group members indeed exists in our model through back-propagating spikes. We first considered the "link back" effect as show in Fig. 3-4. The LGN cell 2's input connection to the dendrite 3 (left input I) and the LGN cell 3's input connection to the dendrite 4 (left input II) belong to the same "left input group". LGN cell 2's input connection to dendrite 1 (right input I) and LGN cell 3's input connection to dendrite 2 (right input II) belong to the same "right input group" (Fig 3-4A). Synaptic calcium concentration changes during a rightward movement trial for all four synapses are shown in Fig. 3-4B. LGN cell 2 spikes at time zero while LGN cell 3 spikes 15ms later. Left input 1's connection strength is below the spiking threshold. In a rightward movement trial, this corresponds to scenario 2 for the left input I: no inhibition, no back propagating spike and the connection strength should be further weakened after the trial. However, 15 ms after left input I's opening, left input II opens. Left input II causes a back propagating spike which also propagates back close to left input I's connection site (dendrite 3). This switches left input I from scenario 2 to scenario 1. The connection strength of left input I increases after the trial instead of decreases. The same spike, however, does not affect right input I and right input II. The inhibitory synapses on dendrite 1 and 2 opens before those two right input connections and thus blocks the back-propagating spike. So this "link forward" effect only benefits group friends but not competitors. Such link effects only exist between adjacent

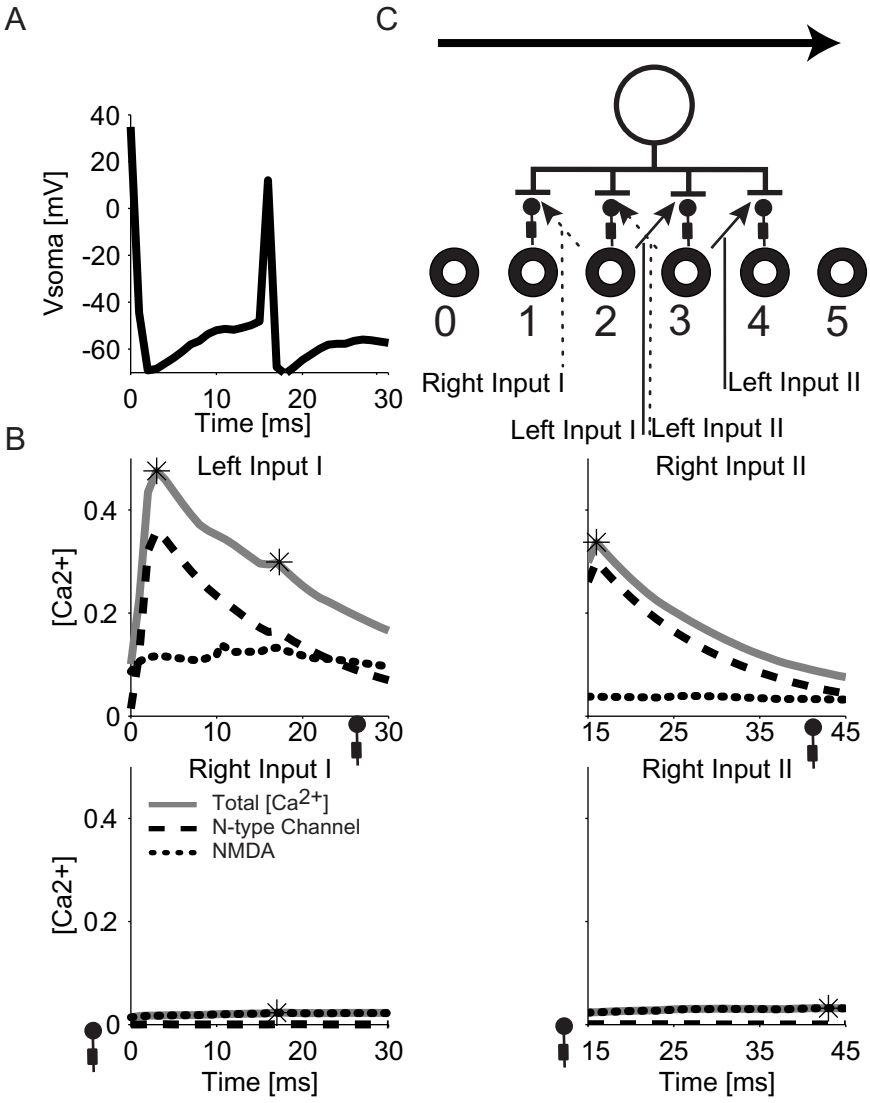

Fig. 3-5. Illustration of the "link-forward" effect between adjacent subunits in the same input group. A. Somatic voltage change. B. Local calcium concentration changes within 30 ms of excitatory synapse firing during a rightward motion trial for all four input connections. Solid line: Total calcium concentration. Dashed line: Calcium concentration buildups due to calcium entering through N-type voltage gated calcium channels. Dotted line: Calcium concentration buildups due to calcium entering through NMDA synapses. LGN cell 2's excitatory input occurs at time 0. LGN cell 3's excitatory input occurs 15ms later. The timing of branch specific inhibitions is marked with closed circle. Calcium concentrations are in arbitrary units. The peak calcium concentration is marked in each case. Left input II is not strong enough to cause a spike initially while left input I is. The second spike due to left input II causes left input one to increase its connection strength without affection the connections in the right input group. C. A schematic drawing of the input connection to the model. Left input I refers to the LGN cell 2's connection to dendrite 3. Right input I refers to the LGN cell 2's connection to dendrite 1. Left input II refers to the LGN cell 3's connection to dendrite 4. Right input II refers to the LGN cell 3's connection to dendrite 2.

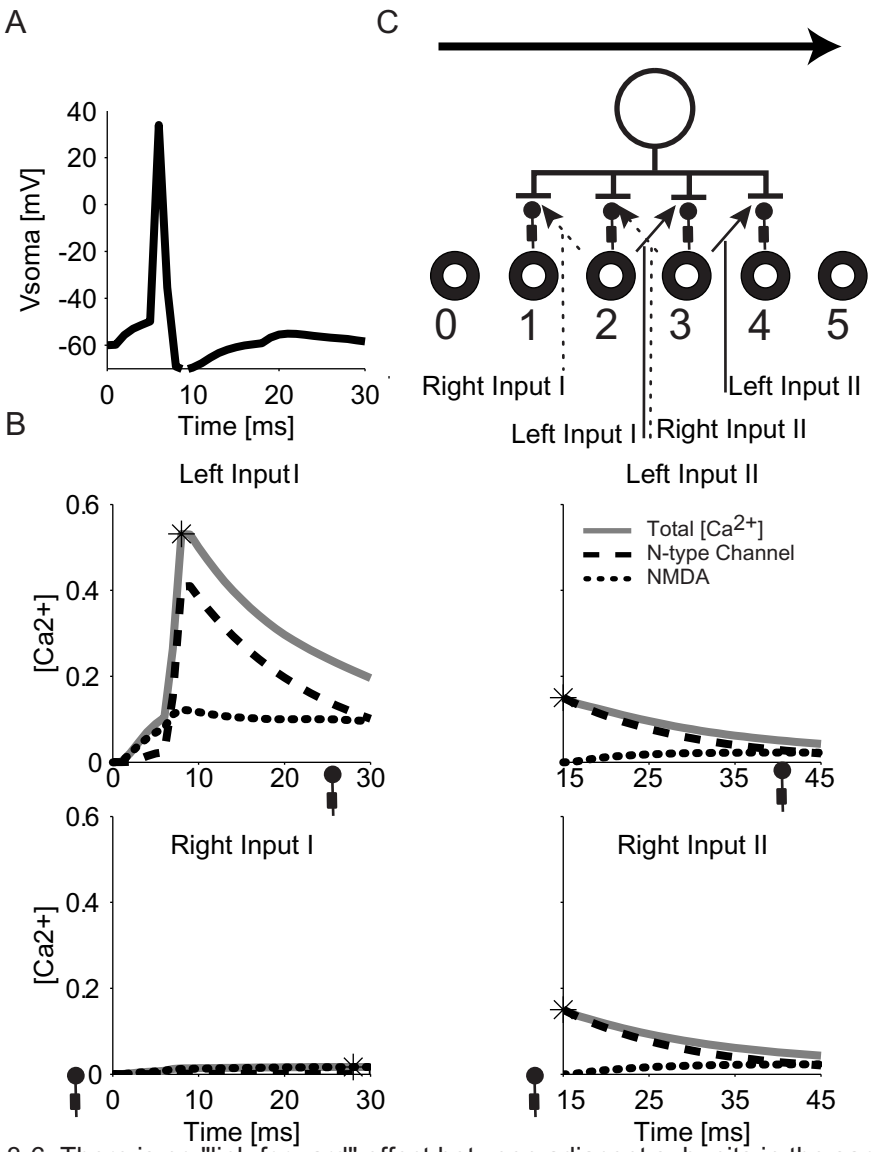

Fig. 3-6. There is no "link-forward" effect between adjacent subunits in the same input group if the LGN input firing rate is not high enough. A. Somatic voltage change. 2. B. Local calcium concentration changes within 30 ms of excitatory synapse firing during a rightward motion trial for all four input connections. Solid line: Total calcium concentration. Dashed line: Calcium concentration buildups due to calcium entering through N-type voltage gated calcium channels. Dotted line: Calcium concentration buildups due to calcium entering through NMDA synapses. LGN cell 2's excitatory input occurs at time 0. LGN cell 3's excitatory input occurs 15ms later. The timing of branch specific inhibitions is marked with closed circle. Calcium concentrations are in arbitrary unit. The peak calcium concentration is marked in each case. Left input II is not strong enough to cause a spike initially while left input I is. The spike due to left input I cannot increase left input II due to the misalignment of both time courses. C. A schematic drawing of the input connection to the model. Left input I refers to the LGN cell 2's connection to dendrite 3. Right input I refers to the LGN cell 2's connection to dendrite 1. Left input II refers to the LGN cell 3's connection to dendrite 4. Right input II refers to the LGN cell 3's connection to dendrite

inputs (adjacent in the visual space) in our model given the various time course settings.

A similar "link forward" effect also exists in our model as shown in Fig. 3-5. In this case the LGN cell's firing rate is elevated to make them spike multiple times during a bar sweep. The connection strength of left input I and left input II are reversed. Left input I now causes the model cell to spike twice during its opening while left input II alone is too weak to cause a spike. During a rightward movement trial, the second spike caused by left input I "rescues" left input II. The spike does not cause either right input I or right input II to increase their connection strength because the inhibitory connections to dendrite 1 and 2 blocks the back-propagating spike. However, if the LGN cell array's firing frequency is held low, the left input I can only cause one spike during its opening. In our model setting, such a spike occurs before left input II's opening and thus can not help increase left input II (Fig. 3-6). In the real case, we expect overlap between each LGN cell's receptive fields. The noise and jitter in spike timing can also help create such a linkage.

3.5 The "majority" rule

The "rescue" effort mentioned above only happens during the preferred direction movement for a group and there are no links between group members during the null direction movement. If a group member is stuck far away from the transition point, it may require long consecutive "same direction" trials to increase its

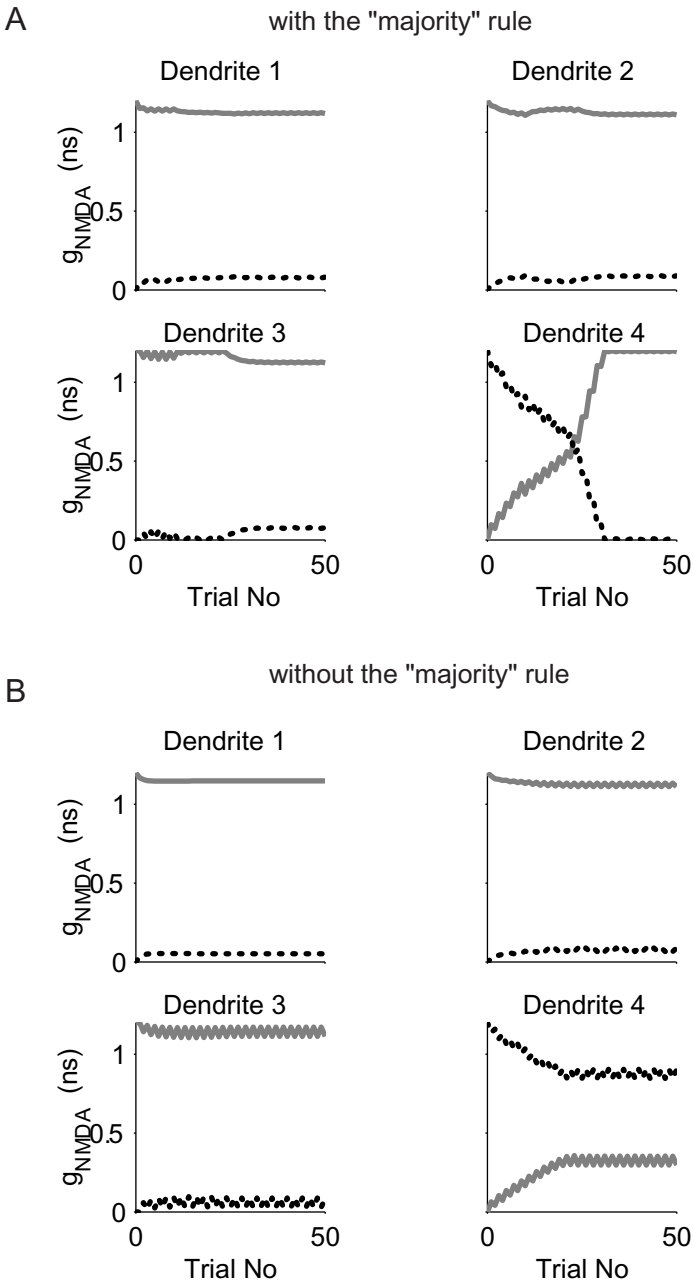

Fig. 3-7. The "majority" rule's effect on the multi-subunits learning model. A. Synaptic weight changes for the left input cells (solid curves) and the right input cells (dotted curves) at each dendrite during one simulation run with the "majority" rule. Subunits on dendrite 1-3 are direction-selective to rightward motion while the subunit on dendrite 4 is direction-selective to leftward motion initially. All subunits converge to the same direction-selective after training with alternating left and right trials. B. A simulation run as shown in A but without the "majority" rule imposed. Dendrite 4 fails to switch to a rightward motion selective unit after training.

connection strength above the spiking threshold. To speed up convergence, we impose an additional "majority" rule. We linearly scale the learning step size of each trial with respect to the total spike numbers of that trial. This creates a direct competition between groups and thus facilitates convergence. The effective learning step size in our model is increased by around four folds when the majority rule is imposed, given the model on average produces three spikes. Fig. 3-7 shows synaptic weight changes for all inputs during two simulation run with (Fig. 3-7A, learning step size 0.025 ns) and without (Fig. 3-7B, learning step size 0.1 ns) the "majority" rule imposed. Initially, dendrites 1-3 are direction-selective to the rightward movement while dendrite 4 is direction-selective to the leftward movement. The learning goal is to have all dendritic subunits converge to the same direction selectivity. The stimuli used in stimulations are alternating left and right moving bars. The subunit on dendrite 4 can not be converted by DS units on dendrites 1-3 without the majority rule. The "rescue" effort during the preferred direction trial (rightward) is canceled by the weight decrease during the null movement trial (leftward). With the "majority" rule, however, dendrite 4 is quickly converted. In this case, the "rescue" effort during the preferred direction is larger (on average four times) than the weight decrease during the null trial because the model cell responds with more spikes during a preferred direction trial and thus has a larger learning step size.

We tested our multi-subunits learning model without imposing the "majority" rule. The challenge facing the multi-subunits model is to coordinate the learning

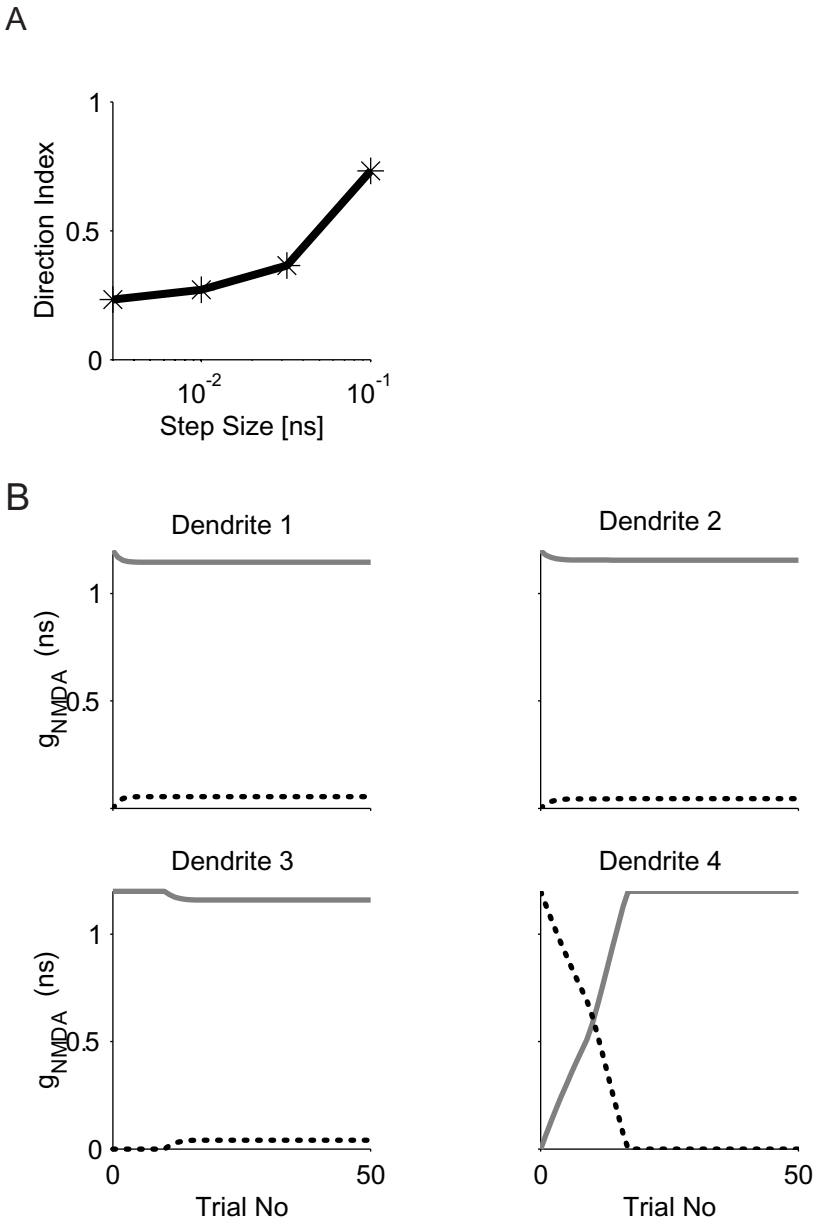

Fig. 3-8. The "majority" rule's effect on the multi-subunits learning model. A. Average DI values of the model cell of 10 simulations each at 4 different learning step size in a "random start" setting. Without the "majority rule", model cell is on average less direction-selective after training. B. Same simulation run without the "majority" rule as in Fig 3-7B except the model is trained with rightward motion stimuli only. All subunits converge to the same direction selectivity.

between subunits. We used the “random start” initial condition to put different subunits into different domains of direction selectivity initially and then tested the model’s ability to converge without the “major” rule. In most cases, the model cell is still direction-selective but the selectivity is less than 1 (Fig. 3-8A).

The “majority” rule greatly speeds up the model’s convergence, but in theory it is not required if the training is long enough. Fig. 3-8B shows a simulation with the same condition as the simulation shown in Fig. 3-7B but using only single direction movements as the training stimuli. In such a case, dendrite 4 is converted to a rightward motion selective unit. It is interesting to see if such a dynamic scaling of learning step size exists in nature. Without the majority rule, the more subunits the neuron has, the longer “single direction training” sequences required to converge all of the units to be selective to the same direction of motion.

3.6 Differential excitation-inhibition learning

Up to now, we fix the inhibitory connection strength throughout our simulations. Here we investigate the possibility of relaxing this constraint and let inhibitory synapses converge to their own optimal connection strength. Given the fact that all inhibitory synaptic connection strengths are the same on all dendrites, we do not need a local, dendrite-specific, learning rule. Neither has it to be a direction-selective one, since the excitatory learning rules we proposed has already accomplished the purpose.

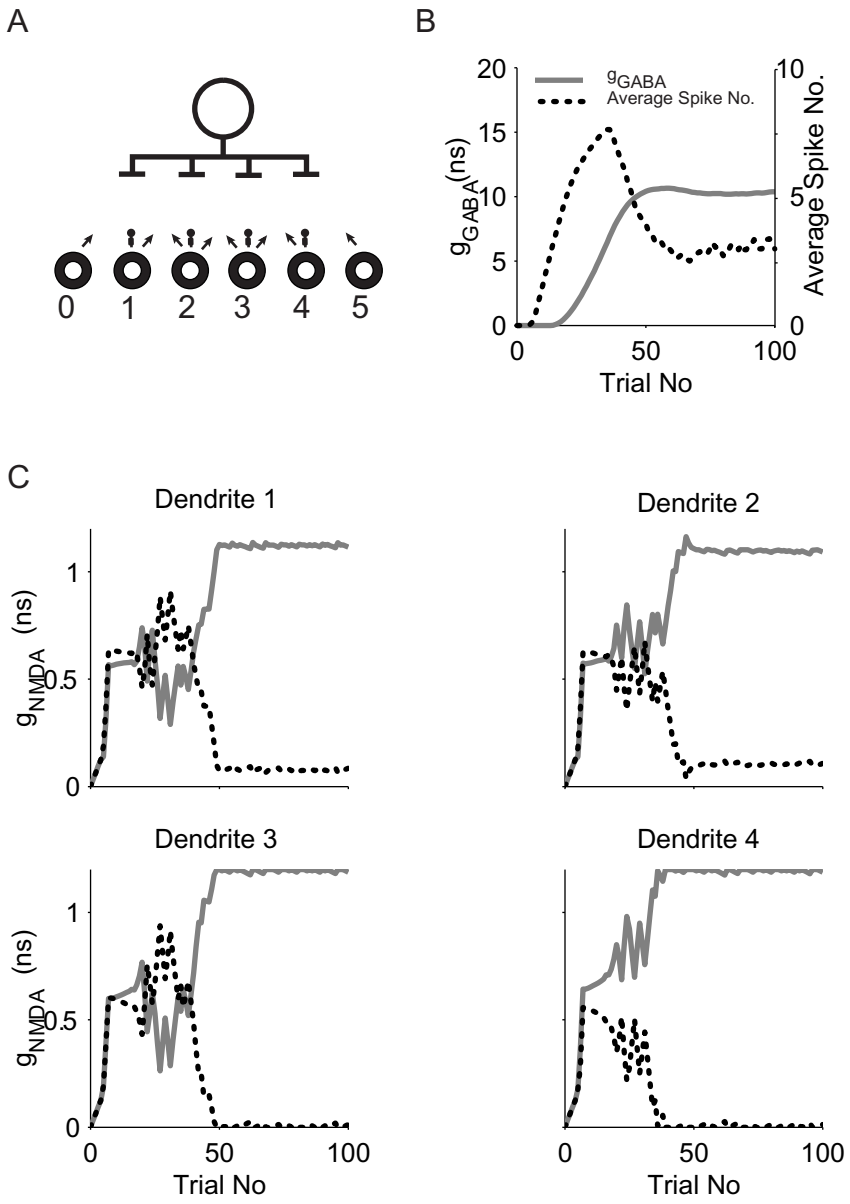

Fig. 3-9. The excitation and inhibition differential learning. A. Schematic drawing of the starting condition. All initial excitatory and inhibitory connection strengths are zero. B. Synaptic weight changes for an inhibitory input cell (solid curve) and the average spike number of the model cell (dotted curve, averaged over 30 trials) during a simulation run. C. Synaptic weight changes for the left input cells (solid curves) and the right input cells (dotted curves) at each dendrite during one simulation run. The model cell is direction-selective after learning.

Therefore we used a simple inhibition learning rule that links the inhibitory synapse strength with the model cell's average response as described by Soto-Trevino *et al*. (2001). We set a target spike number of 3 spikes per trial and keep a 30-trial spiking history. At each trial, the inhibitory synaptic weight change is linear related to the difference between the target value and the average spike number. This learning rule is not a direction-selective one: a DS cell that spikes 6 times in its preferred direction and 0 in its null direction or a non-DS cell that spikes 3 times in both directions fulfills the requirement. Synaptic weight changes for a simulation run with our learning model implementing the inhibition learning rule are shown in Fig. 3-9. Excitatory input weight changes are shown in Fig. 3-9C. The model cell is direction-selective after training. Initially, all excitatory and inhibitory synapses' weights are zero and so is the average spike number. The excitatory synapse weights gradually increase over the spiking threshold because of the "competition" rule. The learning model is not direction-selective because there is no inhibition. The average spike per trial quickly increases over the target value, 3 spikes per trial. Then the inhibitory synapse connection strengths start to increase, so does the competition between excitatory synapses. The inhibitory synapse weights overshoot to a certain value and gradually come down and the model cell stabilizes to become direction-selective. A simulation with extended training periods is shown in Fig. 3-10. In such a setting, the inhibitory synapse weights can go down significantly even after the model converges if extended periods of null direction motion trials cause the average

spike numbers to go down. This in turn causes the excitatory input connections to fluctuate (close to 500 trials in Fig. 3-10). Long consecutive null direction motion trials can force the model cell to start the learning process all over again.

We did not implement a local learning rule for inhibition because it is unclear how inhibitory synapse can obtain local information biophysically. Its strength might also be controlled by local calcium concentration change if it co-localizes with excitatory synapses at the spine. In our model setting, the inhibitory synapse is connected to the main dendrite and it is unlikely that the limited number of calcium ions exiting from spine can cause significant calcium fluctuation at dendrites close to the site of inhibition. The average intracellular calcium concentration is directly linked to the average spike number and can be easily sensed by the inhibitory synapses as we have proposed in our learning rule.

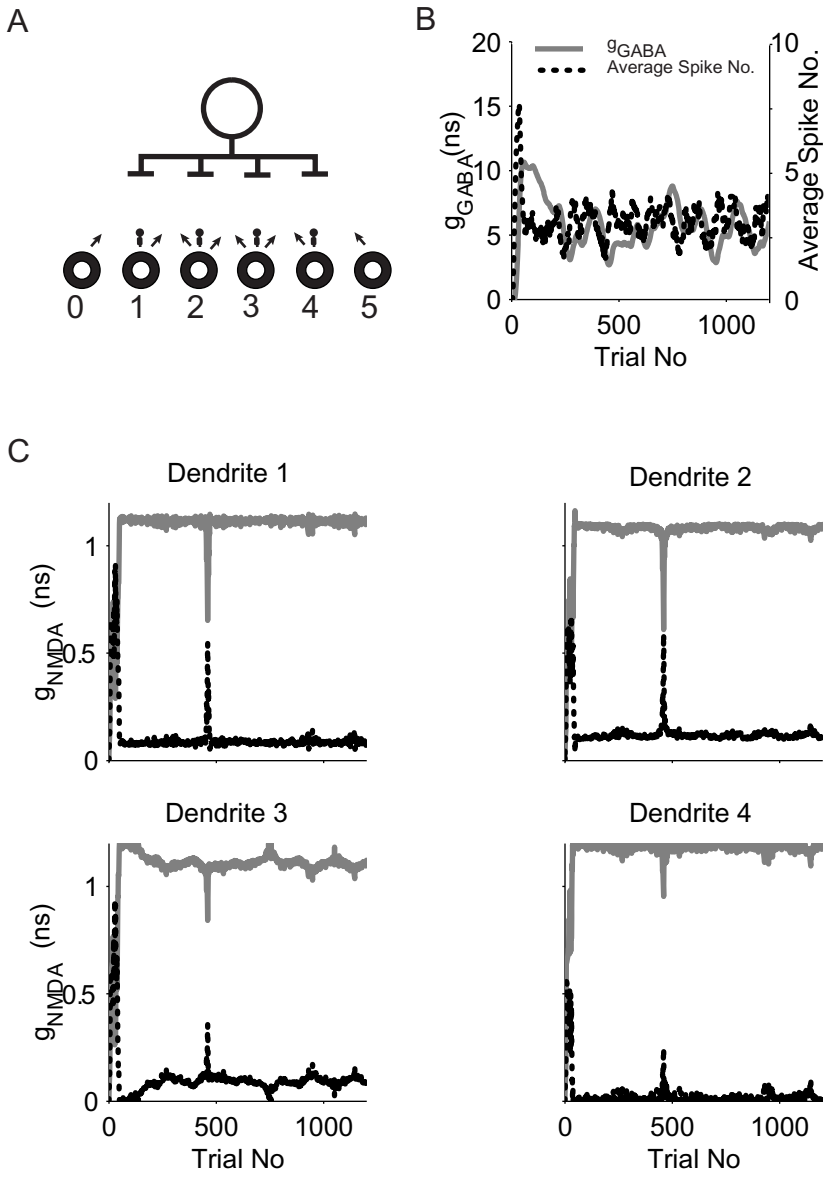

Fig. 3-10. The excitation and inhibition differential learning. The same simulation as shown in Fig 3-9 but with a longer time-scale

Chapter Four

Modeling Reverse-Phi Motion Selective Neurons in Cortex: Double Synaptic Veto Mechanism

4.1 Introduction

Reverse-phi motion was first demonstrated by Anstis (Anstis, 1970; Anstis and Rogers, 1975). Subjects perceive the reverse direction of motion when the contrast of a moving object reverses in the second frame of a two-frame shift experiment. A repetitive 'four-stroke' cycle of reverse-phi motion gives a strong illusion of unidirectional apparent motion (Anstis and Rogers, 1986). The reverse-phi illusion involves the short-range motion process pathway (Chubb and Sperling, 1989). Random dot cinematograms (RDC) studies suggest that D_{max} --- the maximum distance dots can move from one frame to the other while still preserving the sense of motion---for reverse-phi motion is comparable to D_{max} for normal motion, compatible with the notion that the same short-range direction-selective mechanism is most likely responsible for both normal and reverse-phi motion (Sato, 1989). Reverse-phi like effects have also been reported during electrophysiological experiments from direction-selective complex cells in cat striate cortex (Emerson *et al*., 1987), the H1 cell in the fly's lobula plate (Egelhaff and Borst, 1992), and the optical tract of the wallaby (Ibbotson and Clifford, 2001). Recent recordings from direction-selective cells in the alert monkey show that cells in both cortical areas V1 and MT reverse facilitation and suppression

regions in the 2-bar interaction map when two different contrast bars are presented (Livingstone *et al.,* 2000; Conway and Livingstone, 2001). This implies that these cells respond to reverse-phi motion in the reversed direction.

Space-time plots of reverse-phi motion show energy in the reverse direction (Fig. 1A). Although the bar movement direction is to the right, the left motion energy unit aligns better with the stimuli and extracts more motion energy than the right motion energy unit. Therefore both the motion energy model (Adelson and Bergen, 1985) as well as the equivalent Reichardt model (Reichardt, 1961; Santen and Sperling, 1985) can account for the reverse-phi motion. At the core of the Reichardt detector is a correlation step that involves multiplication between inputs. Mathematically, if the sign of one of the inputs that are being multiplied is reversed, as in the case of reverse-phi motion, the sign of the final product is also reversed. However, there is no experimental evidence that either a single neuron or a neural network can perform a clean, four-quadrant multiplication operation. Even for a single identifiable cell that performs multiplication, such as the LGMD neuron in the locust's visual system (Hatsopoulos *et al.*, 1995; Gabbiani *et al*., 1999; Gabbiani *et al.*, 2001), it is unlikely that the sign of the cell's output could be reversed for a reversed signed input, given multiple half-wave rectifications mechanisms and narrow operating ranges for most biophysical processes involved. It is therefore of interest to study a direction-selective mechanism that can be implemented by neurons and that can account for both normal and reverse-phi motion.

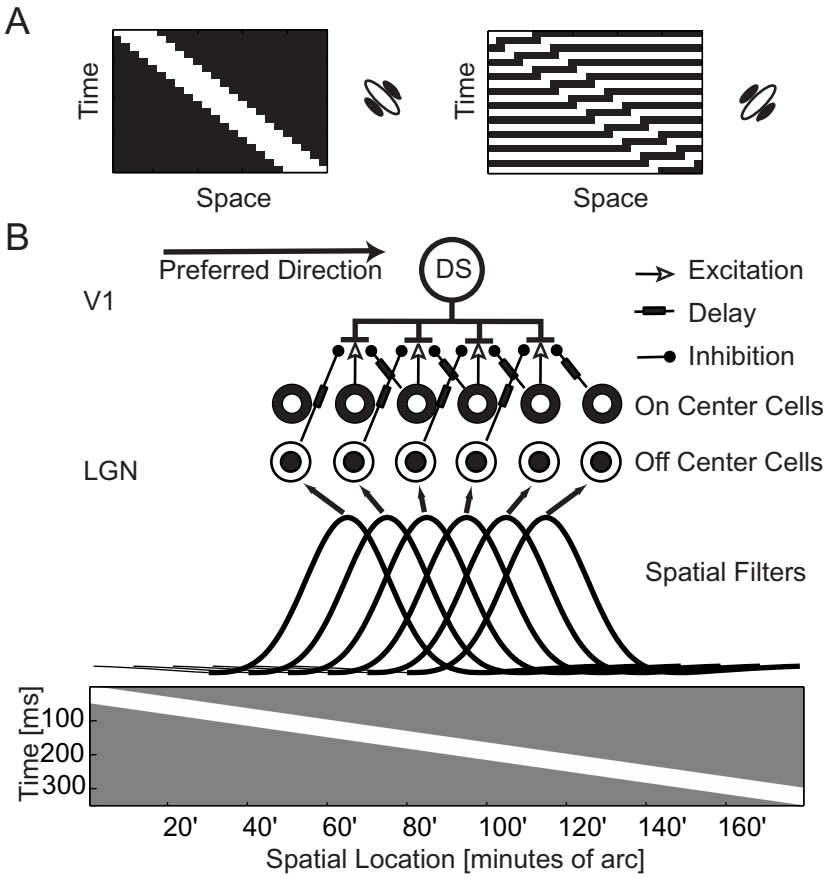

Fig. 4-1. Space-time plot of normal and reverse-phi motion and connectivity diagram of the model that accounts for direction and reverse-phi selectivity. (A) Space-time plot of a one dimension white bar moving from left to right in normal motion (left panel) and in reverse-phi motion (right panel). A right motion energy unit aligns well with the normal motion plot, but triggers a much reduced response for the reverse-phi motion. Instead, this strongly stimulates a left motion energy unit. Adopted from Fig. 16 in (Adelson and Bergen, 1985). (B) Connectivity diagram of normal and reverse-phi motion direction selective model. Input to LGN neurons comes from a one-dimensional array of 179 pixels. The intensities from those pixels were summed through difference of Gaussian spatial filters on to LGN cells. There are one ON and one OFF center geniculate cell at one of six spatially offset locations. Each of the middle four ON center LGN cells provided excitatory input to one branch of the model cell dendrites; while the ON center LGN cell immediately to the right and the OFF center LGN cell immediately to the left provide delayed on-the-path inhibition. The converse connection scheme for the OFF center LGN cells' excitatory inputs are not shown.

The first computational step in visual processing is half-wave rectification and separation into ON and OFF channels. It is unknown whether direction selectivity is generated between non-linear interactions of these half-wave rectified signals or between simple cells that carry the reconstructed full wave signal. DL-2-amino-4-phosphonobutyric acid (APB) reversibly blocks the ON response in the mammalian retina (Schiller, 1982), but the detection of motion direction is largely unaffected in rabbit, cat and monkey in electro-physiological experiments (Knapp and Mistler, 1983; Horton and Sherk, 1983; Sherk and Horton, 1984; Schiller *et al*., 1986). Similarly, existing direction-selective models treat ON and OFF inputs separately (Koch and Poggio, 1985; Suarez *et al*., 1995; Rao and Sejnowski, 2000). However, the nature of reverse-phi motion stimuli suggests an interaction between ON and OFF channels. Different rectification schemes affect the ON-OFF interaction differently and therefore carefully constructed reverse-phi stimuli were used in experiments to separate the firs- order, second-order and third-order motion (Lu and Sperling, 1999; Mather and Murdoch, 1999). The requirement for ON-OFF interactions constrains cellular models of direction selectivity.

V1 direction-selective cells show slanted excitatory regions in their receptive field map (Livingstone, 1998). The asymmetry in the summation of excitatory inputs at dendrites alone was not sufficient to account for the directional response based on modeling study by Anderson *et al*. (1999). Therefore, asymmetrical delayed

inhibition is likely to be the mechanism that underlies direction selectivity. Such a mechanism based on shunting inhibition, *i.e.,* an increase in a chlorine based GABA_A conductance that reverses close to the cell's resting position, was proposed for the cortex by Koch and Poggio (1985). Recent experiments in the retina provide evidence in favor of at least some nonlinear interactions between excitatory and shunting inhibitory inputs that take place within the dendrites of direction-selective ganglion cells (Taylor *et al.*, 2000; for a dissenting view, see Borg-Graham 2001; Borst 2001). Large conductance changes that reverse around the cell's resting potential have been observed in V1 during visual stimuli (Anderson *et al.*, 2000; Borg-Graham *et al*., 1998). Here we show how a double synaptic-veto mechanism, derived from the traditional asymmetrical delayed shunting inhibition model, can account for both normal and reverse-phi motion direction selectivity.

4.2 Methods

We followed a two-step compartmental simulation strategy using the program NEURON (Hines and Carnevale, 1997). We first investigated the performance of an idealized neuron (Fig. 4-4B) before we implemented our synaptic assembly onto a reconstructed V1 cell (Fig. 4-7A). The idealized cell morphology is shown in Fig 4B. Eight dendrites (width 0.5μm, length 100μm) were directly connected to the soma (width 16μm, length 16μm). Each dendrite had 20 compartments, for a total of 180 compartments. The dendrites were passive, while the cell body contained a number of voltage-dependent currents that give rise to fast Hodgkin-

Huxley like action potentials. The biophysical parameters were as follows: R_i=250 Ω•cm, C_m=0.5 μF/cm^2, E_{leak}=-60 mV, R_m=10 kΩ•cm^2, g_{Na}=0.024 S/cm^2, g_K=0.020 S/cm^2, E_{NMDA}=0 mV, g_{NMDA}=2.5 nS, τ_{NMDA} on=0.1 ms, τ_{NMDA} off=80 ms, E_{AMPA}=0 mV, g_{AMPA}=2.5 nS, $\tau_{AMPA\ on}$=0.1ms, $\tau_{AMPA\ off}$=2 ms, E_{GABA}=-60 mV, g_{GABA}=6.0 nS, τ_{GABA_on}=1 ms, $\tau_{GABA\ off}$=80 ms. Synaptic input was modeled using the point process in NEURON (adopted from Archie and Mel, 2000).

We adopted a layer 4 stellate cell model from Mainen and Sejnowski,1996 (Fig. 4-7A). The model cell contained sodium channels at the soma and dendrites, as well as fast potassium channels at the soma and the axon. Both calcium- and voltage-dependent slow potassium channels and high-threshold calcium channels were present at the soma and dendrites. All passive and active parameters were the same as those used in their original paper. All synapse parameters were the same as described above except E_{GABA}=-70 mV, g_{GABA}=6.9 nS.

The input connection scheme to both models is shown in Fig. 4-1B. The spatial resolution of the stimulus was 1 minute of arc and the temporal resolution 0.1 ms. The LGN layer was modeled as a transfer function. Stimuli projected onto the LGN layer consisted of two 6 by 1 arrays of spatial filters modeling ON center and OFF center cells that covered 3 degree of visual space. The spatial kernel was a difference of Gaussian (DOG) function (adopted from Wörgötter and Koch, 1991). The Gaussian kernel was $G(x)=(K/2\pi\sigma^2)\exp(-x^2/2\sigma^2)$, σ_{center}=10.6 minute,

$\sigma_{surround}$=31.8 minute and $K_{center}/K_{surround}$=17/16. Stimuli were first passed through these spatial filters and then through low-pass temporal filters, with a delay between the center and the surround component (τ_{center}=10 ms, $\tau_{surround}$=20 ms $delay_{surround}$=3 ms). The resulting values were scaled to give a time-dependent, stimulus-driven LGN instantaneous firing rate with a maximum value of 200 Hz. A background-firing rate of 5 Hz was added and all negative values were set to 0 (half-wave rectification). OFF center cells were modeled as the reverse of their ON center counterpart.

Each of the middle four ON center LGN cells provided the excitatory input to one branch of the model cell dendrites, while the ON center LGN cell immediately to the right (preferred side) and the OFF center LGN cell immediately to the left (null side) provided delayed inhibition. Each of the middle four OFF center LGN cells provided excitatory input to one branch of the model cell dendrites, while the OFF center LGN cell immediately to the right and the ON center LGN cell immediately to the left provided delayed inhibition. The delay was 12 ms. There were a total of 8 excitatory synapses and 16 inhibitory synapses in the model. Excitatory synapses were mapped to the dendrite compartment 60μm away from the soma; same type inhibitory input was located 50 μm and different type inhibition 40 μm away from the cell body. Given that shunting inhibition was on the direct path between excitation and the soma, it could effectively and specifically veto the excitatory input to that branch while only minimally affecting the excitatory input from neighboring branches (Koch, Poggio and Torre, 1982).

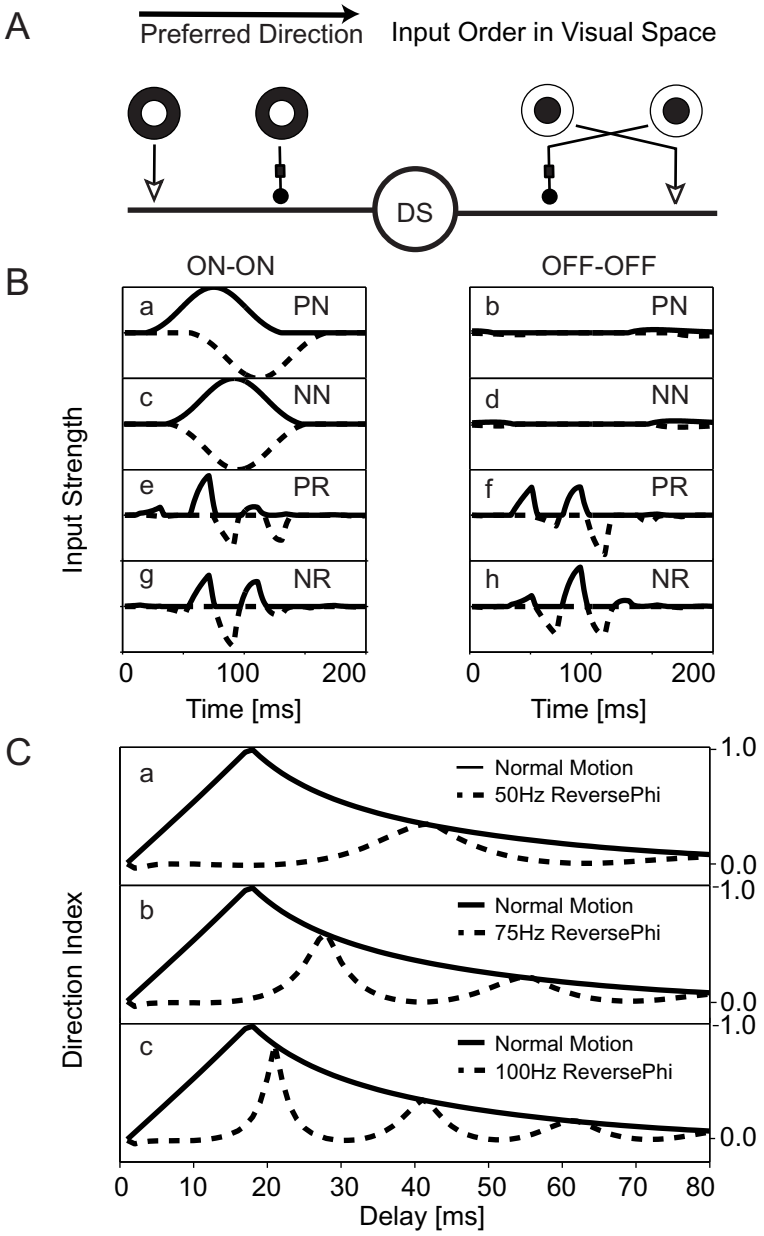

Fig. 4-2. Normal shunting inhibition cannot account for reverse-phi motion. (A) Asymmetrical delayed inhibition scheme resulted in direction selectivity. ON excitation was gated by a delayed ON inhibition at its preferred side and the converse for OFF excitation (symbols as in Fig. 1). (B). Excitatory and inhibitory inputs to model cell when a bright thin bar moves across its receptive field at 10o/s in preferred normal (PN) motion direction (a,b); in null normal (NN) motion direction (c,d), preferred reverse-phi (PR) motion direction (e,f), and null reverse-phi (NR) motion direction (g,h). Solid lines: Excitatory inputs from on center cells (a,c,e,g) and off center cells (b,d,f,h). Dash lines: Delayed Inhibitory inputs (20 ms delay) were plotted in negative. Inputs were calculated as the stimuli passed through the spatial-temporal filters mentioned in the methods section. (C) The direction index DI, for the eight-armed dendritic model cell for different inhibitory delay times and contrast reversal rates. Over a wide range of inhibitory input delay times, the model cell was direction selective to normal motion but only weakly to reverse phi motion.

For the layer 4 stellate cell, 8 triplets of excitatory-inhibitory-inhibitory synapses were mapped to eight separate terminal branches. This arrangement was replicated four times and mapped onto 32 terminal branches. The total synaptic count was 32 excitatory and 64 inhibitory synapses.

4.3 Asymmetric-delayed shunting inhibition model

We started by testing how well the reverse-phi effect was explained by the original asymmetric-delayed inhibition model of Barlow and Levick (1965), as implemented with shunting inhibition (Torre and Poggio,1978; Poggio and Torre,1978; Koch *et al.*,1982) . We then carried out compartmental simulation in NEURON using an idealized dendritic geometry to prove our concept and compare the model against experimental data. Finally, we mapped our synaptic connection scheme to a more realistic cortical cell morphology and demonstrated how it could account for both normal and reverse-phi direction selectivityThe traditional Barlow and Levick (1965) inhibitory based scheme is shown in Fig. 4-2A. Inhibition was assumed to be of the shunting type (that is, with an inhibitory reversal potential around the local resting potential) so that synaptic interactions are restricted to local branches. We plotted the time course of excitatory and inhibitory inputs to the model from two adjacent cells in the LGN input layer (Fig. 4-2B). When a white bar moved in a normal fashion in the preferred direction, there was a temporal shift between excitatory and inhibitory inputs (Fig. 4-2B.a), while in the null direction excitation and inhibition overlapped and therefore

cancelled each other (Fig. 4-2B.c). If the same bar moved in the reverse-phi fashion, there was little difference in the temporal alignment of excitatory and inhibitory inputs between preferred and null direction movement (Fig. 4-2B.e-h). For normal motion only the ON branch received significant input, while for reverse-phi motion the input was spread between ON and OFF channels. The combined areas under the excitation or inhibition curves for both branches were much less for reverse-phi motion than normal motion. Because of the low-pass filtering and the rectification inherent in the LGN layer, both the excitatory and inhibitory inputs to the model cell during reverse-phi motion were reduced.

We compared the direction index (DI) of the model cell using different stimulus reversal rates and the delay factor for the inhibition (Fig. 4-2C). DI was calculated as the response in the preferred direction minus the null direction response, divided by the sum of the preferred and the null direction. The value of preferred direction was calculated as the sum of excitation minus inhibition with all negative values set to zero. Thus DI ranges from 0, for a non-discriminatory system, to 1, for a system that does not respond at all to null direction motion. The model was direction-selective to normal motion for a wide range of delay values but was only weakly direction-selective to reverse-phi motion. DI for reverse-phi motion increased when the stimulus reversal rate increased, but the direction preference was the same as that of normal motion, contrary to the experimental data. Therefore, it appears that a traditional inhibition scheme cannot easily account for reverse-phi motion.

Given the nature of reverse-phi motion, a direct non-linear interaction between ON and OFF branches, missing in traditional schemes, is needed to account for reverse-phi motion direction selectivity. We here propose a "reversed" shunting inhibition scheme (Fig. 4-3A), in which an ON excitation is gated by a delayed OFF inhibition at its null side and an OFF excitation is gated by a delayed ON inhibition at its null side (see Poggio, 1982; Koch and Poggio, 1987 for other synaptic logic models involving ON-OFF interaction). Not surprisingly, this model responds equally strongly to both directions for normal motion, as inhibition is only activated by a bar of the opposite contrast from that of excitation. However, there is a difference in the temporal alignment of excitatory and inhibitory inputs between the preferred and null direction reverse-phi movement. When the inhibitory delay matches the stimuli reversal rate, DI is close to 1. DI decreases when the stimulus reversal rate increases. We conclude that the ON-OFF and OFF-ON vetoing scheme can discriminate the direction of reverse-phi motion. Given that the experimental data demonstrated that reverse phi motion in the cell's null direction elicited more vigorous responses than reverse phi motion in the preferred direction (DI < 0), the delayed inhibitory input needs to reside at the excitatory input's preferred side instead of its null side.

4.4 Double synaptic veto mechanism

A traditional shunting inhibition scheme can account for normal motion direction selectivity while a "reversed" shunting inhibition scheme can account for reverse-

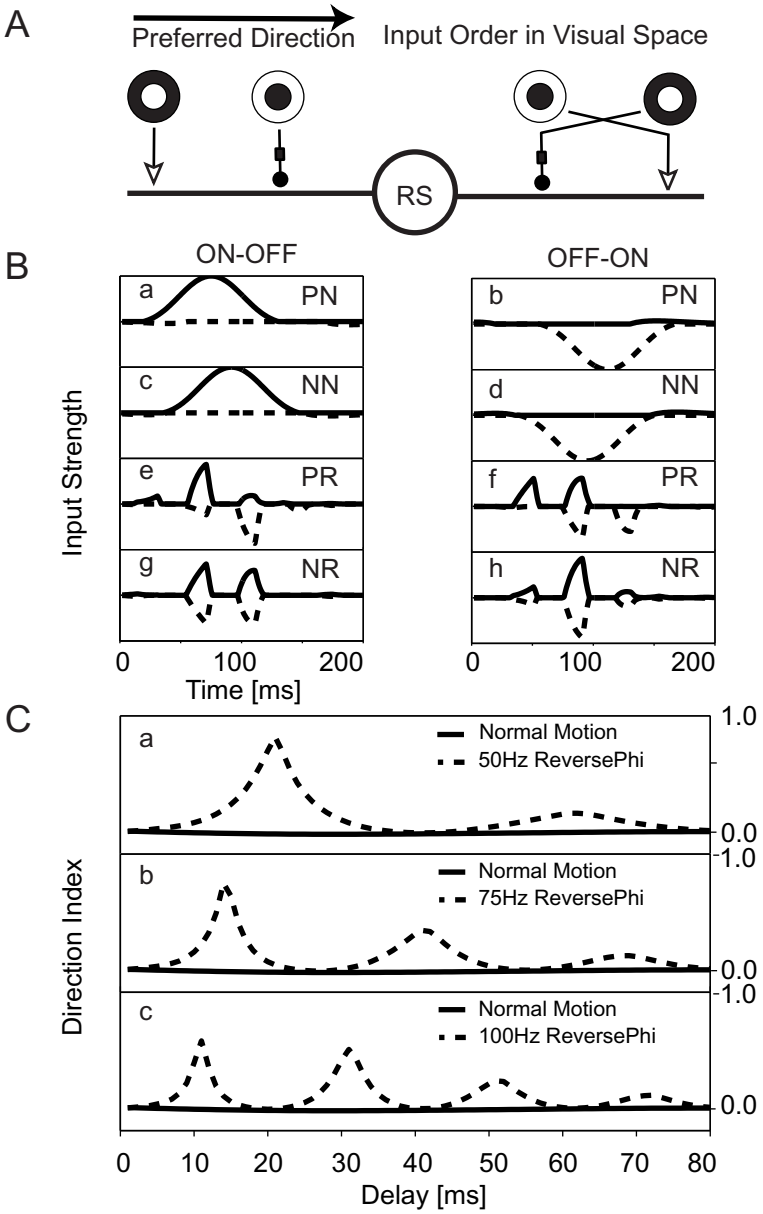

Fig. 4-3. Reversed shunting inhibition scheme was direction selective to reverse-phi motion. (A) Reversed asymmetrical delayed-inhibition scheme. ON excitation was gated by a delayed OFF inhibition at its preferred side and the converse for OFF excitation. (B) Excitatory and inhibitory inputs to the model cell when a bright thin bar moves across its receptive field at 10o/s in the preferred normal (PN) motion direction (a,b); in the null normal (NN) motion direction (c,d), the preferred reverse-phi (PR) motion direction (e,f), and the null reverse-phi (NR) motion direction (g,h). Solid lines: Excitatory inputs from on center cells (a,c,e,g) and off center cells (b,d,f,h). Dash lines (Delayed Inhibitory inputs (20 ms delay) are plotted in a reverse negative. (C) The DI calculated for reverse-phi motion. The model is not direction selective to normal motion but when inhibitory input delay is optimal, the model was direction selective to reverse phi motion.

phi motion direction selectivity. In order to account for both, we need to combine both synaptic schemes. One way to achieve this is to construct a model cell with four dendritic branches. Two of them implement a traditional shunting inhibition scheme while the remaining two implement a “reversed” shunting inhibition scheme. Such a connection scheme will be selective to both types of motion. However, the “traditional” branches offer a non-gated path for reverse-phi excitatory inputs, while the “reversed” branches offer a non-gated path for normal motion excitation. Such non-gated excitatory inputs results in a high background level of depolarization at the soma and therefore low DI values.

We propose here a double synaptic veto mechanism that combines the two synaptic schemes in a more sophisticated way at the microcircuitry level (Fig. 4-4A). In the new connection scheme, an ON excitatory synapse is gated by both a delayed ON inhibition at its null side (Fig. 4-1B, right side of the cell) and by a delayed OFF inhibition at its preferred side (Fig. 4-1B, left side of the cell) and an OFF excitatory synapse is gated by both a delayed OFF inhibition at its null side and by a delayed ON inhibition at its preferred side. Same type inhibition at the null side vetoes null direction normal motion, while different type inhibition at the preferred side vetoes preferred direction reverse-phi motion. We mapped this triplet of synapses, one excitatory and two shunting inhibitory ones, onto the abstract cell model with a soma and eight dendritic branches (Fig. 4-4B), creating a simulacrum with four direction-selective subunits, each of which implements

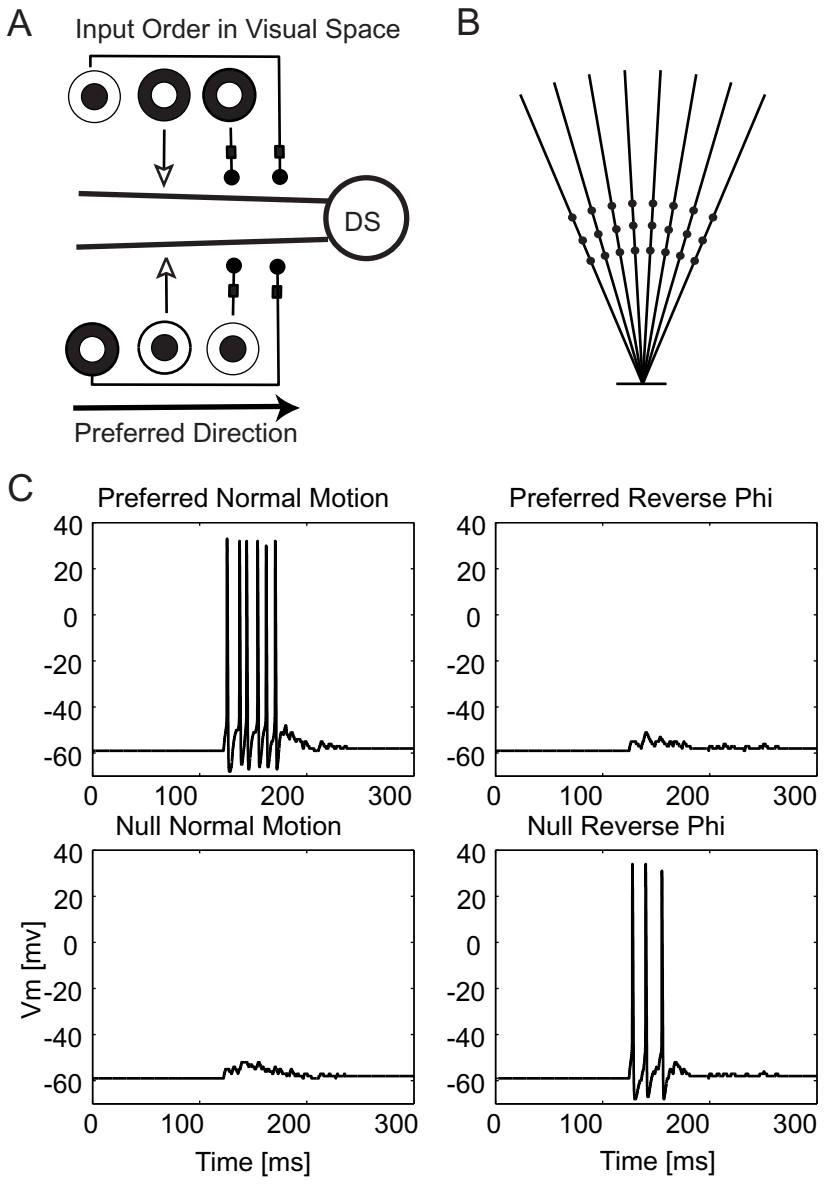

Fig. 4-4. A double synaptic veto mechanism can account for both normal as well as reverse-phi motion direction selectivity. (A) Connection scheme of the double synaptic veto mechanism. ON excitation is gated by a delayed ON inhibition at its preferred side and by a delayed OFF inhibition at its null side and the converse for off excitation. (B) Mapping the double synaptic veto scheme onto the eight-armed cable model with spiking at the cell body. Each excitation-inhibition-inhibition triplet is mapped onto its own dendritic branch with the excitation at the far side of cell body. (C) Model cell's response to a bright bar moving at 10o/s across its receptive field. The model cell responds best when a normal motion stimulus moves in its preferred direction and when a reverse-phi motion stimulus moves in its null direction. The stimuli reverse rate is 75Hz.

the synaptic connection of Fig. 4-4A (the detailed connection scheme is explained in the methods section).

The model responded best to normal motion in its preferred direction (DI=1) and reverse-phi motion (DI=-1) in its null direction (Fig. 4-4C). Note that the amplitude of the response to normal motion (6 spikes) was twice as large as the amplitude to reverse-phi motion (3 spikes), reflecting the fact that both the excitatory and inhibitory inputs for normal motion stimuli were stronger. In a broad range of model parameters, Cm=0.5 to 1$\mu F/cm^2$, E_{leak}=-70 to -60mV, $Delay_{inhibitory\ input}$=8 to 15ms, $g_{AMPA} + g_{NMDA}$ =1 to 10nS, gAMPA / g_{NMDA} =0.1 to 10,and gGABA / (g_{NMDA} + g_{NMDA}) =1 to 10, the simulation showed direction selectivity for both types of motion, but only specific parameter sets resulted in high DI. When DI was small, null direction normal motion or preferred direction reverse-phi motion also elicited spikes, but the timing of the first spike was late compared to the case of the preferred direction movement (data not shown). Even if gNMDA was set to zero, the cell responded in a differential way to null and preferred direction motion. Since sodium and potassium channels are only placed at the soma, the voltage-dependent dendritic current was not required for the model's direction selectivity. However, NMDA currents increased somatic voltage during preferred direction movement and thus increased DI. The inhibitory synapses were always located between the excitatory input and the spike-triggering zone at the cell body, thereby fulfilling the "on-the-path" condition (Koch *et al.*, 1982). The inhibitory

conductance change in most cases only needs to be a little bit larger than the excitatory conductance change to achieve a “veto” effect.

To test whether shunting inhibition was required for the direction selectivity we observed, we decreased the GABA channel reversal potential from –60 mV to –90 mV in 5 mV steps. At the same time we decreased the amplitude of gGABA accordingly so that the model always responded to a preferred direction normal motion stimuli with 6 spikes and null direction reverse-phi stimuli with 3 spikes. DI for both types of motions decreased when the GABA channel reversal potential was decreased. At –90 mV, the model responded with 5 spikes to null direction normal motion stimuli and with 3 spikes to preferred direction reverse-phi motion stimuli. Thus the direction selectivity was lost.

4.5 Receptive field and two-bar interaction maps

The direction-selective cell shows a slant in the space-time plot (Fig. 4-5A). A recent study of direction-selective cells in awake monkey V1 shows an excitatory region on the cell’s preferred side and an inhibitory region on the cell’s null side, consistent with our connection scheme (Livingstone, 1998). To compare the experiment data with our model, we incorporated a synaptic noise source (AMPA conductance only) at the soma to achieve a reasonably high background firing rate and then presented flashing bar stimuli at 20 different spatial locations across the receptive field (Fig. 4-5B). There was good agreement between the experimental data and the response of our eight-arm model. Both space-time

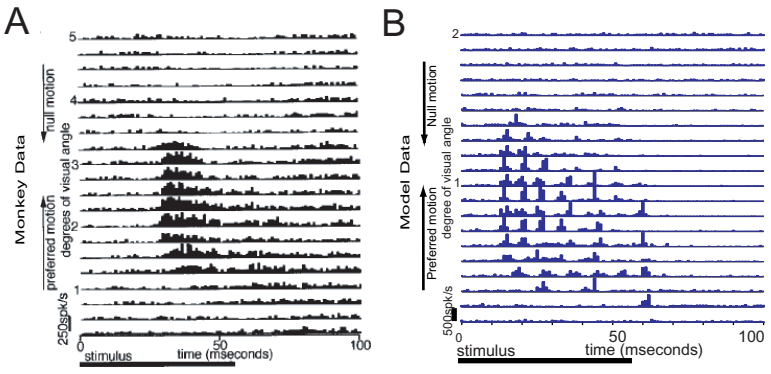

Fig. 4-5. Comparison of space-time response mapping of monkey V1 cell and model cell. (A) PSTHs obtained from a layer 5/6 complex cell in primary visual cortex of the alert macaque monkey in response to flashed bars, presented in random orders at a series of positions across the cell's receptive field. (from Livingston, 1998. Figure 3A). This cell's preferred direction was from the bottom towards the top. Flash bar duration =56 ms; inter-stimulus delay =100 ms; 75 stimulus presentations. (B) PSTHs obtained from the model neuron to flashed bars at 20 spatial locations across its receptive field. The model's preferred direction is from the bottom towards the top. It shows a decrease in the response onset time and an increase in the response transiency, as does the V1 complex cell.

plots showed a progressive shortening of the response onset time and a more transient response going from the cell's preferred side to its null side. In our model, the shortening of response onset time and the increasing in response transiency were due to asymmetrical delayed inhibition and the basic property of integrate-and-firing neurons of LGN layer. The response onset time was determined mainly by the excitatory input since the inhibitory input was relatively small and delayed. Going from the preferred to the null side, the bar moves from the edge to the center of the receptive field of the first LGN cell that provided excitatory, increasing the excitatory input amplitude and decreasing the time needed to charge the membrane to fire the first spike. The response transiency is primarily determined by how quickly inhibition can overcome excitation and shut off the response. Moving towards the null side, excitatory input strength decreases, while inhibitory input strength increases as well as the response transiency. The slant of the excitatory and inhibitory regions in the space-time plot is related to the cell's velocity tuning (Livingstone, 1998; McLean and Palmer, 1989; Reid *et al.*, 1991). Since we did not include any synaptic delay between the retina and V1, the model responds much earlier to the visual stimulus than actual striate cortex neurons. The periodic firing is caused by the deterministic synaptic input. Random noise channels at the soma are responsible for the background firing and jitter of spikes around the peak firing time. Rao and Sejnowski (2000) showed a similar space-time plot for their direction-selective model. In their network model, the decrease of response onset time was due to the increase of the excitatory synaptic input strength from the

cell at the preferred side toward the model cell itself. This effect is expected for any direction-selective model that is based on asymmetrical inhibition.

The experimental data also show reversed excitatory and inhibitory regions in the two-bar interaction map of direction-selective cells in V1 and MT when opposite contrast bars instead of same contrast bars were presented (MT: Fig. 4-6A. Livingstone, 2001. Fig 1. V1: Livingstone, unpublished data). To compare with the experimental data, we tested our model's response to two sequentially presented bars (Fig. 4-6B). The X-axis corresponds to the position of the first flashed bar and the Y-axis corresponds to the position of the second flashed bar. The diagonal line corresponds to both bars being presented at the same spatial location. A non-direction-selective cell should have excitation regions both above and below the diagonal line while a direction-selective cell should have asymmetric excitation regions with respect to the diagonal line. When the two bars are of the same contrast, the excitatory region of our model cell's response map is mostly above the diagonal, where the second presenting bar's position is located more toward the null side of the first presenting bar. However, when the two bars have opposite signs of contrast, the excitatory region is mostly below the diagonal, whereas the second presenting bar's position is located more toward the preferred side of the first bar, signaling a reverse in the direction preference of the model. There is no difference between the white-white and black-black plots, given the symmetric ON and OFF inputs the model receives (likewise for the black-white and black-white plots). The difference of the

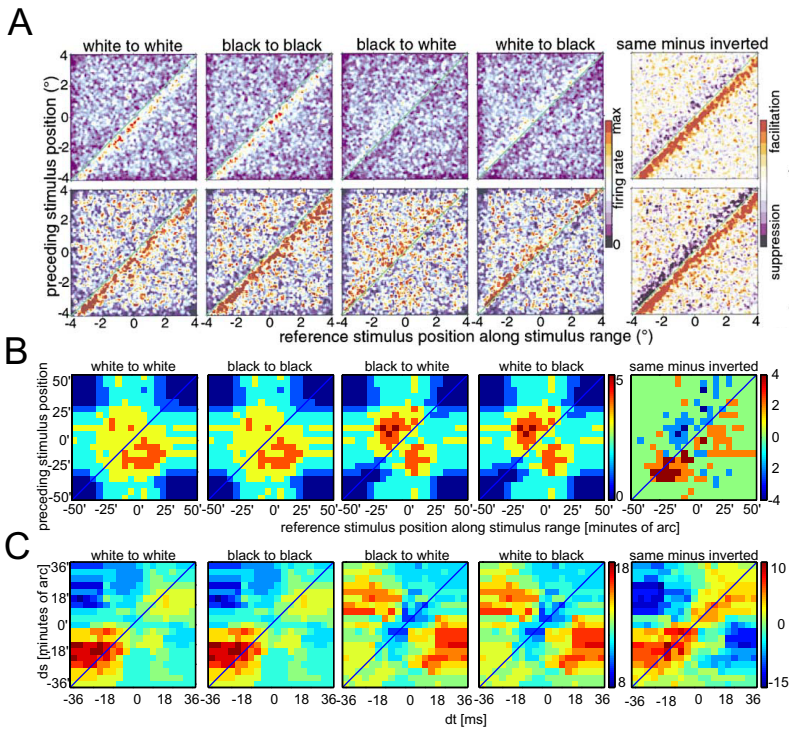

Fig.4-6. Two-bar interaction maps. (A) Interaction map for two MT cells in the alert monkey (Fig. 1 in Livingstone et al., 2001). (B) Same interaction map for the eight-armed model neuron. Pairs of bars (8' of width) were flashed sequentially for 13 ms each at different spatial locations. Spikes were counted for 100 ms from the start of the first bar flash. X-axis is the first flash bar's position and Y-axis is the second bar's position. Diagonal line is where two bars presented at the same spatial location. From left to right, Panel 1: Both bars were white. Areas above the diagonal line, where the second bar position was more positive than the first bar position, were more active than the area below the diagonal line. Panel 2: Both bars were black. Panel 3: The first bar was black and the second bar was white. Areas below the diagonal line were more active than the area above the diagonal line. Panel 4: The first bar was white and the second was black. Panel 5: The same contrast conditions minus the inverted contrast conditions (1+2-3-4). Model neuron preferred two same contrast bars flashed sequentially in its preferred direction and two inverted contrast bars flashed sequentially in its null direction. Given the symmetrical input, the white-to-white and black-to-black model interactions are identical, as are the black-to-white and the white-to-black one. (C) Space-time two bar interaction map of the model cell following the technique pioneered by (Emerson et al., 1987). The reference bar was presented at time 0 at four different locations across the receptive field. For each reference bar position, the probing bar was presented at different locations and times relative to the reference bar. Spikes were counted for 100 ms from the start of the first bar flash. Four such maps were added together to give a position invariant ds-dt map of two bar interactions. From left to right, Panel 1: Both bars were white. Areas along the diagonal line, where the two bar presenting sequence matched the preferred direction and speed, were more active than areas orthogonal to the diagonal line, where the two bar presenting sequence matched the null direction. Panel 2: Both bars were black. Panel 3: The reference bar was black and the probing bar was while. Panel 4: The reference bar was white and the probing bar was black. Panel 5: Same contrast conditions minus inverted contrast conditions. The model neuron preferred two same contrast bars flashed sequentially in its preferred direction and two inverted contrast bars flashed sequentially in its null direction.

excitatory and inhibitory regions between the same and inverted contrast bar presentations is more clearly evident in Fig. 4-6B: excitation is mostly above and inhibition mostly below the diagonal. Note that excitation was stronger at the model cell's preferred side (minus side of spatial scale), while inhibition was stronger at the model cell's null side (plus side of spatial scale). This was again due to the spatial asymmetry of excitation and inhibition. Although the model is direction-selective to both presentations, direction selectivity was higher for same contrast bar presentations than for different contrast bar presentations. This translates into a weaker response to reverse-phi than to normal motion. The experiment data from MT cells in Fig. 4-6A shows the same overall trend but with a much larger receptive field and better overall position invariance across the receptive field. There were a few major differences between the empirically determined MT cell response maps (Fig. 4-6A) and our V1 model cell response (Fig. 4-6B). Fig. 4-6A shows a diagonal organization, while Fig. 4-6B shows a more circular organization. Part of this difference can be explained by the receptive field size difference between MT and V1 cells. This difference can also arise due to differences in the number and density of direction-selective subunits along the preferred direction and the extent of the non-linear boost of the final output stage. Some V1 direction-selective complex cells do show a circular interaction region while other V1 complex cells reveal a more diagonal organization (M. Livingstone, unpublished data). In addition, the diagonal region in the model (Fig. 4-6B) is above baseline, whereas it appears to be below baseline in the data (Fig. 4-6A). This elevation is likely due to the reverse

correlation technique used in the experiment and further non-linear excitation mechanisms that are missing from our model.

Despite these differences, the “same minus inverted” maps (the rightmost panel in Figs. 4-6A and 4-6B), which demonstrate the non-linear interactions, do show a substantial amount of similarity. Lastly, the cross-shaped backdrop in Fig. 4-6B does not appear in the experimental data. Again, this is due to the difference in receptive field size between the recorded MT cell and our V1 model cell. If Fig. 4-6A were evaluated within a larger spatial range (for example, within +/- 10°), the same cross-shaped background would appear (personal communication with M. Livingstone).

We also generated space-time two bar interaction maps (Fig. 4-6C) to compare with the experimental data published by Emerson *et al.* (1987) on complex cells in cat striate cortex. The X-axis corresponds to the time of the flashed probe bar relative to the time of presentation of the flashed reference bar. The Y-axis corresponds to the position of the flashed probe bar relative to the position of the flashed reference bar (for more details, see Emerson *et al.*, 1987). A direction-selective cell should have obliquely oriented excitatory regions (Fig. 2 in Emerson *et al.*, 1987). When the two bars are of the same contrast, the excitatory region of our model cell’s response map is mostly found along the diagonal, whereas the second presenting bar’s position is located more toward the null side of the first presenting bar. However, when the two bars presented

have opposite contrast sign, the excitatory region mostly flanks the diagonal area, whereas the second presenting bar's position is located more toward the preferred side of the first bar, signaling a reverse in the direction preference of the model. The difference of excitatory and inhibitory regions between the same and inverted contrast bar presentations is more clearly evident in Fig. 4-6C: excitation is mostly along the diagonal line while inhibition mostly flanks the diagonal area. Note that excitation is stronger at the model cell's preferred side (minus side of spatial scale), while inhibition is stronger at the model cell's null side (plus side of spatial scale). This is due to the spatial asymmetry of excitation and inhibition. The non-linear facilitation observed in the experiment by Emerson and colleagues may derive from a specific excitatory directional interaction that is not addressed in our model or from generic non-directional facilitations (such as network feedback or active channels on the dendrites that are masked by directional suppressions).

4.6 The layer 4 stellate cell model

Although all our parameters are physiologically plausible, and the model displayed direction selectivity for a broad range of parameters, we wanted to ensure that the effect we observed was not due to the model cell's cable structure. We therefore mapped our double synaptic-veto arrangement onto an anatomically correct layer 4 stellate cell model (Mainen and Sejnowski, 1996; Fig. 4-7A). All active and passive parameters of the original model cell remained unchanged. The new model's response to different types of motions is illustrated

in Fig. 4-7B. The stellate cell showed direction selectivity for normal motion and the opposite selectivity for reverse-phi motion with DI=1 in both cases. We also tested our connection scheme on the layer 5 pyramidal cell model from (Mainen and Sejnowski, 1996). The pyramidal cell model showed the same directional preference when we mapped our synapse triples onto basal dendrites alone or basal and apical dendrites together (data not shown).

4.7 Discussion

We demonstrate here that our double synaptic-veto mechanism can account for the reversal of direction selectivity in reverse-phi motion. Our biophysical simulations are, obviously, a mere proof of concept that such a scheme might be implemented in a plausible manner by cortical cells. Given the large number of degrees of freedom of any detailed biophysical simulations and the few constraints, except for order of magnitude estimations on the relevant parameters, little else is possible at this point in time. However, the fact that different cell models with distinct dendritic morphologies and voltage-dependent currents can be driven by the same synaptic arrangement to replicate the experimental data in terms of direction selectivity shows that our double synaptic-veto mechanism is not implausible from a physiological point of view.

This scheme makes several predictions that can be evaluated using extra cellular recordings. Firstly, the non-direction-selective zone for reverse-phi motion should reside at the cell's null side instead of the preferred side. Due to our

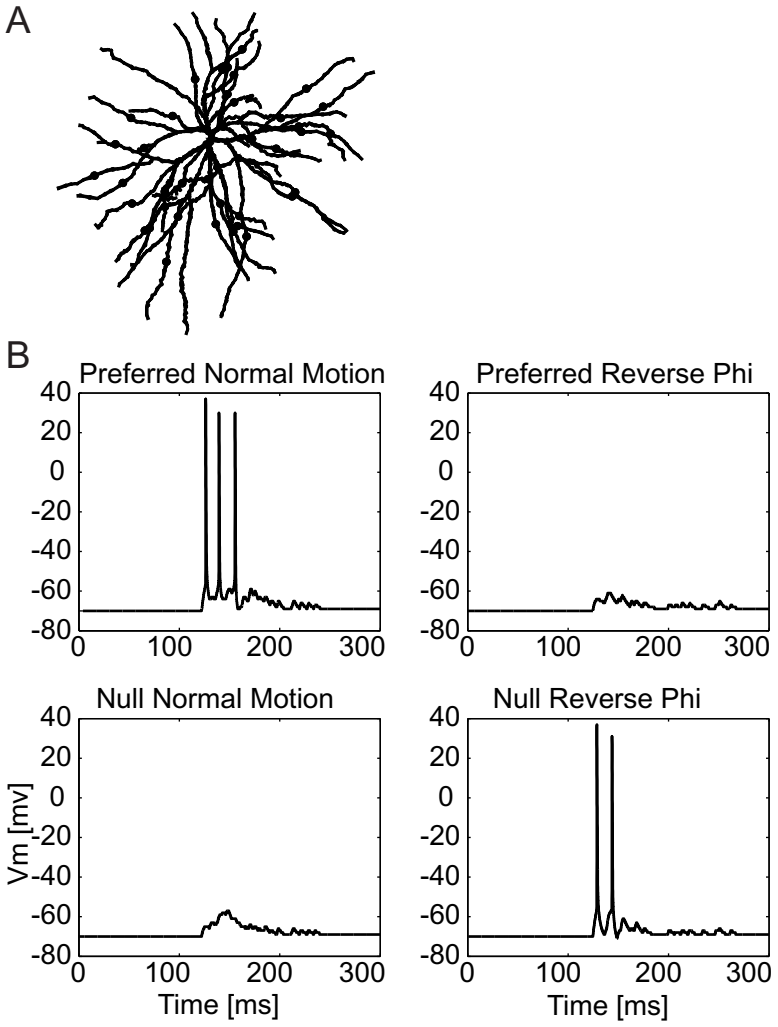

Fig. 4-7. Mapping the double synaptic veto mechanism onto a layer 4 stellate cell model caused it to respond differentially for both normal as well as reverse-phi motion. (A) Input synapse location on a layer 4 stellate cell. (Cell model was taken from Mainen and Sejnowski, 1996). (B) Stellate cell model's response to a bright bar moving at 10o/s across its receptive field. The model responds best when a normal motion stimulus moves in its preferred direction and when a reverse-phi motion stimulus moves in its null direction, as do many V1 cells in the macaque monkey (Livingstone, 2000).

inhibitory synaptic connection scheme, the non-discriminating zone of direction-selective cells demonstrated experimentally in retinal and cortical neurons (Livingstone, 1998; He *et al.*, 1999) should also reverse its location for reverse-phi stimuli. Secondly, the response amplitude to normal motion in the preferred direction should be larger than to reverse-phi in the null direction (Figs. 4-4C and 4-7B). The inputs from the LGN layer to the model cell are weaker and spread into both ON and OFF channels for reverse-phi stimuli. Thirdly, DI for reverse-phi motion should be more sensitive to parameter tuning than normal motion, especially for inhibitory input delay. Our input time course analysis (Figs. 4-2 and 4-3) suggests DI of reverse-phi motion is quite sensitive to the reversal rate: the higher the reversal rate, the weaker the input signals feeding into the direction-selective cell. This last property might show up in appropriate psychophysical studies as an increase in the motion detection threshold (increase of percentage of motion coherence or a decrease of Dmax).

In this study, we assume that direction selectivity is generated at the single cell level in a feed-forward manner, without the aid of local feedback circuits. There are extensive feedback interactions among V1 cells and these feedback currents are likely to be important for sharpening directional tuning (Douglas *et al.*, 1995; Maex and Orban, 1996). As we stated before, our models respond in an appropriate direction-selective manner to both types of motions over a broad parameter range, although DI was not always high. When DI was low, the response onset time for the preferred direction motion was less than for the null

direction motion. A network could use this difference in response onset time to increase DI if we assume neurons with the same direction preference have more excitatory feedback connection among themselves. In fact this difference alone is enough to generate direction selectivity through network interaction (Maex and Orban, 1996; Suarez, Koch and Douglas, 1995; Suarez 1995). Excitatory feedback might also help to produce balanced response amplitude for normal motion and reverse phi motion. In psychophysics experiments, human subject have the same detection threshold for normal motion and reverse-phi motion (Sato, 1989). Monkey V1 cell's response amplitudes to normal motion and reverse-phi motion are also comparable (M. Livingstone, personal communication). In our simulation, although DI=1 for normal motion and DI=-1 for reverse-phi motion, our model responds with many more spikes for the normal motion due to the low-pass nature (Krukowski and Miller, 2001) and half-wave rectification of our vision system. This difference can be decreased by network interactions if the feed-forward input triggers the cortical response and sets the directional bias, while the network itself determines the amplitude of the response. Of course, the use of shunting inhibition to compute the normal and reverse-phi direction selectivity does not rule out additional biophysical mechanisms to sharpen up this selectivity (Mel, 1993; Archie and Mel, 2000; Mel and Archie, 1998) such as facilitation in the preferred direction (Emerson *et al.*, 1987).

We use the term “excitation” and “inhibition”, rather than “facilitation” or “suppression” in this report. Facilitation and suppression usually refer to the non-linear part of a cell's response. We did not isolate linear responses from non-linear responses in our analysis, although the “same minus inverted” map (Fig. 4-6B and C) is a plot of the non-linear interaction and thus shows facilitation and suppression (Emerson *et al.*, 1987; Livingstone *et al.*, 2001). The non-linear suppression in the null direction comes from shunting inhibition. There is no significant non-linear facilitation in our model other than NMDA synaptic inputs. This might provide positive non-linear interaction in the real neuron. Because the excitatory input for reverse-phi motion spreads between ON and OFF channels, such facilitation could further increase the difference of response amplitudes. Excitatory feedback, missing in our feed-forward model, might underlie the facilitation in the preferred direction and might fill in the gap of response amplitude difference between normal and reverse phi motion.

In the traditional inhibition-based direction-selective scheme, shunting inhibition is not necessarily required if the neuron does not possess subunit structures. However, shunting inhibition is required for our double synaptic veto mechanism to restrict the interaction to local branches. As we stated in the results section, direction selectivity for both normal and reverse-phi motion decreases to almost zero when the inhibitory channel reversal potential decrease from –60 mV to –90 mV. Our double synaptic veto scheme requires branch-specific computations that cannot be achieved by non-shunting inhibition. Archie and Mel (2000)

demonstrated disparity tuning and reverse-phi like effects (Cogan *et al*., 1993; Cogan *et al*., 1995; Cumming and Parker, 1997; Ohzawa *et al*., 1997; Livingstone and Tsao, 1999) without shunting inhibition in a similar modeling study. The non-linear interaction underlying disparity tuning in their model is clustering (non-linear excitatory interaction). The basic non-linear direction interaction in our model is between the excitation and shunting inhibition; shunting inhibition is required for the on-path veto and direction selectivity. We only used one type of GABA synapse that has a long off ramp (80 ms) in our simulation. This long off ramp is only necessary to shut off the long lasting NMDA currents. If we set NMDA conductance to zero and GABA synapse off ramp to 2ms, the model is still direction-selective. In real neuron, fast and slow inhibitions co-exist.

The key to our double synaptic gating mechanism is that excitatory inputs are half-wave rectified and carry separate ON or OFF signals, while the inhibitory input carries both ON and OFF signals (in a spatially segregated manner). In our model, inhibition originates (via interneurons) from LGN ON and OFF center cells. The inhibition could, in principle, also be supplied by a cortical simple cell, with spatially offset ON and OFF regions within its receptive field. The separation of ON and OFF channels occurs at the very first mammalian visual processing stage in the retina (Rodieck, 1998). Within the mammalian visual system it is not until V1 that these two channels combine their information. Since the detection of reverse-phi requires interaction between ON and OFF channels and the simple

cell might be the first place that this interaction occurs, it was proposed (Livingstone *et al.*, 2001) that direction selectivity in the monkey might arise between the interactions of two simple cells that carry the full-wave signal. In the visual system of the fly, the reverse-phi effect observed in higher-order visual cells (Egelhaaf and Borst, 1992) was used to support the argument that there is no ON-OFF channel separation. Although ON-OFF interaction is necessary to account for reverse-phi motion, our results suggest only inhibition needs to carry the full-wave signal. The excitation to the direction-selective cell can originate from direct geniculate projection.

The synaptic triplet arrangement proposed here for our double synaptic veto scheme requires rather sophisticated synapse placement during the development process. Two inhibitory ON and OFF inputs need to make synapse close by their associated excitatory input or between this input and the cell body in order to be able to effectively veto excitation (Koch *et al.*, 1982). This is in contrast to traditional shunting inhibition schemes that only require the pairing of one inhibitory process for each excitatory one. It is possible that activity-dependent, temporally asymmetric Hebbian learning rules (Markram, 1997) might be used to establish such specific connection schemes as shown for normal direction selectivity by Rao and Sejnowski (2000). It does remain a major challenge to understand how direction-selective neurons with subunit structures could be established in an unsupervised manner on the basis of such learning rules.

Reverse-phi motion stimuli do not appear to be a common feature of natural spatiotemporal scenes. It therefore remains unclear why cortical cells should invert their direction selectivity for reverse-phi motion. We believe that the synaptic circuitry responsible for detecting reverse-phi motion has to be established as a by-product of developing normal direction selectivity, rather than as a stand-alone training process. If the inputs to direction-selective cortical neurons have a significant background-firing rate, then OFF inhibition at the preferred side of ON excitation is released when a white bar moves in the preferred direction and thus helps to increase direction preference. If the inhibition comes from simple cells, it naturally contains spatially offset ON and OFF signals. The challenge is to properly align the ON and OFF regions with excitatory inputs. We are currently investigating learning rules that could account for our double synaptic veto mechanism. The “prediction and sequence learning” mechanism proposed in (Montague and Sejnowski, 1994 and Montague *et al*., 1995) might play an important role in the establishment of the reverse-phi motion detection circuit.

Chapter Five

Models' Dependency on Shunting Inhibition

5.1 Introduction

The shunting inhibition refers to an increase in a chlorine based GABA_A conductance that reverses close to the cell's resting position. Such an inhibition is most effective when it fulfills the on-the-path condition. Our models require branch specific inhibitions which are implemented using shutting inhibition as illustrated in Fig. 5-1A. Inhibition 1 needs to decrease excitation 1 more than it does excitation 2. If we reverse excitation and inhibition locations, inhibition 1 still affects excitation 1 more than excitation 2. The excitatory input's effect on the soma increases while the inhibitory input's effect decreases in this case. In natural condition, inhibitory inputs are likely to be close to soma than excitatory inputs. Such a local veto effect breaks if we switch the locations of inhibition 1 and inhibition 2 or simply map al four synapses into a single dendritic compartment.

It is unclear if such local shunting effects exist in the real cells. Active channels tend to clamp membrane voltages during high frequency firing and thus reduce the shunting effect (Holt and Koch, 1997). Many experiments using white noise or depolarization to elevate cell's back ground firing rate to uncover inhibition (Citron and Emerson, 1983;Livingstone, 1998; Monier *et al*, 2003). Such

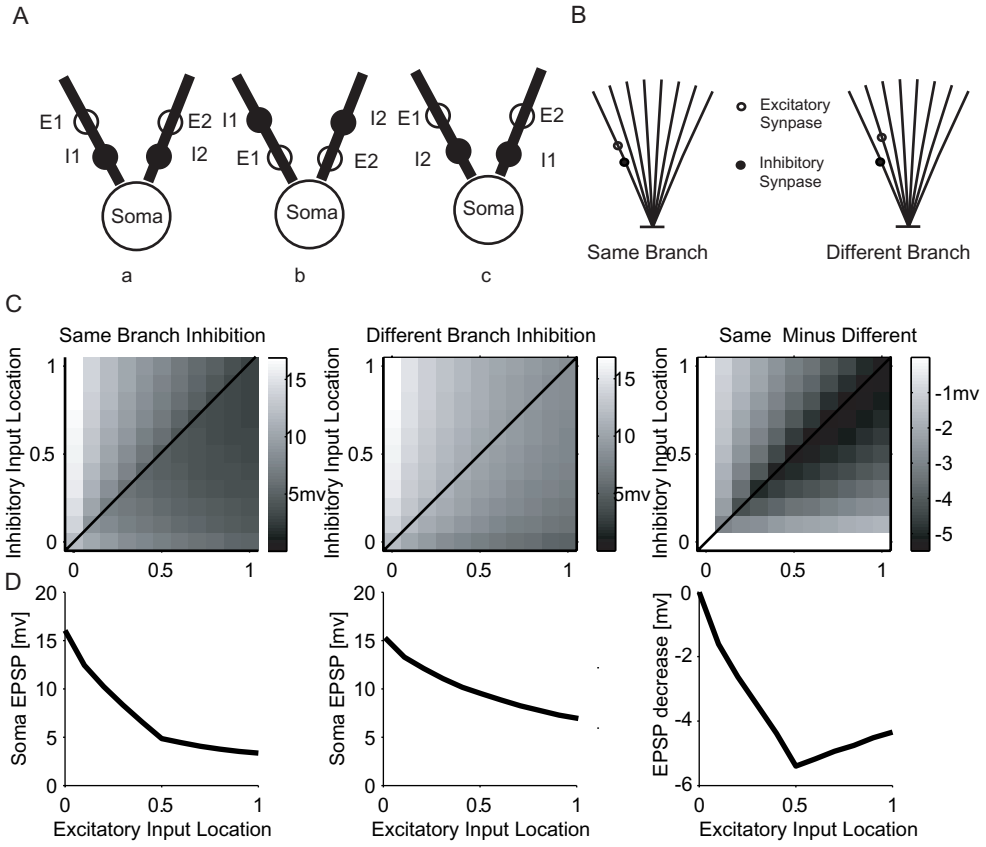

Fig. 5-1. The "local" effect of the shunting inhibition A schematic drawing of shunting inhibition's local effect. B Schematic drawing of the relative excitatory and inhibitory synapse locations. C. EPSP sizes measured at soma with same branch inhibitions, different branch inhibitions and the different between them. The 0 end of the dendrite is connected to the soma while 1 is the distal end. The inhibition and excitation co-locate at the diagonal line. The excitation is always to the distal end of inhibition (on-path) in the area below the diagonal line, where the inhibition is more effective than the area above the diagonal line. D. A line plot of C with inhibition fixed at the middle of the dendrite.

techniques drive the average membrane potential up and thus reduce the shunting effect. Recent experiments in the retina provide evidence in favor of at least some nonlinear interactions between excitatory and shunting inhibitory inputs that take place within the dendrites of direction-selective ganglion cells (Taylor *et al.*, 2000; for a dissenting view, see Borg-Graham 2001). Large conductance changes that reverse around the cell's resting potential have been observed in V1 during visual stimuli (Anderson *et al.*, 2000; Borg-Graham *et al*., 1998). In this chapter, we tested both our reverse-phi model and learning model's dependency on the shunting inhibition.

5.2 Optimal inhibitory and excitatory input locations on dendrite.

We first considered the optimal location for the shunting inhibition using our model cell. We varied the excitation and inhibition input location on dendrites and measure the EPSP amplitude at the soma as shown in Fig. 5-1C. The diagonal line shows the case where excitation and inhibition co-locate (in the "different branch inhibition" case, they are located on the same position in different dendrites). The excitation is always distal to the inhibition (on-the-path) in the area below the diagonal line of the "same branch inhibition" plot. Here the inhibition is more effective than above the diagonal line, where inhibition is distal to the excitatory synapse. The "same minus difference" plot shows shunting inhibition's local veto effect. Shunting inhibition is more effective in blocking the "same branch excitation" compared to the "different branch excitation" when the "on-the-path" condition is fulfilled. Such local veto effect decreases to zero when

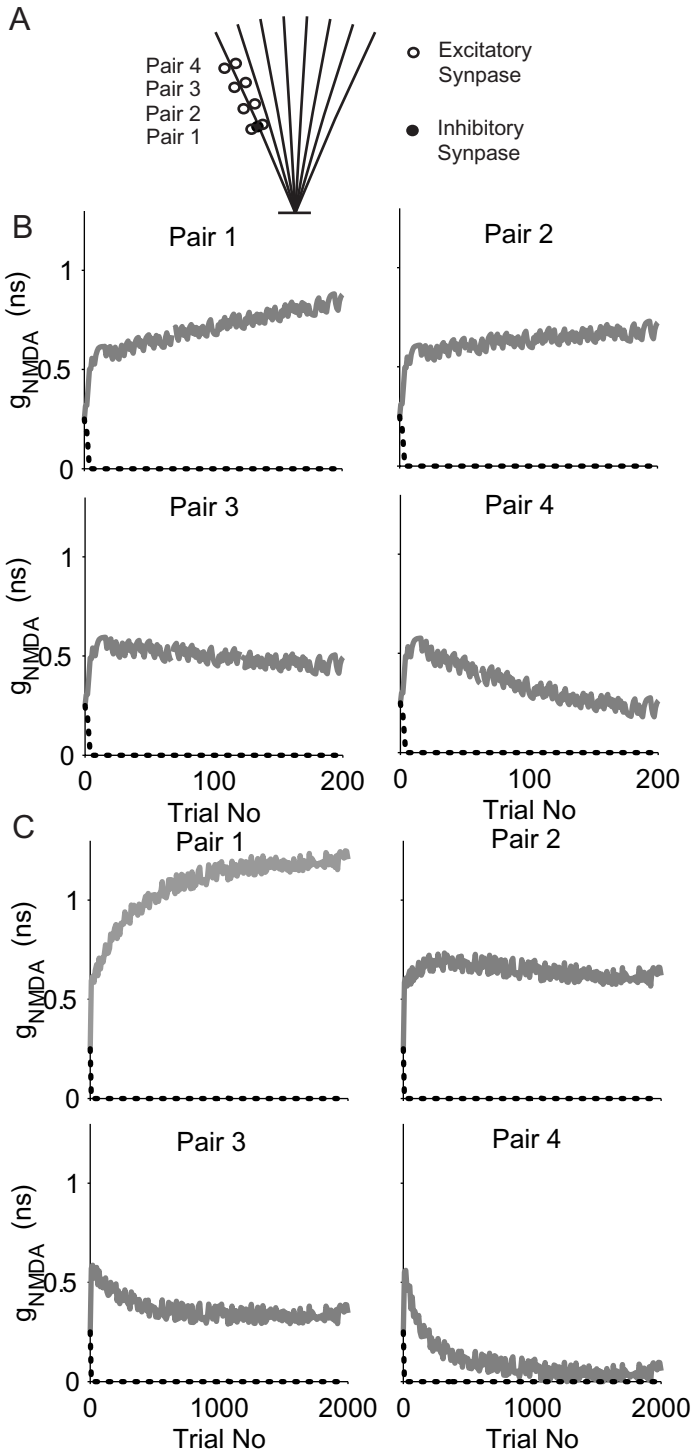

Fig. 5-2. The relative position of excitatory synapse on dendrites affect learning A. 4 pairs (one left, one right, 0.3 ns) of excitatory inputs are mapped onto one dendrite of the model cell, position 0.5, 0.6, 0.7, 0.8, respectively. The inhibitory input is mapped onto position 0.5. B. The closer the excitatory synapse to the soma, the larger its final weight. Solid line: synaptic weight changes for all the left inputs during training. Dashed line: synaptic weight changes for all the right inputs during training. C. Same simulation as in B but with a longer training period.

the inhibition input location is too close to the soma. In our learning model, the inhibitory input location is fixed at the middle of the dendrite (0.5).

We also considered the optimal excitatory input location when the inhibitory input location is fixed at the middle of the dendrite. Four pairs of excitatory synapses were mapped onto different locations on one dendrite, all of which fulfilling the "on-the-path" condition. The "competition" rule worked over all eight excitatory synapses. Fig. 5-2 shows the closer the excitation to the soma, the larger the connection weight after learning. This is expected, given the decrease in the amplitude of the back action potential propagating back from the soma to the distal dendrites. The excitatory connections to the distal end did not drop to zero after training, but rather settled to a lower value than those toward the proximal end. This was due to the sliding threshold we imposed: the smaller the connection weight, the lower the peak calcium concentration required for an increase in the weight of the excitatory synapse. Excitatory connections tend to reside at the distal end of dendrites in real cells with some possible scaling at the distal ends to keep the amplitude of the somatic EPSP constant. If there is an underlying mechanism that favors distal excitatory connection, our learning rule, which works against this trend, can help produce a balanced dendritic tree.

5.3 The Reverse-phi Mode's dependency on shunting inhibition

To test whether shunting inhibition is required for the direction selectivity we observe, we decreased the GABA channel reversal potential from –60 mV to –90

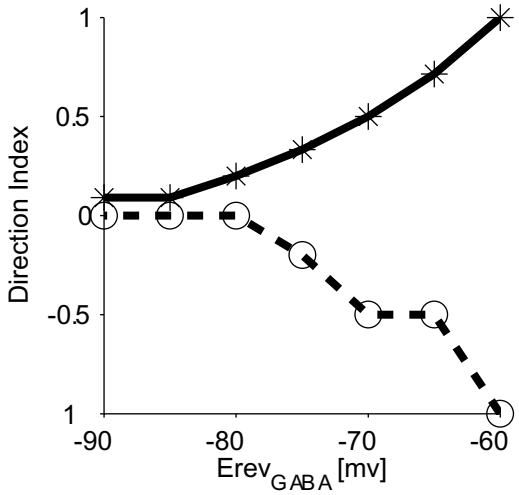

Fig. 5-3. The reverse-phi model requires shunting inhibition. Solid line: Model's direction selectivity for the normal motion given different GABA channel reversal potentials. Dashed line: Model's direction selectivity for the reverse-phi motion given different GABA channel reversal potentials

mV in 5 mV steps. At the same time we decreased the amplitude of g_{GABA} accordingly so that the model always responded to a preferred direction normal motion stimuli with 6 spikes and null direction reverse-phi stimuli with 3 spikes. DI for both types of motions decreased when the GABA channel reversal potential was decreased (Fig. 5-3). At –90 mV, the model responded with 5 spikes to null direction normal motion stimuli and with 3 spikes to preferred direction reverse-phi motion stimuli. Thus the direction selectivity was lost.

The reverse-phi model's dependency on the shunting inhibition is expected. Our double veto mechanism involves null side same-type inhibitions and preferred side different-type inhibitions. If we mix these inhibitions from different dendritic branches, the model will receive symmetric input in space-time and thus has neither normal nor reverse-phi motion selectivity.

5.4 The learning model's dependency on shunting inhibition

To test whether the shunting inhibition is required for our learning model, we decreased the GABA channel reversal potential from –60 mV to –80 mV in 5 mV steps. Note that the cell's resting potential was always -60mV. 10 simulation runs were conducted for each reversal potential. The average DI of the model cell after training is shown in Fig. 5-4A. Our results show that the single-unit learning model is not dependent on the shunting inhibition. This is not surprising since the single-unit learning model has no dendritic subunit and thus local inhibition is not required. Any global inhibition can fulfill its requirement. However, the

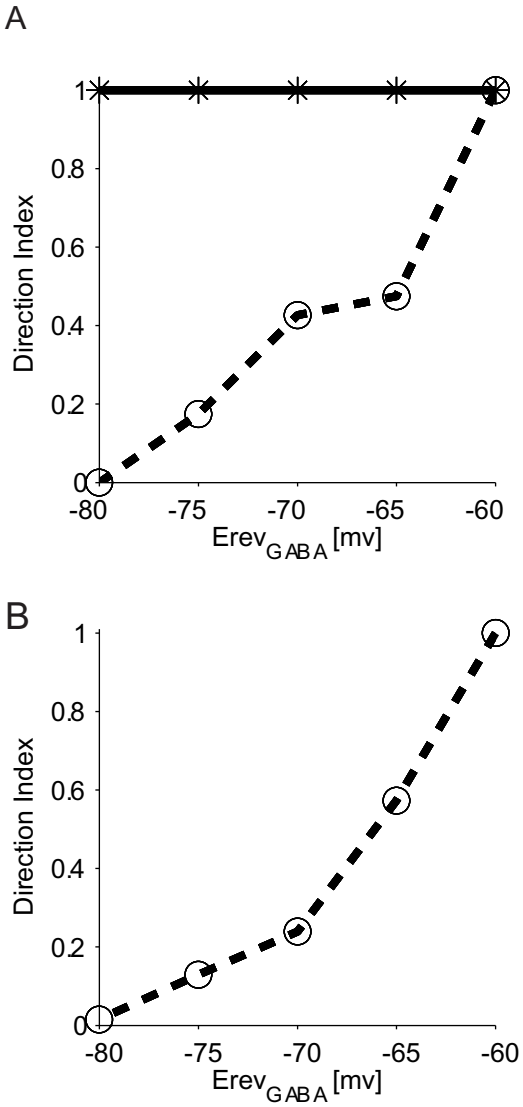

Fig. 5-4. Learning model's dependency on the shunting inhibition. A. The single-unit learning model doesn't require shunting inhibition while the multi-subunits learning model's performance decreases with respect to GABA channel reversal potentials. Solid line: Average DI values of the single-unit learning model at different GABA channel reversal potentials. Dashed line: Average DI values of the multi-subunits learning model at different GABA channel reversal potentials. B. Multi-subunits learning model's performance decreases with respect to the GABA channel reversal potential. The overall inhibitory connection strength is decreased to allow the model to produce equal number of spikes in a preferred direction movement.

assumption here is that the model cell has zero or very low background firing rate. The threshold thus performs the non-linear operation between two spatial offset inputs, which is required by all direction-selective models. If, however, the model cell has a high background firing rate, then the model cell will not even be direction-selective if we use non-shunting type inhibition and look for the time averaged response (Borst and Egelhaaf, 1989). Shunting inhibition is required in this case to generate basic direction selectivity.

The multi-subunits learning model's performance is dependent on the shunting inhibition. At -80 mV, 20 mV away from the resting potential, all direction selectivity is lost. In such simulation runs, the overall inhibitory current became larger as we gradually decreased the GABA channel's reversal potential. To control for such variations we used two types of compensation. In the first scheme, we decreased the amplitude of g_{GABA} accordingly, so that the model always responded to a preferred direction normal motion stimulus with 7 spikes if all connections within an entire input group reached their maximum connection values and those of the other input group dropped to zero. The average DI after trainings with respect to the GABA channel reversal potential is shown in Fig. 5-4B. The learning model's performance still decreased dramatically when the shunting condition was not met. At -60mv, the model cell responded with 7 spikes in its preferred direction and no spike in its null direction. The direction index was 1. At -80mv, when we lowered the g_{GABA} to allow 7 spikes in the

preferred direction, the model cell responded with 3 spikes in the null direction. Therefore the DI of the learning product was less than 1 in this case.

In the second scheme, we relaxed the spike number requirement for the learning model. At each reversal potential, we lowered the inhibitory synaptic connection strength until the model cell started to spike in the null direction given the maximum excitatory connection strength. Thus the inhibitory synapse weight we used in this scheme was greater than the value used in the above case. The DI of the ultimate learning product was 1 at all reversal potentials but the model produced less spikes when the inhibition was away from the resting values. The average DI and spike numbers for learning models with 4 subunits (solid curve), 6 subunits (dashed curve), and 8 subunits (dotted curve) are shown in Fig. 5-5. The spike number refers to the maximum number of spikes the model cell can generate in its preferred direction while maintaining DI=1. Our results suggest the more subunits the model cell has, the more its performance depends on the shunting inhibition. In the four subunits model, the excitatory inputs to dendrite 1 and dendrite 2 open before any inhibition opens, given the spatial offset and temporal delay of the inhibition. Therefore only 2 of 4 subunits' learning are affected by the non-shunting type later inhibitory current. 4 of 6 units and 6 of 8 units are affected in the 6 and 8 subunits models, making them rely more and more on shunting inhibition. Synaptic weight changes during a simulation run for the 6 subunits model and for the 8 subunits model are shown in Figs. 5-6 and 5-7. The GABA channel reversal potential for these two simulations was -80mV.

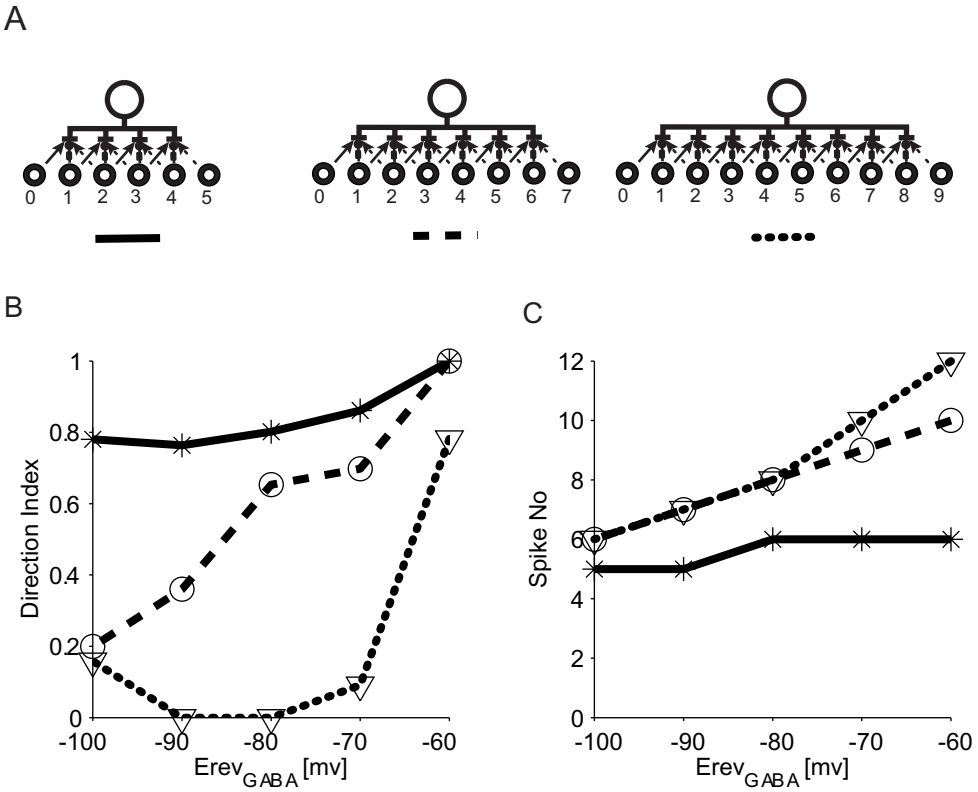

Fig. 5-5. Multi-subunits learning model requires the inhibition to be of the shunting type. A. A schematic drawing of model cells with four (solid curve), six (dashed curve) and eight subunits (dotted curve) on their dendrites. B. Average DI values of the multi-subunits learning model at different GABA channel reversal potentials. The more subunits the learning model has, the more it depends on shunting inhibition. C. Maximum number of spikes the model cell can produce during a preferred direction run at DI=1 given different GABA channel reversal potentials.

We can see from the weight change that the late subunits lost synchronization with the first few subunits and learned to be selective to a different direction. The model cell was less direction-selective compared to the case of shunting inhibition.

The other important aspect of shunting inhibition is that it allows more subunits to contribute to the cell's overall response. This is most obvious when going from 4 units to 8 units; the model cell produced much more spikes in the shunting condition than the non-shunting condition (Fig. 5-5B). A model cell implementing the non-shunting type inhibitions faces a dilemma: if it allows the late subunits to contribute to the cell's response in the preferred direction, the inhibitory input strength has to be decreased as in our first compensation scheme and the model cell's DI suffers; if it keeps its DI value at 1, then the inhibition input strength has to be increased and all late responses are wiped out. Therefore shunting inhibition and its local veto property are desirable for direction-selective cells with subunit structures on their dendrites.

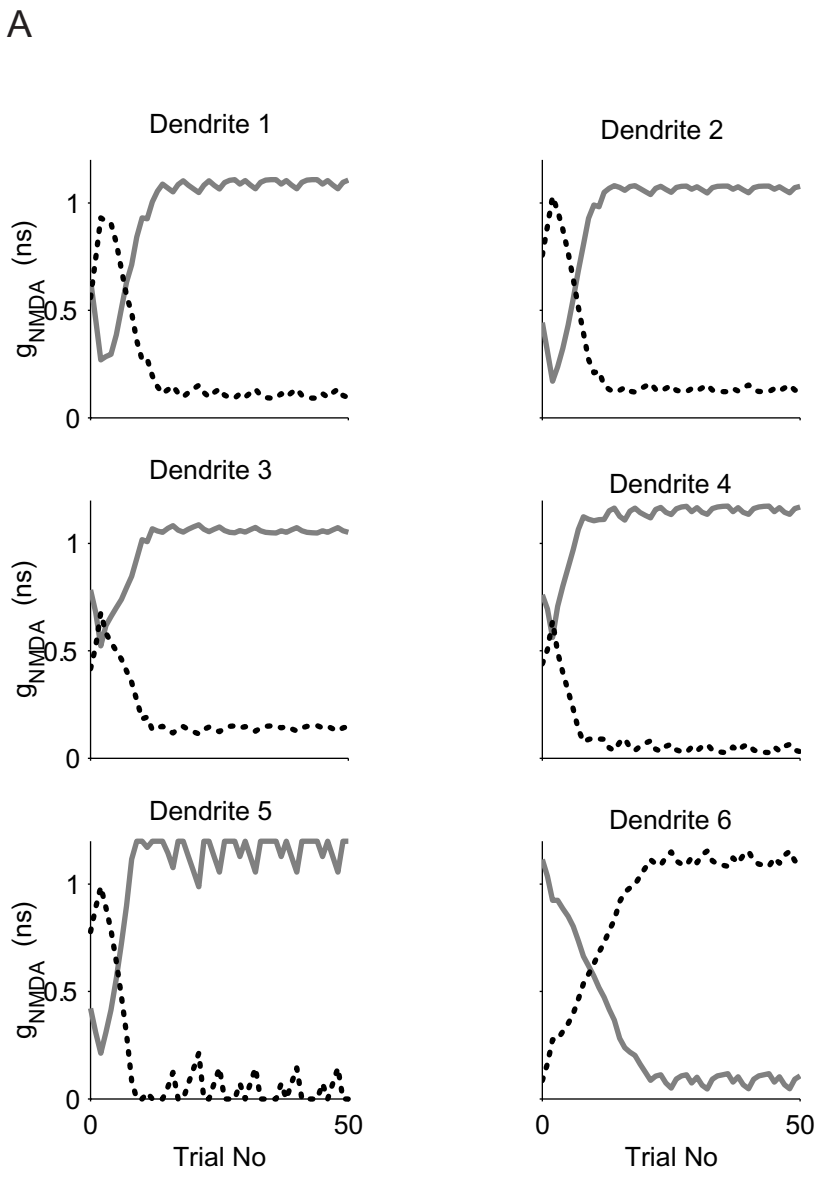

Fig. 5-6. GABA channel's reversal potential affects learning model's performance. Synaptic weight changes for the left input cells (solid curves) and the right input cells (dotted curves) at each dendrite during one simulation run. GABA channel's reversal potential is set to -80mv. The subunit on dendrite 6 fails to reach the same direction selectivity as the rest subunits.

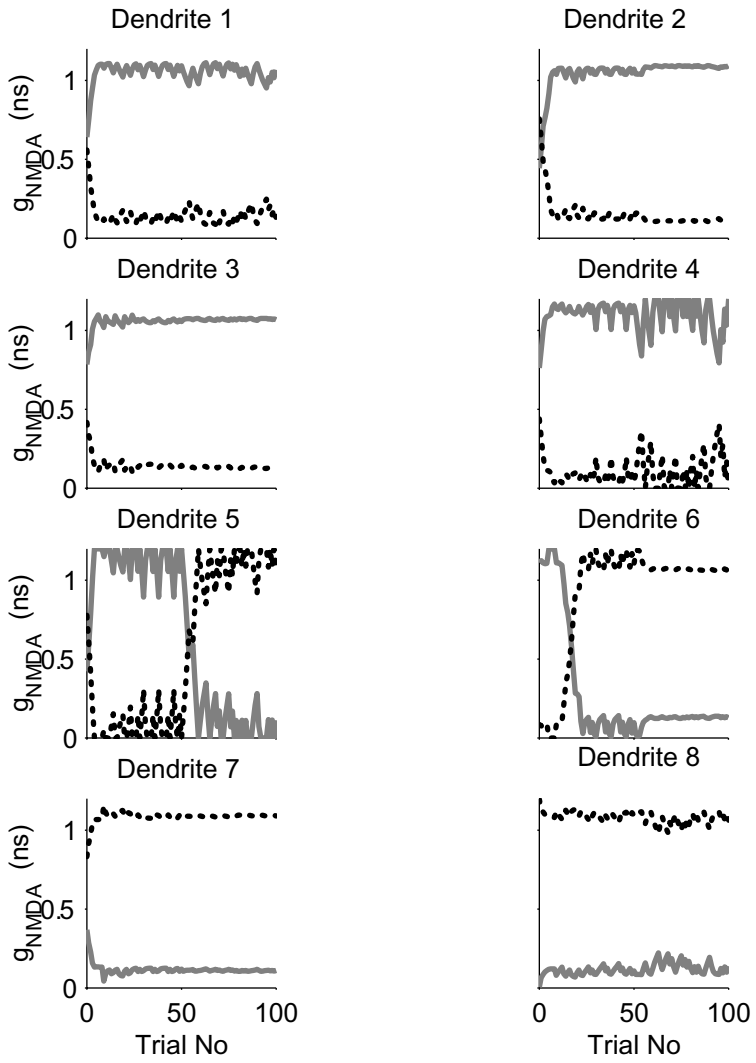

Fig. 5-7. GABA channel's reversal potential affects learning model's performance. Synaptic weight changes for the left input cells (solid curves) and the right input cells (dotted curves) at each dendrite during one simulation run. GABA channel's reversal potential is set to -80mv. The direction selectivity of subunits on dendrite 1-4 is different from that of subunits on dendrite 5-8.

Chapter Six

A Learning Rule for the Reverse-Phi Selective Synaptic Placement

6.1 Introduction

Our “double veto” mechanism described in Chapter Four can account for the reverse-phi effect first observed by Anstis (Anstis, 1970; Anstis and Rogers, 1975). Subjects perceived the reverse direction of motion when the contrast of a moving object reversed in the second frame of a two-frame shift experiment. Reverse-phi motion stimuli do not appear to be a common feature of natural spatiotemporal scenes. It therefore remains unclear why cortical cells should invert their direction selectivity for reverse-phi motion. We believe that the synaptic circuitry responsible for detecting reverse-phi motion has to be established as a by-product of developing normal direction selectivity, rather than as a stand-alone training process. Here we show such a connection might be established due to the background firing of inhibitory input cells, which causes bias in the learning outcome.

6.2 The reverse-phi learning scheme

In our learning model, the incoming stimuli sequence plays the key role of breaking the balance of initially balanced excitatory inputs and pushes the model beyond the divergent point. If the input connections are biased, the learning

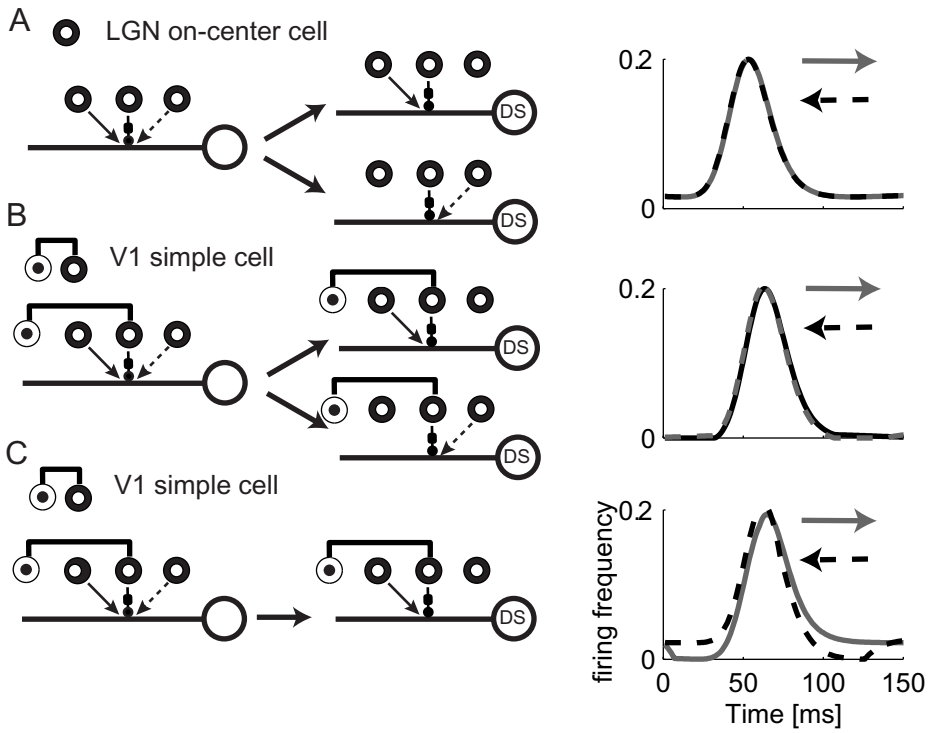

Fig. 6-1. Receptive field substructures of the inhibitory input cell can bias learning outcomes. (a) A model cell receiving input from an inhibitory cell with only an ON receptive field has equal chances to become a left or a right motion-selective cell. Instantaneous firing frequencies of the inhibitory cell during bar movement presentations are shown on the right. Solid curve: Rightward motion. Dashed curve: leftward motion. (b) A model cell receiving input from an inhibitory cell with an OFF-ON simple cell-like receptive field and no background firing has equal chance to become a left or to become a right motion-selective cell. (c) A model cell receiving input from an inhibitory cell with an OFF-ON simple cell like receptive field and a 20Hz, 10% background firing is biased to become a right motion selective cell. The resulting "double veto" is equivalent to a tri-synapse connection proposed by Mo and Koch, 2003.

outcomes are also expected to be biased. Receptive field substructures of the inhibitory input cell can play such a role to bias the learning outcomes. Fig. 6-1A shows a model cell receiving inputs from an inhibitory cell with only an ON receptive field which is the same single-unit learning model as described in chapters two and three. Instantaneous firing frequencies of the inhibitory cell during a bar moving to the right (solid line) and to the left (dashed line) are shown in the right of the figure. There is no difference in the inhibitory time course with respect to the motion direction. Therefore, in the absence of any other biases, the model cell is as likely to become a left motion-selective cell as a right one after learning. However, if the inhibitory input comes from a simple cell with spatially offset ON-OFF regions (Bishop *et al*., 1973; Heggelund, 1986; Jones and Palmer, 1987;Ferseter, 1988; Deangelis *et al*. 1993), the situation is more complicated. Two such inhibitory inputs with OFF excitatory regions to the left side of the ON excitatory regions are shown in Fig. 6-1B (background firing rate 0) and Fig. 6-1C (background firing rate 20Hz 10% of the peak firing rate). In the case of 10% background firing (in the absence of any input), there is a difference in the inhibitory input time course with respect to motion direction. If a white bar moves from the left to right (solid curve), it reaches the OFF region of the inhibitory input cell first and thus drops the cell's firing rate to 0. It then reaches the left excitatory input cell. The excitatory input causes the model to spike. The bar finally reaches the ON region of the inhibitory input cell. The inhibition blocks input from the right excitatory input cell. The left excitatory cell's connection strength is increased and the right excitatory cell's connection is decreased

according to our learning model. However, if the bar moves from the right to left (dashed curve), there is no such clamping of inhibitory firings by the OFF region. If the inhibitory input cell spikes before the right input cell due to its random background firing, the right excitatory input's connection strength won't be increased although the bar moves in its preferred direction during this trial. Such a scenario gives the left excitatory cell advantage in competition. The advantage doesn't exist if the inhibitory input has a zero background firing rate as shown in fig. 6-1B.

6.3 The background firing of inhibitory inputs can facilitate the " double veto" synaptic placement

We implemented the learning scheme described above in our learning model. To account for the inhibitory background firing, we used a stochastic model for inhibitory synapse. At any moment during the simulation, the probability of an inhibitory synapse opening was related to its instantaneous firing frequency based on its background firing rate plus the stimuli driven firing. Histograms of synaptic opening events during a simulation run for all the leftward and rightward movements trials during a simulation run are shown in Fig. 6-2A. The background firing rate was 20Hz. Note the shape of the histograms resembles the instantaneous firing frequency curves of Fig. 6-1C. Synaptic weight changes from both excitatory inputs during the simulation are shown in Fig. 6-2B. The model cell learned to be direction-selective after training with DI=1.

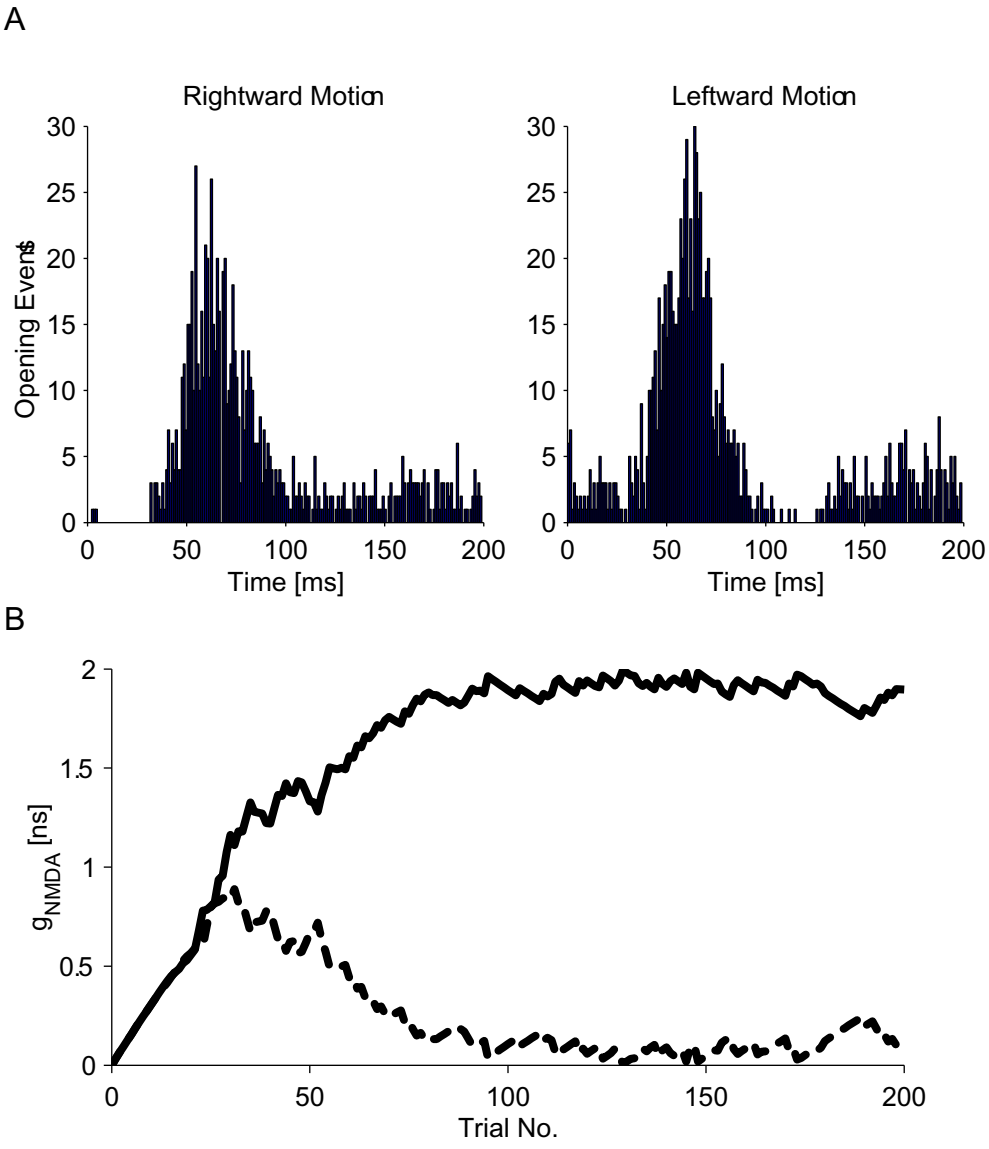

Fig. 6-2. A simulation run of the learning model receiving simple cell-like inhibitory input. A. Inhibitory synaptic opening events during the whole training process. The histograms resemble the LGN instantaneous firing frequency curves shown in Fig 6-1c. B. Synaptic weight changes for the left input cell (solid curve) and the right input cell (dotted curve) during one simulation run.

There are two possible learning outcomes for such learning model; one is reverse-phi selective; the other is not (Fig. 6-3A). We looked at the relationship between the percentage of simulation converged to be reverse-phi selective versus the inhibitory input's background firing rate (Fig. 6-3B). DI values represented the average of 20 simulations at each different background firing frequency). At 20Hz, 10% of the 200 HZ peak firing rate, the model cell converged to the reverse-phi synapse placement 100% times. Therefore, it is possible that such a "double veto" synaptic placement, as we propose, can be established as a byproduct of the normal direction selectivity development process.

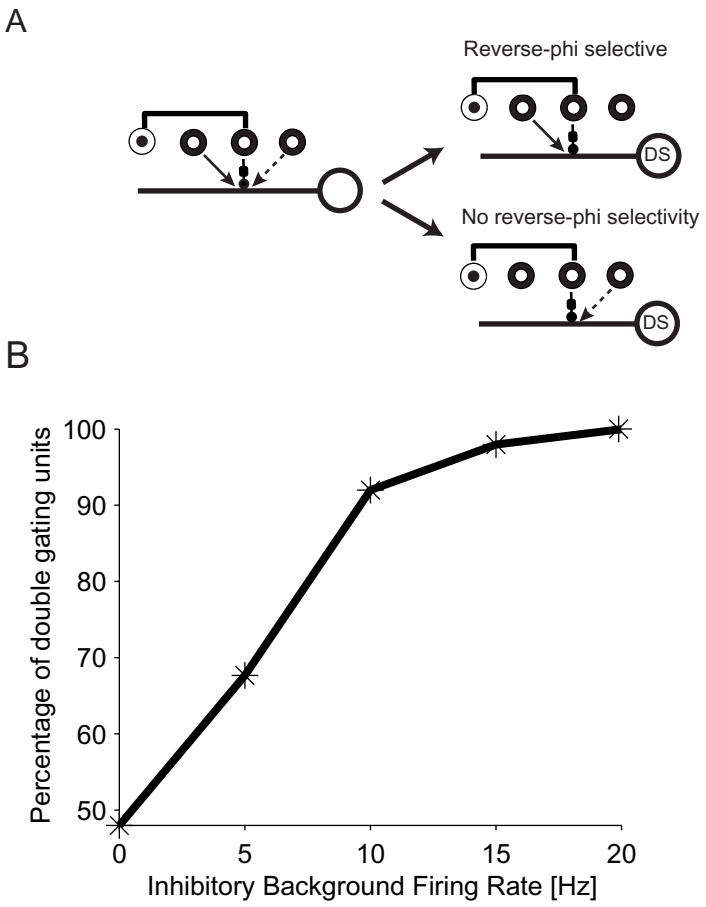

Fig. 6-3. The rate of convergence to the double synaptic veto connection depends on the inhibitory input's background firing rate. A. A schematic drawing of the two possible outcomes of the learning model. B. The percentage of the double veto units increases with the inhibitory background firing rate. The peak inhibitory background firing rate is held at 200Hz.

Chapter Seven

Summary

There is considerable interest in activity based synaptic learning rules. Given the complexity of our brain, it is impossible to genetically specify each synaptic connection exactly. Instead, the development process may involve experience-dependent neural plasticity (Quartz and Sejnowski, 1997; Quartz, 1999). In this thesis, a learning model for direction-selective synapse placement based on local calcium concentration at spines is proposed. The same principle can be applied to other learning scenarios that require specific excitation-inhibition interactions.

We tested our learning rule in compartmental simulations. We implemented a simple calcium scheme and used the computed calcium concentration at spines during simulations to direct synaptic weight changes. The model cell implementing our learning rule is direction-selective after learning. The learning model is stable under a variety of starting conditions. Jacobs *et al*. (2001) demonstrated that cortical regions involved in later stages of information processing have more complex dendritic/spine system than that of early stages of processing. Dendritic subunit learning rules are likely to be even more important in the proper development of these areas. Our model cell's simple geometry allows us to simulate dendritic subunits learning scenarios. Our simulation results prove our learning rule is indeed local: the input connection

strength after training depends on its post-synaptic location. In our model, the difference among locations is caused by inhibitory inputs to different branches. Based on our model, we made a few predications in the discussion section of Chapter Two that can be tested in experiments. Possible extension of modeling studies is also discussed.

We also proposed a global inhibition learning rule this is dependent on the overall excitatory state of the cell. The inhibition learning rule works together with our excitation to achieve excitation-inhibition differential learning. A model cell implementing such learning rules is direction-selective after training. Much less is known about the learning mechanism of inhibitory synapses than that of excitatory synapses. It will be interesting to see if our inhibitory learning scheme exists in nature.

Reverse-phi is an interesting visual illusion. It can help us to understand the direction-selective scheme evolution chose to adopt given the fact that the cellular reverse-phi equivalent has been discovered in a variety of animal systems. In this thesis work, we presented for the first time a biophysical model that can account for both the normal and reverse-phi direction selectivity. The model's response to bar stimuli was compared with the response of real cells recorded in monkey V1. Our double synaptic-veto mechanism, in which ON excitatory synapses are gated by both delayed ON inhibition at their null side and by delayed OFF inhibition at their preferred side, is an extension of the original

asymmetric-delayed shunting inhibition scheme. We reason such a double veto can come from cortical simple cells.

We used shunting inhibition in both of our models to achieve branch specific veto of excitations. We discussed shunting inhibition's local effect and our model's dependency on this special type of inhibition. Our reverse-phi model and multiple subunits learning model depend on the shunting inhibition while the single-unit learning model does not. We showed in our simulations how shunting inhibition can help to achieve dendritic specific local learning. Shunting inhibition can clamp membrane voltage and thus reduce the amount of calcium flow through nearby NMDA channels. Shunting inhibition can block back-propagating spikes from reaching its distal side. Given the local nature of the shunting inhibition, both of these effects only affect the dendritic branch that the inhibition resides within a certain parameter tuning range. Although no experimental evidence exists, so far, on such effects of shunting inhibition, there is evidence suggesting that shunting inhibition is important to cell's direction selectivity (Taylor *et al*., 2000). Large conductance changes of cortical cells have been observed during visual stimuli, which is also consistent with the existence of shunting inhibition (Anderson *et al*., 2000; Borg-Graham *et al*., 1998). It is interesting to see if nature can use the shunting inhibition not only to achieve local dendritic specific computation but also learn the appropriate synaptic placement.

Finally, our learning rule can facilitate the placement of the double synaptic veto connections proposed to account for the reverse-phi selectivity. This can be achieved through an inhibitory input with simple cell-like receptive field structure and low background firing rate. This is consistent with our idea that the reverse-phi selectivity is formed as a by-product of the normal direction selectivity, given that there are no substantial reverse-phi stimuli in the natural scenes.

References

Abbot, LF. and Nelson, SB. (2000) Synaptic plasticity: taming the beast. *Nature Neuroscience* ***3*** **Suppl**:1178-1183

Adelson, EH. and Bergen, JR. (1985) Spatiotemporal energy models for the perception of motion. *J. Opt. Soc. Am. A* **2:**284-299

Anderson, JC., Binzegger, T., Kahana, O., Martin, KAC. and Segev, I. (1999) Dendritic asymmetry cannot account for directional responses of neurons in visual cortex. *Nature Neuroscience* **2:**820-824

Anderson, JS., Carandini, M. and Ferster, D. (2000) Orientation tuning of input conductance, excitation, and inhibition in cat primary visual cortex. *J. Neurophysiology* **84:**909-926

Anstis, SM. (1970). Phi movement as a subtractive process. *Vision Research* **10:**1411-1430

Anstis, SM. and Rogers, BJ. (1975). Illusory reversal of visual depth and movement during changes of contrast. *Vision Research* **15:**957-961

Anstis, SM. and Rogers, BJ. (1986). Illusory continuous motion from oscillating postive-negative patterns: implications for motion perception. *Perception* **15:**627-640

Archie, KA. and Mel, BW. (2000) A model for intradendritic computation of binocular disparity. *Nature Neuroscience* **3:**54-63

Barlow, HB., Hill, RM. And Levick, WR (1964) Retinal ganglion cells responding selectively to direction and speed of image motion in the rabbit. *J.*

Physiology. **173**:377-407

Barlow, HB. and Levick, WR. (1965) The mechanism of directional selectivity in the rabbit's retina. *J. Physiology* **173:**477-504

Benison G, Keizer J, Chalupa LM, Robinson DW. (2001) Modeling temporal behavior of postnatal cat retinal ganglion cells. *J Theor Biol* **210**:187-199

Bienenstock, EL., Cooper, LN., and Munro, PW. (1982) Theory for the development of neuron selectivity: orientation specificity and binocular interaction in visual cortex. *J Neuroscience* **2**:32-48

Bishop, PO., Goodwin, AW. and Henry, GH. (1973) Direction selective sub-regions in striate simple cell receptive fields. *J. Physiology* **238**:25-27

Bito, H., Deisseroth, K. and Tsien, RW. (1997) Ca2+-dependent regulation in neuronal gene expression. *Curr Opin Neurobiol*. **7**:419-429

Blais, B., Cooper, LN., and Shouval, H. (2000) Formation of direction selectivity in natural scene environments. *Neural Computation* **12**:1057-1066

Bliss TV, Lomo T. (1973) Long-lasting potentiation of synaptic transmission in the dentate area of the anaesthetized rabbit following stimulation of the perforant path. *J Physiol* **232**:331-356

Borg-Graham, LJ., Monier, C. and Frégnac, Y. (1998) Visual input evokes transient and strong shunting inhibition in visual cortical neurons. *Nature* **393**:369-373

Borg-Graham, LJ., (2001) The computation of directional selectivity in the retina occurs presynaptic to the ganglion cell. *Nat Neurosci*. **4**:176-183

Borst, A. (2001) Direction selectivity in ganglion cells: pre or post? *Nat Neurosci*.

4:119-20.

Borst, A. and Egelhaaf, M. (1989) Principles of visual motion detection. *Trends Neurosci*. **12**:297-306

Carmignoto, G. and Vicini, S. (1992) Activity-dependent decrease in NMDA receptor responses during development of the visual cortex. *Science.* **258**:1007-1011

Castellani, GC. Quinlan, EM., Cooper, LN., and Shouval, HZ. (2001) A biophysical model of bidirectional synaptic plasticity: Dependence on AMPA and NMDA receptors. *PNAS* **98**:12772-12777

Chance, FS., Abbott, LF., and Reyes, AD. (2002) Gain modulation from background synaptic Input. *Neuron* **35**:773-782

Chubb, C. and Sperling, G. (1989) Two motion perception mechanisms revealed through distance-driven reversal of apparent motion. *Proc. Natl. Acad. Sci. USA* **86:**2985-2989

Citron, MC. and Emerson, RC. (1983) White noise analysis of cortical directional selectivity in cat. *Brain Res*. **279**:271-279

Clifford, CW. and Ibbotson, MR. (2003) Fundamental mechanisms of visual motion detection: models, cells and functions. *Prog Neurobiol*. **68**:409-37

Cogan, AI., Lomakin, AJ. and Rossi, AF. (1993) Depth in anticorrelated stereograms: effects of spatial density and interocular delay. *Vision Res*. **33**:1959-1975

Cogan, AI., Kontsevich, LL., Lomakin, AJ., Halpern, DL., and Blake R. (1995) Binocular disparity processing with opposite-contrast stimuli. *Perception.*

24:33-47

Collingridge, GL., Kehl, SJ., and McLennan, H. (1983) Excitatory amino acids in synaptic transmission in the Schaffer collateral-commissural pathway of the rat hippocampus. *J. Physiol.* **334**:33-46

Conway, BR. and Livingstone, MS. (2001) Space-time maps and two-bar interactions of direction-selective cells in macaque V-1. *(in press)*

Cumming, BG., and Parker, AJ. (1997) Responses of primary visual cortical neurons to binocular disparity without depth perception. *Nature* **389**:235-237

Cummings, JA., Mulkey, RM., Nicoll, RA. and Malenka, RC. (1996) Ca2+ signaling requirements for long-term depression in the hippocampus. *Neuron.* **16**:825-833

Cynader, M. and Chernenko, G. (1976) Abolition of direction selectivity in the visual cortex of the cat. *Science* **193**:504-505

DeAngelis GC, Ohzawa I, Freeman RD. (1993) Spatiotemporal organization of simple-cell receptive fields in the cat's striate cortex. I. General characteristics and postnatal development. *J Neurophysiol*. **69**:1091-1117

Destexhe, A., Mainen, ZF., and Sejnowski, TJ. (1994) Synthesis of models for excitable membranes, synaptic transmission and neuromodulation using a common kinetic formalism. *J Comput Neurosci* **1**:195-230

Dingledine, R. (1983) N-methyl aspartate activates voltage-dependent calcium conductance in rat hippocampal pyramidal cells. *J Physiol.* **343**:385-405

Douglas, RJ., Koch, C., Mahowald, M., Martin, KAC. and Suarez, HH. (1995)

Recurrent excitation in neocortical circuits. *Science* **269:**981-985

Dudek, SM and Bear, MF (1992) Homosynaptic long-term depression in area CA1 of hippocampus and effects of N-Methyl-D-Aspartate receptor blockade *PNAS* **89**:4363-4367

Egelhaaf, M. and Borst, A. (1992) Are there separate ON and OFF channels in fly motion vision? *Visual Neuroscience* **8**:151-164

Emerson, RC. (1997) Quadrature subunits in directionally selective simple cells: spatiotemporal interactions. *Vis Neurosci* **14**:357-371

Emerson RC, Bergen JR, Adelson EH. (1992) Directionally selective complex cells and the computation of motion energy in cat visual cortex. *Vision Res.* **32**:203-128

Emerson, RC., Citron, MC., Vaughn, WJ. and Klein, SA. (1987) Nonlinear directionally selective subunits in complex cells of cat striate cortex. *J. Neurophysiology* **58:**33-65

Emerson, RC. and Gerstein, GL. (1977) Simple striate neurons in the cat. II. Mechanisms underlying directional asymmetry and directional selectivity. *J Neurophysiol.* **40**:136-155

Ernst, UA., Pawelzik, KR., Sahar-Pikielny, C. and Tsodyks, MV. (2001) Intracortical origin of visual maps. *Nat Neurosci.* **4**:431-436

Feidler, JC., Saul, AB., Murthy, A. and Humphrey, AL. (1997) Hebbian learning and the development of direction selectivity: the role of geniculate response timings. *Network: Comput. Neural Syst*. **8**:195-214

Ferster, D. (1988) Spatially opponent excitation and inhibition in simple cells of

the cat visual cortex. *J Neuroscience* **8**:1172-1180

Fischer, M., Kaech, S., Wagner, U., Brinkhaus, H. and Matus A. (2000) Glutamate receptors regulate actin-based plasticity in dendritic spines. *Nat Neurosci.* **3**:887-894

Gabbiani, F., Krapp, HG. and Laurent, G. (1999) Computation of object approach by a wide-field, motion-sensitive neuron. *J Neurosci* **19**:1122-1141

Gabbiani, F., Mo, C. and Laurent, G. (2001) Invariance of angular threshold computation in a wide-field looming-sensitive neuron. *J. Neuroscience* **21:**314-329

Gamble E, Koch C. (1987) The dynamics of free calcium in dendritic spines in response to repetitive synaptic input. *Science*.**236**:1311-1315

Ganz, L. and Felder, R. (1984) Mechanism of directional selectivity in simple neurons of the cat's visual cortex analyzed with stationary flash sequences. *J Neurophysiol.* **51**:294-324

Goodwin, AW., Henry, GH. and Bishop, PO. (1975) Direction selectivity of simple striate cells: properties and mechanism. *J Neruophysiol*. **38**:1500-1523

Grigonis, AM., Zingaro, GJ. and Murphy, EH. (1988) The development of orientation and direction selectivity in the rabbit visual cortex. *Brain Res.* **468**:315-318

Hatsopoulos N, Gabbiani F, Laurent G. (1995) Elementary computation of object approach by a wide-field visual neuron *Science* **270**:1000-1003

He, S., Jin, ZF. and Masland, RH. (1999) The nondiscriminating zone of directionally selective retinal ganglion cells: Comparison with dendritic

structure and implications for mechanism. *J. Neuroscience* **19**:8049-8056

Hebb, DO. (1949) The Organization of Behavior: A Neuropsychological Theory. *Wiley, New York*.

Heggelund, P. (1986) Quantitative studies of enhancement and suppression zones in the receptive field of simple cells in cat striate cortex. *J Physiol*. **373**:293-310

Helmchen, F., Svoboda, K., Denk, W. and Tank, DW. (1999) In vivo dendritic calcium dynamics in deep-layer cortical pyramidal neurons. *Nat Neurosci*. **2**:989-996

Hines, ML. and Carnevale, NT. (1997) The NEURON simulation environment. *Neural Computation* **9:**1179-1209

Holt, GR. and Koch, C. (1997) Shunting inhibition does not have a divisive effect on firing rates. *Neural Comput*. **9**:1001-1013

Holthoff, K., Tsay, D. and Yuste, R. (2002) Calcium dynamics of spines depend on their dendritic location. *Neuron.* **33**:425-437

Horton, JC. and Sherk, H. (1983) Receptive field properties in the cat's lateral geniculate nucleus in the absence of ON-center retinal input. *J. Neuroscience* **4:**374-380

Humphrey, AL. and Saul, AB. (1998) Strobe rearing reduces direction selectivity in area 17 by altering spatiotemporal receptive-field structure. *J Neurophysiol*. **22**:2945-2955

Ibbotson, MR. and Clifford, CWG. (2001) Interactions between ON and OFF signals in directional motion detectors feeding the NOT of the Wallaby. *J.*

Neurophysiol. **86**:997-1005

Ibboston, MR. and Price, NSC. (2001) Spatiotemporal tuning of directional neurons in mammalian and avian pretectum: A comparison of physiological properties. *J Neurophysiol.* **86**:2621-2624

Jacobs, B., Schall, M., Prather, M., Kapler, E., Driscoll, L., Baca, S., Jacobs, J., Ford, K., Wainwright, M. and Treml, M. (2001) Regional dendritic and spine variation in human cerebral cortex: a quantitative golgi study. *Cereb Cortex.* **11**:558-571

Jagadeesh, B., Wheat, HS. and Ferster, D. (1993) Linearity of summation of synaptic potentials underlying direction selectivity in simple cells of the cat visual cortex. *Science.* **262**:1901-1904

Jones, JP. and Palmer, LA. (1987) The two-dimensional spatial structure of simple receptive fields in cat striate cortex. *J Neurophysiol*. **58**:1187-1211

Kalikulov, K., Ismailov, I., Hester, FW. and Friedlander, MJ. (2002) Intracellular calcium imaging in neonatal visual cortical neurons during paring Induced synaptic potentiation. *Neuroscience Abst* **443.1**

Kennedy, MB. (2000) Signal-processing machines at the postsynaptic density. *Science.* **290**:750-754

Knapp, AG. and Mistler, LA. (1983) Response properties of cells in rabbit's lateral geniculate nucleus during reversible blockade of retinal ON-center channel. *J. Neurophysiology* **50:** 1236-1245

Koch, C. (1999) Biophysics of Computation: Information processing in single neurons. *Oxford University Press*.

Koch, C., Mo, C. and Softky, W. (2003) Single Cell Models. In *Handbook of Brain Theory and Neural Networks, 2nd edition, MIT press* .p1044-1049

Koch, C. and Poggio, T. (1987). Biophysics of computation: Neurons, Synapses, and Membranes. *Synaptic Function. G.M. Edelman, W.E. Gall and W.M. Cowan, eds., Neurosciences Research Foundation, John Wiley and Sons*, 637-697

Koch, C. and Poggio, T. (1985). The synaptic veto mechanism: does it underlie direction and orientation selectivity in the visual cortex? *In models of the visual cortex. D. Rose and V. Dobson, eds., John Wiley & Sons Ltd*. 408-419

Koch C, Poggio T, Torre V. (1982) Retinal ganglion cells: a functional interpretation of dendritic morphology *Philos Trans R Soc Lond B Biol Sci.* **298**, 227-263

Koch, C. and Segev, I. (2000) The role of single neurons in information processing. *Nat Neurosci*. **3 Suppl**:1171-1177

Krukowski, AE, and Miller, KD. (2001) Thalamocortical NMDA conductances and intracortical inhibition can explain cortical temporal tuning. *Nat Neurosci* **4**:424-430

Livingstone, MS. (1998) Mechanisms of direction selectivity in Macaque V1. *Neuron* **20:**509-526

Livingstone, MS., Pack, CC. and Born, RT. (2001) 2-D substructure of MT receptive-fields. *Neuron* **30**:781-93

Livingstone, MS., Tsao, DY. (1999) Receptive fields of disparity-selective neurons in macaque striate cortex. *Nat Neurosci* **2**:825-32

Livingstone, MS., Tsao, DY. and Conway, BR. (2000) What happens if it changes contrast when it moves? *Society for Neuroscience Abstracts* **26:**162.6.

Lynch, G., Larson, J., Kelso, S., Barrionuevo, G. and Schottler, F. (1983) Intracellular injections of EGTA block induction of hippocampal long-term potentiation. *Nature* **305**:719-721

Lu, ZL. and Sperling, G. (1999) Second-order reversed phi. *Perception & Psychophysics* **61:**1075-1088

MacDermott, AB., Mayer, ML., Westbrook, GL., Smith, SJ. and Barker, JL. (1986) NMDA-receptor activation increases cytoplasmic calcium concentration in cultured spinal cord neurones. *Nature*. **321**:519-522

Maex, R. and Orban, (1996) GA. Model circuit of spiking neurons generating directional selectivity in simple cells. *J. Neurophysiol*. **75**:1515-1545

Mainen, ZF. and Sejnowski, TJ. (1996) Influence of dendritic structure on firing pattern in model neocortical neurons. *Nature* **382:**363-366

Malenka, R. and Nicoll R. (1999) Long-term potentiation—a decade of progress? *Science.* **285**:1870-1874

Markram H., Lubke J., Frotscher M. and Sakmann B. (1997) Regulation of synaptic efficacy by coincidence of postsynaptic APs and EPSPs. *Science*. **275**:213-215

Mather, G. and Murdoch, L. (1999) Second-order processing of four-stroke apparent motion . *Vision Research* **39:**1795-1802

McLean, J., and Palmer, L.A. (1989). Contribution of linear spatiotemporal receptive field structure to velocity selectivity of simple cells in area 17 of cat. *Vision Res*. **29**:675-679

Meister, M., Wong, RO., Baylor, DA. and Shatz, CJ. (1991) Synchronous bursts of action potentials in ganglion cells of the developing mammalian retina. *Science*. **252**:939-43

Mel, BW. (1993) Synaptic integration in an excitable dendritic tree. *J Neurophysiol.* **70**:1086-1101

Mel, BW., Ruderman, DL. and Archie, KA. (1998) Translation-invariant orientation tuning in visual "complex" cells could derive from intradendritic computations. *J. Neuroscience* **18:**4325-4334

Mel, BW. (2002) Have we been Hebbing down the wrong path? *Neuron*, **34**, 275-88

Majewska, A., Brown, E., Ross, J. and Yuste, R. (2000a) Mechanisms of calcium decay kinetics in hippocampal spines: role of spine calcium pumps and calcium diffusion through the spine neck in biochemical compartmentalization. *J Neurosci.* **20**:1722-1734

Majewska A, Tashiro A, Yuste R. (2000b) Regulation of spine calcium dynamics by rapid spine motility. *J Neurosci*. **20**:8262-8268

Mo, CH. and Koch, C. (2003) Modeling reverse-phi motion selective neurons in cortex: double synaptic veto mechanism. *Neural computation*

Montague, PR., Dayan, P., Person, C. and Sejnowski, TJ. (1995) Bee foraging in uncertain environments using predictive hebbian learning. *Nature*

377:725-728

Montague, PR. and Sejnowski, TJ. (1994) The predictive brain: temporal coincidence and temporal order in synaptic learning mechanisms. *Learn Mem* **1**:1-33

Ohzawa, I., DeAngelis, GC., Freeman, RD. (1997) Encoding of binocular disparity by complex cells in the cat's visual cortex. *J Neurophysiol* **77**:2879-909

Oja, E. (1982) A simplified neuron model as a principal component analyzer. *J. Math. Biology* **15**:267-273

Poggio, T. (1982) Visual Algorithms. *In Massachusetts Institute of Technology Aritifical Intelligence Laboratory, A.I. Memo No. 683*. 1-28

Poggio, T. and Torre, V. (1978) “A new approach to synaptic interactions." In: *Lecture Notes in Biomathematics: Theoretical Approaches to Complex Systems*, **Vol. 21.** Heim, R., and Palm, G., editors, pp. 89-115. Springer Verlag: Berlin, Germany

Poirazia, P., Brannon, T. and Mel, BW. (2003) Pyramidal neuron as 2-layer neural network. *Neuron*, in pres

Quartz, SR. (1999) The constructivist brain. *Trends in Cognitive Sciences.* **3**:48-5

Quartz, SR. and Sejnowski, TJ. (1997) The neural basis of cognitive development: A constructivist manifesto. *Behavioral and Brain Sciences*. **20**:537-596

Rao, RPN. and Sejnowski, TJ. (2000) Predictive sequence learning in recurrent

neocortical circuits, *Advances in Neural Information Processing Systems 12,* S. A. Solla, T. K. Lee, and K.-R., Muller (Eds)., MIT Press, 164-170

Rao, RPN. and Sejnowski, TJ. (2001) Spike-timing-dependent Hebbian plasticity as temporal difference learning. *Neural Computation* **13**:2221-2237.

Reichardt W. (1961) Autocorrelation, a principle for the evaluation of sensory information by the nervous system. In *Sensory Communication* (edited by W. A. Rosenblith). Wiley, NewYork.

Reid, RC., Soodak, RE. and Shapley, RM. (1991) Directional selectivity and spatio-temporal structure of receptive fields of simple cells in cat striate cortex. *J. Neurophysiol*. **66**: 505-529

Rodieck, RW. (1998) The first steps in seeing. *Sinauer Associates, Inc.* 102-121.

Sabatini, BL., Maravall, M. and Svoboda, K. (2001) Ca(2+) signaling in dendritic spines. *Curr Opin Neurobiol.* **11**:349-356

Sabatini BL, Oertner TG, Svoboda K. (2002) The life cycle of Ca(2+) ions in dendritic spines. *Neuron* **33**:439-52

Santen, JPH. and Sperling, G. (1985) Elaborated Reichardt detectors. *J. Opt. Soc. Am. A* **2:**300-320

Sato, T. (1989) Reversed apparent motion with random dot patterns. *Vision Res.* **29:**1749-1758

Saul, AB. and Feidler JC. (2002) Development of response timing and direction selectivity in cat visual thalamus and cortex. *J Neurosci*. **22**:2945-55

Schiller, PH. (1982) Central connections of the retinal ON and OFF pathways. *Nature* **297:**580-583

Schiller, PH., Sandel, JH. and Maunsell, JHR. (1986) Functions of the ON and OFF channels of the visual system. *Nature* **322:**824-825

Schuman, EM. (1997) Synapse specificity and long-term information storage. *Neuron* **18**:339-342

Sherk, H. and Horton, JC. (1984) Receptive field properties in the cat's area 17 in the absence of on-center geniculate input. *J Neurosci* **4**:381-93

Song, S., Miller, KD., and Abbott, LF. (2002) Competitive Hebbian learning through spike-timing-dependent synaptic plasticity. *Nature Neuroscience* **3**:919-926

Soto-Trevino, C., Thoroughman, KA., and Marder, E., Abbott, LF. (2001) Activity-dependent modification of inhibitory synapses in models of rhythmic neural networks. *Nature Neurosci*. **4**:297-303

Suarez, H. (1995) Modeling motion detection in striate visual cortex using massive excitatory feedback. *Ph.D thesis. California Institute of Technology, Pasadena, California, 91125*

Suarez, H., Koch, C. and Douglas, R. (1995) Modeling direction selectivity of simple cells in striate visual cortex within the framework of the canonical microcircuit. *J. Neuroscience* **15**:6700-6719

Taylor, WR., He, S., Levick, WR. And Vaney, DI. (2000) Dendritic computation of direction selectivity by retinal ganglion cells. *Science.* **289**:2347-2350

Torre, V. and Poggio, T. (1978) A synaptic mechanism possibly underlying directional selectivity to motion. *Proc. Roy. Soc. Lond. B* **202:**409-416

Tsay, D. and Yuste, R. (2002) Role of dendritic spines in action potential

backpropagation: a numerical simulation study. *J Neurophysiol*. **88**:2834-45

Turrigiano, GG., Leslie, KR., Desai, NS., Rutherford, LC., and Nelson, SB. (1998) Activity-dependent scaling of quantal amplitude in neocortical neurons. *Nature* **391**:892-896

Yang, SN., Tang, YG., and Zucker, RS. (1999) Selective induction of LTP and LTD by postsynaptic [Ca2+]i elevation. *J Neurophysiol* **81**:781-787

Vaney, DI., He, S., Taylor, WR. and Levick, WR. (2001) Direction-selective ganglion cells in the retina. In Motion Vision- Computational, Neural, and Ecological Constraints. *Springer Verlag, Berlin Heidelberg New York*, p14-56

Wong, RO., Meister, M. and Shatz, CJ. (1993) Transient period of correlated bursting activity during development of the mammalian retina. *Neuron*. **11**:923-38

Wö rgö tter, F. and Koch, C. (1991) A Detailed model of the primary visual pathway in the cat: comparison of afferent excitatory and intracortical inhibitory connection schemes for orientation selectivity. *J. Neuroscience* **11:**1959-1979

Zador, AM., Koch, C., and Brown, T. (1990) Biophysical model of a Hebbian Synapse. *PNAS.* **87**:6718-6722

Zucker, RS. (1999) Calcium - and activity-dependent synaptic plasticity. Curr Opin *Neurobiol.* **9**:305-313